Real-Time Steam Allocation Optimization

by

Najmudeen Sibaweihi

A thesis submitted in partial fulfillment of the requirements for the degree of

Doctor of Philosophy

in

Petroleum Engineering

Department of Civil and Environmental Engineering

University of Alberta

Abstract

Traditionally, reservoir model-based open-loop optimization is used to allocate an amount of steam to each injector well. In Steam-Assisted Gravity Drainage (SAGD) recovery, the optimal real-time steam allocation from a shared steam generator to physically connected multi-pads can significantly improve long-term performance goals. However, in real-time optimization (RTO), general-purpose optimization algorithms decide based on short-term responses, unlike long-term optimization processes. Using economic Key Performance Indicators (KPI) such as Net Present Value (NPV) in a single objective, the RTO determines the smallest amount of steam allocation that results in the highest economic returns. Injecting a small amount of steam reduces steam chamber heat loss, growth, and long-term ultimate bitumen recovery. Furthermore, when the oil price is volatile, maximizing steam allocation and non-condensable gas (NCG) at the wind-down stage is essential to ensuring a profit while reducing risk. This research addresses the SAGD RTO workflow limitations of handling oil price volatility and balancing steam chamber development and economics to achieve long-term goals.

An adaptive data-driven predictive model developed based on typical Athabasca oil reservoir properties is employed for real-time short-term forecasting of the KPI, reducing the computational cost. A modified version of Modigliani's risk-adjusted performance is proposed and integrated into the workflow as a tradeoff selector of expected returns and risk when handling oil price volatility. Additionally, the workflow is tested on multi-pad steam allocation using an

Alternating Direction Method of Multipliers (ADMM) for single-, multi- and many-objective optimization problems. Finally, an alternating set of RTO objectives is proposed to ensure that both short- and long-term KPIs are achieved.

The performance of the RTO workflow introduced is tested on single and multi-pad field scale SAGD first principle models. In addition, the cases are designed to mimic SAGD operations steam availability, wind-down, single, multi, and many objective RTO. The impact of the developed workflow is the improved short-term strategies, improved long-term economics, and reduced carbon footprints

Preface

The research presented in this dissertation was accomplished under the supervision of Dr. Japan Trivedi. In chapters Chapter 2, Chapter 3, Chapter 4, and Chapter 5, he contributed to the concept formulation, reviewed and edited the initial draft composed by me.

A version of Chapter 2 has been published as Najmudeen Sibaweihi, Patel R.G., Jose L. G., Ian D. G. Trivedi J., 2021 "Real-time steam allocation workflow using machine learning for digital heavy oil reservoirs", Journal of Petroleum Science and Engineering, volume 199, article 108168. Also, a full-length paper based on this chapter has been published in the proceedings of the SPE Western Regional Meeting 2019. I was responsible for coding of real-time workflow, running optimization and manuscript composition. Dr. Patel R.G. developed the reservoir and data analytic models and manuscript review. Mr. Jose L. G. manuscript review and optimization coding support. Dr. Ian D. G. was the supervisory author. Dr. Trivedi J. was responsible for optimization coding support and manuscript composition and review.

A version of Chapter 3 has been published as Najmudeen Sibaweihi, Trivedi J., 2022 "Risk Management and Optimization in Real-Time NCG Co-Injection Under Economic Uncertainty", SPE Reservoir Evaluation & Engineering, pages 1-21. I was responsible for coding of real-time workflow, running optimization, reservoir and data analytic models development and manuscript composition. Dr. Trivedi J. was responsible for optimization coding support and supervisory author.

A version of Chapter 4 is submitted as Najmudeen Sibaweihi, Trivedi J., 2022 "Distributed Real-Time Optimization of Multi-Pad Steam Allocation" to SPE Reservoir Evaluation & Engineering. Also, a full-length paper based on this chapter has been accepted in the proceedings of the SPE Canadian Energy Technology Conference and Exhibition 2023. I was responsible for coding of real-time workflow, running optimization, reservoir and data analytic models development and manuscript composition. Dr. Trivedi J. was responsible for optimization coding support and supervisory author.

A version of Chapter 5 is submitted as Najmudeen Sibaweihi, Trivedi J., 2022 "Multi-Criteria Real-Time Optimization of Multi-Pad Steam Allocation" to Journal of Petroleum Science and Engineering. I was responsible for coding of real-time workflow, running optimization, reservoir and data analytic models development and manuscript composition. Dr. Trivedi J. was responsible for optimization coding support and supervisory author.

Dedicated to my parents, wife, children, siblings and friends

For their love, support and understanding.

Acknowledgements

First and foremost, I thank Allah (SWT) for all His blessings, which made it possible for me to complete this research and earn a Ph.D.

My supervisor, Dr. Japan Trivedi, has been a tremendous source of motivation throughout this doctoral journey. He has been an inspiration and a source of immense knowledge, direction, and motivation in enhancing my research experience and education. I appreciate the freedom he has allowed me to explore and implement new ideas despite the numerous research obstacles.

My appreciation also goes to my defense committee members, Dr. Juliana Leung, Dr. Zukui Li, Dr. Deepak Davegowda, and Dr. Alireza Nouri, for their valuable feedback on my research. Finally, I am also grateful to my past and present research group members for their stimulating discussions and moral support. I thank my late, much-loved father, Sibaweihi Y. Muhydeen, and my mother, Mariyat Suweid. Their unselfish love and support helped me reach this goal and allowed me to go to college. I also thank my wife, Iman S. Madugu, and my children, Mariyat N. Sibaweihi, Sibaweihi N. Sibaweihi, and Najma N. Sibaweihi, for their patience and duas during my Ph.D.

I gratefully acknowledge the University of Alberta's Future Energy Systems research initiative, which made this research possible research thanks to funding from the Canada First Research Excellence Fund (CFREF). I also acknowledge financial support from the University of Alberta through the Doctoral Recruitment Scholarship and Computer Modelling Group (CMG) for providing academic licenses for the thermal reservoir simulator STARS.

Contents

List of Tables

List of Figures

Chapter 1

Introduction

1.1 Background

According to Natural Resources Canada, Canada's proved oil reserve totals 168.5 *billion* barrels in 2014, of which 164.1 *billion* (˜97%) are oil sands (NRCAN, 2016). Between 2019 and 2039, the Canadian Energy Research Institute (CERI) predicts that in-situ thermal recovery, solvent, primary, and EOR cold bitumen projects will cost $CAD200$ *billion* in capital costs. The CERI study also says that the oil sands are expected to add $1.01 *trillion* to Canada's GDP over the next 11 years (Millington, 2019). Oil sands are made of bitumen, sand, and water, which are mined or heated because of their highly viscous nature. The main in-situ bitumen recovery methods are cyclic steam stimulation (Escobar et al., 2000; Frenette et al., 2016; Patel et al., 2005; Vittoratos et al., 1990) and steam-assisted gravity drainage (Aboorvanathan et al., 2019; Butler, 1991; Edmunds and Chhina, 2001). This work focuses on the real-time optimization of the steam-assisted gravity drainage (SAGD) recovery method.

Even though SAGD has been used successfully in western Canadian oil reservoirs, many research questions still need to be answered to improve bitumen recovery, lower the cost of steam injection, and improve energy efficiency to reduce the carbon footprint. Achieving the goals require in-depth knowledge of integrated SAGD process management decision-making under uncertainty. Uncertainty can arise from the bitumen price, the reservoir's geology, the water supply for steam generation, or technical issues with a steam generator.

Improvements in intelligent field technology make it possible to make better decisions about the SAGD process in real-time.

1.1.1 Data-Driven SAGD Reservoir Models

Management of SAGD reservoirs requires a production forecasting tool for optimal decision-making. Typically, a decision-making tool is needed. The tool can be analytic (i.e., Butler's model), numerical (i.e., reservoir simulator), or data-driven models (i.e., system identification, neural network). Historically, assisted or manual history matching has mainly been conducted using a reservoir simulator. The computational expense of assisted or manual history matching with reservoir simulators presents a challenge. Other problems, like the cost of getting new data to update the model, can make it hard to use reservoir simulators for making quick decisions. Reservoir simulators are the most effective tool for long-term screening of different recovery methods. The dissertation focuses on real-time optimal short-term decision making, which faces decisions such as bitumen price uncertainties, availability of steam supply, steam-non-condensable gas injection, single and multiple objective multi-pad steam allocation (optimized control variable). System identification is selected as a tool to simulate the dynamic state of the SAGD recovery process. The selected data-driven tools main advantages are

- Computationally less expensive
- Use of routine data (i.e., temperature, rate) at no extra cost, unlike the simulator, which requires well logs, seismic data updating, which is expensive.
- It does not requires highly skilled engineers to operate it in production operations.

Using observed data from a dynamic system to construct a representative mathematical model is called system identification (Ljung, 1999). Petroleum reservoirs are dynamic systems because pressure and saturation change over time and space. System identification techniques can be used to model these changes. System identification in the SAGD model can be described as an inverse problem. Identification of the reservoir (system) state is defined as history matching, a critical step in SAGD process optimization.

A general model structure (Ljung, 1999) for dynamic systems can be represented as

$$y(t) = G_p\left(z^{-1}, \theta\right) u(t) + G_l\left(z^{-1}, \theta\right) e(t) \tag{1.1}$$

$G_p\left(z^{-1}, \theta\right)$ is the process transfer function that relates the input ($u(t)$, steam injection rate) at any time(t) to the output ($y(t)$, oil or water rate). $G_l\left(z^{-1}, \theta\right)$ is the disturbance transfer function that relates the input noise to the output. z^{-1} is the backward shift operator; this allows the process and disturbance transfer functions to include the effects of the past inputs on the current output. θ represents the vector of parameters to be estimated. The general prediction error model (PEM) for history matching SAGD reservoir model is expressed as (Huang and Kadali, 2008);

$$A\left(z^{-1}\right) y(t) = \frac{B\left(z^{-1}\right)}{F\left(z^{-1}\right)} u(t) + \frac{C\left(z^{-1}\right)}{D\left(z^{-1}\right)} e(t) \tag{1.2}$$

$$A\left(z^{-1}\right) = 1 + a_1 z^{-1} + \ldots + a_{na} z^{-na} \tag{1.3a}$$

$$B\left(z^{-1}\right) = b_1 z^{-1} + \ldots + b_{nb} z^{-nb} \tag{1.3b}$$

$$C\left(z^{-1}\right) = 1 + c_1 z^{-1} + \ldots + c_{nc} z^{-nc} \tag{1.3c}$$

$$D\left(z^{-1}\right) = 1 + d z^{-1} + \ldots + d_{nd} z^{-nd} \tag{1.3d}$$

$$F\left(z^{-1}\right) = 1 + f_1 z^{-1} + \ldots + f_{nf} z^{-nf} \tag{1.3e}$$

The process (Equation 1.4) and disturbance (Equation 1.5) transfer functions are defined as the rational backward shift operator, respectively, as

$$G_p\left(z^{-1}\right) = \frac{B\left(z^{-1}\right)}{A\left(z^{-1}\right)F\left(z^{-1}\right)} \tag{1.4}$$

History matching using system identification is conducted by re-writing Equation 1.2 as a general linear regression model (Equation 1.5).

$$y(t) = \varphi^T(t)\theta + e(t) \tag{1.5}$$

The formulation now reduces the optimal parameter θ, which minimizes the error between the measured and predicted historical data. The matrix of Equation 1.5 for a historical measurement is

$$Y = \Phi\theta + e(t) \tag{1.6}$$

Where

$$Y = \begin{pmatrix} y_1 \\ \vdots \\ y_N \end{pmatrix} \qquad \Phi = \begin{pmatrix} \varphi^T(1) \\ \vdots \\ \varphi^T(N) \end{pmatrix} \qquad e = \begin{pmatrix} e_1 \\ \vdots \\ e_N \end{pmatrix}$$

The minimization loss function is

$$J(\theta) = \frac{1}{N}(Y - \Phi\theta)^T(Y - \Phi\theta) \tag{1.7}$$

The derivative of Equation 1.7 with respect θ and equating to zero reformulates the loss function with regularization to reduce overfitting as

$$\min_{\theta} J(\theta) = J\left(\widehat{\theta}\right) = \frac{1}{N}\left[Y^TY - Y^T\Phi\left(\Phi^T\Phi\right)^{-1}\Phi^TY\right] + \frac{1}{N}\lambda\left\|\theta\right\|^2 \tag{1.8}$$

The SAGD recovery process is developed in stages (ramp-up, regular, and blow-down). Steam is prioritized for hundreds of well-pairs or pads at various stages of maturity. Although the data-driven model can help short-term SAGD recovery decision-making under uncertainty, it can produce suboptimal decisions as decision variables grow.

Over the years, various researchers have presented data-driven models as a proxy for a high-fidelity first-principle model to make production optimization decisions. Ma et al. (2015) studied the uncertainties of parameters of an artificial neural network SAGD model. Principal component analysis was used to reduce the size of the problem's dimensions to avoid overfitting and make better predictions. SAGD performance is affected by interbedded shale barriers. Kim and Shin (2017) studied the effects of interbedded shale barriers on SAGD performance. Their study used linear, linear-log, log-log two-factor interaction, and two-factor with a log transform regression models to build a data-driven SAGD model. The study showed that the key parameters affecting the peak and drop (inflection point) in bitumen production rate and increase of Steam-Oil-Ratio (SOR) are reservoir thickness, shale width, shale length, and vertical location of shale barriers. In addition, integrating convolutional neural networks and data analytic techniques were studied to infer the distribution of shale barrier impedance to steam chamber growth (Ma and Leung, 2019). The data-driven SAGD models use temperature profiles from vertical observation wells and horizontal SAGD well-pair production profiles to infer shale barriers' size. Also, the data-driven SAGD model generates an ensemble of heterogenous SAGD input production and temperature time-series data. In the same way, Kumar and Hassanzadeh (2021) used random forest regression to create a data-driven SAGD model to study how random shale barriers affect SAGD performance. Their results showed that shale with a length of less than 20% of the reservoir and increasing shale distance away from the producer had no significant effect on production performance. Yu et al. (2021) developed a data-driven model for forecasting SAGD cumulative oil production. The model is based on an artificial neural network, and the performance was tested using the Von Bertalanffy indicator with a 0.52% error after 20 years of cumulative oil production forecast. Based on the comparison of ANN, XGBoost, and LightGBM SAGD data-driven models, Huang and Chen (2021) showed that training performance improves with increasing sample size and randomness (i.e. sampling distribution), with LightGBM showing the best performance. However, the ANN model shows the best performance with the

worst randomness. A recent study by Huang et al. (2023) of ANN, GRU, LSTM, CatBoost, XGBoost, and LightGBM SAGD data-driven models on three sets of PetroChina Canada field data. The test results showed that the recurrent-based algorithms (GRU, LSTM) have better predictive performance but require higher training time than boosting-based algorithms (CatBoost, XGBoost, LightGBM) and ANN, with GRU being the best predictive algorithm. System identification, a recurrent-based algorithm that requires less training time, will be used in this dissertation.

System identification for data-driven models has been applied over the years in the petroleum industry for waterflooding design (Hourfar et al., 2016), oil PVT properties estimation (Salehinia et al., 2016) and production optimization (Elgsaeter et al., 2008). System identification, which will be used to build a data-driven SAGD model, has proven to be effective in SAGD operations over the years. Yao et al. (2015) studied the use of system identification in developing a data-driven studied the use of system identification in developing a data-driven SAGD model which showed the Box-Jenkins model structure has higher accuracy for one-step-ahead predictions of non-recursive prediction error methods and for a seven-step ahead prediction, recursive autoregressive with exogenous input model structure performs better. It was also observed from the study that, better predictive performance is achieved when SAGD data-driven model is structured with inputs of steam injection rates and bottom-hole pressure and outputs of bitumen and water production rate. The results from Yao et al. (2015) study informs the choice of Box-Jenkins model structure as the data-driven model development for this work. Purkayastha et al. (2018) further showed MIMO system identification of the SAGD model outperforms a multi-input and single-output (MISO) model structure. In the study, the MIMO model was used for the steam trap and oil rate controls, while the steam trap was the control for MISO. MIMO configuration showed a 171% improvement in NPV when compared with MISO. Sibaweihi et al. (2019) used Output-Error (OE) system identification model structure as SAGD data-driven model to study the economic performance of SAGD under different scenarios of steam availability and prioritization.

Data-driven models using system identification proxy models will learn the SAGD process parameters for real-time short-term forecasting and optimization in this work. The underlying equations used in building data-driven models may be applied to multiple decision processes and usually leads to not honoring the physics of the process under study. Using first-principle models requires setting boundary conditions or constraints for development strategy (i.e., minimum or maximum rates, flowing bottom hole pressure) to ensure feasible solutions are produced. In the reported works using data-driven models, normalizing historical data aims to improve the data-driven model's prediction performance. Constraints are imposed on the first principle model prediction but not in data-driven models, making them susceptible to producing infeasible future production forecasting. In the work of Purkayastha et al. (2018), the model predictive control (MPC) was used. Using MPC with system identification means setting many constraints (i.e., 32) to make the controller moderately aggressive or ensure prediction stays within bounds. Having many constraints results in poor optimization algorithm performance because it has to honor all the constraints. The methodology section will further describe normalization to reduce constraints and ensure improved prediction performance. The following subsection presents a literature review on using data-driven models in real-time SAGD optimization.

1.1.2 Real-Time Production Optimization

Advances in intelligent field technologies present a unique opportunity for real-time production optimization. Daily SAGD recovery process monitoring and surveillance program collects data such as rates, temperature, and pressure information of well-pairs or pads. The collected data are processed into helpful information used in management decision-making. Future development plans for SAGD reservoirs are designed using life-cycle optimization to maximize economic benefit. The dynamic nature of SAGD reservoirs means the initial SAGD reservoir model used in creating future development plans needs updating. Decisions such as well-pairs or pad drilling schedules, exploitation strategy, production, and injection allocations due to changes in market forces

and geological or operational challenges introduce conflict in long-term and short-term goals. Short-term (weekly, daily, or monthly) updates and optimization of SAGD reservoir model input parameters in real-time to minimize deviations from long-term goals become essential.

The life cycle of SAGD recovery projects involves making capital-intensive decisions and has a high risk of failure. Thermal recovery techniques cost is affected significantly by steam supply and water handling accounts for more than half of cost (Edmunds and Chhina, 2001). Traditionally, predetermined steam is allocated using the reservoir model to optimize the SAGD process. Allocating steam using proration can lead to a suboptimal return on investment and, hence, optimize steam allocation to maximize NPV. Unexpected operational challenges or water availability for a steam generation have a significant constraint on the steam amount injected into a well-pair or well-pad or field SAGD operation. SAGD project life-cycle requires well-pairs or well-pads added to the production stream at different project stages. Adding well-pairs or pads introduces an additional steam generation capacity requirement, affecting the project performance . Hence, optimal operation maximizes NPV, identifying which well-pair or well pad in the SAGD project being allocated excess steam becomes essential. Environmental and low oil prices constrained the optimal performance of SAGD. Hence, optimal operation maximizes NPV and identifying which well-pair or well pad in the SAGD project being allocated excess steam becomes essential. In addition to low oil prices, environmental factors constrains the optimal performance of SAGD. Accordingly, it becomes essential to coordinate steam supply to each well-pair or well-pad in real-time steam allocation optimization. Challenges such as steam chamber conformance control and uniform steam chamber distribution along well-pairs due to heterogeneity in geological properties further support the need for real-time production optimization. The geological heterogeneity encountered as the steam chamber spreads vertically and laterally can positively or negatively affect bitumen production and steam injection. Real-time optimization ensures the adaptation of injection and production rates to reflect the dynamic state of the reservoir.

SAGD data-driven model is coupled with an optimization algorithm and data acquisition setup to form a real-time production optimization workflow. The workflow dynamically sets controller setpoints from ramp-up, normal and wind-down stages of SAGD (i.e., from greenfield to brownfield). Dynamic optimization under uncertainty is performed in real-time to maximize short-term Key Performance Indicators (KPI). SAGD recovery method KPIs typically optimized is Net Present Value (NPV), Steam-Oil-Ratio (SOR), water loss or balance, and recovery factor. For the annual In Situ Performance Presentations oil and gas companies submit to the Alberta Energy Regulator (AER), the the in situ recovery method performance is formulated as multi-objective to balance economic, engineering, and environmental goals (EEE-G).

Presentations in the literature have yet to formulate the real-time workflow that balances EEE-G submitted to AER annually. As well-pairs and pads are added to the SAGD reservoir, it can produce sub-optimal decisions as decision variables grow. Typically, in the literature, the optimization problem is presented as a single problem. For real-time SAGD production optimization, the optimization problem can be decomposed into units (well-pair or well-pad), and each unit can be optimized.

The primary tool in SAGD operations decision-making is utilizing a reservoir simulator (first principle model). Improvement in real-time data acquisition presents an opportunity for real-time short to medium-term SAGD operations decision-making. Saputelli et al. (2006) define real-time as making decisions at a frequency commensurate with the corresponding level's timescale. The challenge long-term SAGD operating strategies face is dynamic changes in the reservoir because heterogeneity requires continuous updating of operating strategies. Holanda et al. (2015) listed some challenges of reservoir management decision-making: high uncertainty of measured data, time-consuming nature of analyzing data, and expensive data acquisition. Various researchers have presented workflows demonstrating improved key performance indicators (KPI) of SAGD real-time optimization. Mohajer et al. (2010) proposed a four staged workflow that uses artificial intelligence and data mining algorithms coupled with a thermal reservoir simulator to analyze real-time data from

SAGD operations. Gonzalez et al. (2012) proposed a real-time workflow to optimize SAGD well-pairs inflow performance. The workflow uses fiber optic downhole array temperature measurements and pressure-temperature downhole gauges to guide steam injection rates and pressures during the start-up and production stages of the SAGD process in real-time. Purkayastha et al. (2015) used MPC with proactive steam injection rates determined recursively to describe the relationship between subcool temperature difference and input heat rate. The goal was to find the optimal steam conformance, which resulted in an NPV improvement of 35.7%. Patel and Trivedi (2017) presented a real-time SAGD production optimization using Adaptive and Gain-Scheduled MPC. Adaptive MPC recursively estimates model parameters while Gain-schedule decomposes the subcool control problem into a dynamic nonlinear reservoir system's multiple-controller problem. The economic performance of SAGD was optimized in real-time, which realized an NPV increase of 23.69% and 10.36% for adaptive and gain-Scheduled MPC, respectively. Kumar et al. (2018) proposed workflow with coupled machine learning and numerical simulation to predict future SAGD performance. The workflow uses field surveillance data to determine the optimal field and well steam injection rate, duration of steam injection, and the rate of reduction of steam injection to mature ells for redistribution to newly developed regions. When the workflow was implemented in a middle eastern reservoir, the results showed that NPV increased by 42.4%, and the cumulative steam-oil ratio decreased by 24%. Vembadi et al. (2018) presented rea-time feedback control of SAGD subcool and steam chamber development optimization under uncertainty. It was demonstrated that MPC real-time realized an 18% improvement in NPV than standard open-loop optimum rates typically practice in the field. Hunyinbo et al. (2022) proposed a real-time SAGD forecast uncertainty workflow with Monte Carlo sampling to handle uncertainty quantification. The approach to handling uncertainty is based on the probabilistic approach, while in this dissertation, a scenario-based approach is implemented in a robust optimization framework.

The SAGD recovery process is developed from single well-pair pilot test-

ing to multi-well pair pad and multi-pad as field development moves from greenfield to brownfield. Real-time optimization of SAGD operations results in increasing optimization problem size with competing demand for steam allocation between mature and younger well-pairs or pads. The real-time SAGD optimization workflows presented in the literature assume a single well pair (Guevara et al., 2018) or well-pad (Guo et al., 2018) or multi-pad (Shahandeh et al., 2016) over the life-cycle of the project. The formulation of real-time SAGD optimization as a single problem can be susceptible to producing sub-optimal results. In this work, real-time SAGD optimization is formulated as a distributed control optimization.

1.1.3 Decomposition-based Optimization

The decomposition approach can be applied to break large-scale multi-pad optimization problems into sub-problems and solved either in parallel or sequentially. Even in situations where decomposed solution methods are slower than centralized solutions methods, decomposed solutions are preferred since it allows coordination of subsystems to achieve global optimality (Boyd et al., 2008). For the multi-pad steam allocation problem (Equation 1.9), the variable (steam allocation, U) for which N_{pad} is the number of pads, is decomposed into subvectors $u_1, \ldots, u_{N_{pad}}$ and the sum of the objectives of steam allocation u_i solved in parallel honouring the local constraint to each pad is the field-wide objective. A coupling constraint (Equation 1.10a) does not allow the optimization problem to be solved separately. The local constraint can be the maximum allowable change in steam allocation for controller stability (Equation 1.10b) and the local bounds constraint for the allocation variable to each operating well-pair in the pad (Equation 1.10c). Hence decomposition techniques are applied to solve the sub-problems iteratively in parallel to achieve an optimal global solution.

$$\max_{u} \quad \sum_{i=1}^{N_{pad}} f_i\left(u_i\right) \tag{1.9}$$

$$s.t. \sum_{i=1}^{N_{pad}} u_i \ \leq \overline{U} \qquad i = 1, \ldots, N_{pad} \tag{1.10a}$$

$$\Delta u_{i,j}^{\min} \leq \Delta u_{i,j} \leq \Delta u_{i,j}^{\max} \quad j = 1, \ldots, N_{wells} \tag{1.10b}$$

$$u_{lb} \leq u_{i,j} \leq u_{ub} \tag{1.10c}$$

Primal and dual decomposition techniques can be applied to split the optimization problem (Equation 1.9) into sub-problems. In this work, the dual decomposition technique will be used. The dual decomposition of Equation 1.9 is formed by introducing partial Lagrangian to reformulate (Equation 1.9) as a decentralized problem (Equation 1.11). Where $h_i\left(u_i\right)$ is the vector of the resource allocated to each pad.

$$L\left(u_{_i}, \lambda\right) = \sum_{i=1}^{N_{pad}} f_i\left(u_i\right) + \lambda^T \sum_{i=1}^{N_{pad}} h_i\left(u_i\right) \tag{1.11}$$

$$L\left(u_{_i}, \lambda\right) = \left[f_1\left(u_1\right) + \lambda^T h_1\left(u_1\right)\right] +, ... + \left[f_{N_{pad}}\left(u_{N_{pad}}\right) + \lambda^T h_{N_{pad}}\left(u_{N_{pad}}\right)\right] \tag{1.12}$$

$$s.t. \qquad u_i \in C_i \tag{1.13a}$$

$$\Delta u_{_j}^{^{min}} \leq \Delta u_{i,j} \leq \Delta u_{_j}^{^{max}} \quad j = 1, ..., N_{wells} \tag{1.13b}$$

$$u_{lb} \leq u_{i,j} \leq u_{_{ub}} \tag{1.13c}$$

Equation 1.11 can be optimized separately given the dual variable (λ) or the price vector by forming the dual function (Equation 1.13)

$$g(\lambda) = \ g_1(\lambda) +, \ldots, + g_{N_{pad}}(\lambda) \tag{1.14}$$

Where $g_1(\lambda)$ is

$$\max f_1(u_1) + \lambda^T h_1(u_1) \tag{1.15a}$$

$$s.t \qquad u_1 \in \mathcal{C}_1 \tag{1.15b}$$

$$\Delta u_{1,j}^{\min} \leq \Delta u_{1,j} \leq \Delta u_{1,j}^{\max} \quad j = 1, \ldots, N_{wells} \tag{1.15c}$$

$$u_{lb} \leq u_{1,j} \leq u_{ub} \tag{1.15d}$$

$$\tag{1.15e}$$

The master problem (Equation 1.14) updates λ iteratively based on the subgradient (Equation 1.16) until consensus is reached. Where α is the step-size and k is the iteration counter.

$$\lambda := \lambda - \alpha(k) \sum_{i=1}^{N_{pad}} h_i(u_i) \tag{1.16}$$

The concept of distributed optimization dates back to the early 1960s (Benders, 1962; Dantzig and Wolfe, 1960). The idea behind using a distributed optimization method for real-time large-scale multi-pad steam allocation is to optimize a global objective based on local well-pair or well-pad dynamics. The optimization problem is approached using decomposition methods by decomposing the global optimization problem into subproblems. The global constraint (maximum Steam generator capacity or gas supply) is imposed on local KPI, which ensures communication between the local KPI's, which leads to global optimum KPI. Large-scale optimization problems are solved with three approaches as summarized from Cheng et al. (2007) work:

- **Centralized:** explicitly account for all interactions between subproblems. They are designed to be implemented on a single computer. Require high-efficiency computers and optimization algorithms. As the SAGD process expands, the optimization problem size grows with the possibility of hundreds or a thousand well-pairs. Centralized real-time or life-cycle optimization becomes impossible to solve even with high-performing computers.

- **Decentralized:** Recommended for real-time optimization of decomposable problems like multi-pad SAGD operations. High-efficiency optimization algorithms, high-performance computers and subproblem interactions are not a requirement. The decentralized approach is susceptible to sub-optimal results because of ignoring subproblem interactions.

- **Coordinated decentralized:** is a trade-off between centralized and decentralized approaches by accounting for essential subproblem interactions. A coordinated decentralized approach can be modeled using the following strategies.

  - Centralized modeling, decomposition and then coordination.
  - Decentralized modeling, linking constraints and then coordination.

The structure of the multi-pad SAGD process can be decomposed into a series of subproblems. In this case, subproblems refer to individual well-pairs or well-pads to solve the optimization problem efficiently. Two approaches are typically used to decompose the large-scale decomposable optimization problem: primal decomposition (Johansson et al., 2006) and dual decomposition (Conte et al., 2012; Dantzig and Wolfe, 1960). When the optimization problem has a coupling or shared decision variable or constraints, primal or dual decomposition is used (HomChaudhuri, 2013). A survey of the petroleum literature revealed a little-reported work in applying decomposition techniques in large-scale optimization. Dual decomposition techniques using Lagrangian (Foss et al., 2009; Krishnamoorthy et al., 2018) and Dantzig-Wolfe (Gunnerud et al., 2009) for Troll west oil have been reported for real-time production optimization.Knudsen et al. (2014) presented a Lagrangian relaxation-based decomposition for multi-well pad well scheduling for shale-gas systems. The dual decomposition by the authors assumed a strongly convex optimization problem and also a constant $\alpha(k)$ was assumed for calculating the price vectors in Equation 15 (Fixed stepsize Gradient method). This work explores non-strongly convex (Alternating direction method of multipliers (ADMM) techniques to handle Lagrangian decomposed optimization problem.

1.2 Multi-Criteria Decision-Making (MCDM)

Multi-criteria (NPV, recovery factor, water balance, steam chamber conformance) optimization of SAGD operations can be challenging with conflicting objectives. Single objective economic optimization of SAGD projects may not be safe for the environment or meet safe engineering standards (steam chamber pressure above fracture gradient). NPV is the main criterion that has been primarily used for real-time SAGD optimization (Mohajer et al., 2010; Patel et al., 2014; Vembadi et al., 2018). Recently, multi-objective optimization of steam alternating solvent (Coimbra et al., 2019) and warm solvent (Hunyinbo et al., 2021) injection have been presented using the Pareto-based approach. The works mentioned above on multi-objectives were not implemented in a real-time framework. Implementing multi-objective optimization in real-time SAGD operations comes with a challenge of non-uniqueness of the optimal solutions (non-dominated solutions) to be executed the current prediction horizon. Hence, a mechanism is required to rank and prioritize the non-dominated solutions. The dissertation uses a compromise programming method at each control horizon to choose the best control strategy from the set of non-dominated solutions in a multi-pad, multi-criteria steam allocation. To the best of my knowledge, this is the first time a multi-pad, multi-criteria, and compromise programming approach with real-time workflow is presented.

1.3 Problem Statement

The critical challenge in the steam allocation of steam-assisted gravity drainage (SAGD) projects is evaluating hundreds of wells or pads at different stages of production (ramp-up, regular, and wind-down). Additional challenges affect the SAGD project's efficiency facility constraints, well performance (Steam-oil-ratio, Water-steam ratio, Water-cut), and the capital competition to drill new wells. Since steam supply cost significantly contributes to bitumen's overall production cost, dynamic and intelligent steam allocation to various wells or pads in the oilfield deserves further attention. In addition, a comprehensive

real-time SAGD workflow adaptive to SAGD production stages from greenfield to brownfield requires additional attention.

Using the first principle model in real-time SAGD operations optimization is computationally expensive. Data-driven SAGD models are used as a SAGD reservoir proxy to reduce the computational head. Unlike first principle models, which have boundary problems, data-driven models do not have constraints and forecasts outside the feasible region. Minimizing unfeasible data-driven model forecasting in real-time optimization requires additional constraints, which increases computational time, as in MPC (Patel and Trivedi, 2017). Designing data-driven models that ensure feasible forecasting and minimizing computational time requires further attention SAGD multi-pad recovery system can be described as a large-scale interconnected, well-pairs, and well-pads through shared resource allocation. Individual well-pairs and pads work to maximize bitumen recovery at well-pair and pad drainage areas to maximize field-wide ultimate recovery in a coordinated fashion. Thus, the steam allocation optimization problem deals with allocating steam from one well-pair or pad to another set of well-pair or pads in a multi-pad system to optimally achieve the overall economic, engineering, and environmental goals. Multi-pad SAGD steam allocation optimization with different well-pairs or pad steam requirements at different maturity stages is a high dimensional optimization problem because of hundreds of well-pairs. Computational complexity increases with a centralized optimization problem with hundreds of well-pairs and scales poorly for real-time multi-pad steam allocation. In addition, uncertainty in steam availability, the dynamic nature of SAGD reservoir models, and uncertainty of its parameters coupled with distributed steam generation without central control complicate the optimization process. In this proposal, distributed optimization workflow in real-time operates independently and parallel, utilizing local well-pair or pads dynamic state to improve field-wide KPI in a coordinated manner. Distributed steam allocation optimization reduces the high dimensionality of current real-time SAGD optimization and mitigates scalability and flexibility issues. The efficient operations of SAGD reservoirs require monitoring and optimizing several operating parameters and KPIs.

Balancing conflicting EEE-G makes the problem a multi-objective optimization problem, which results in nondominated solutions. Furthermore, selecting which solutions to implement in real-time control problems under parameter uncertainty can further complicate the optimization problem, hence exploring alternative decision criteria that incorporate expert input.

Based on the gaps and potential room for improvement of the current approach as enumerated in the current section, the following hypothesis is proposed:

1. Real-time multi-pad steam allocation optimization can be improved using decomposition-based algorithms to ensure feasible solutions and better control strategies.

2. Expert knowledge can be incorporated either through the use of compromise programming or Modigliani risk-adjusted performance to prioritize the efficient control strategy in a real-time multi-objective steam allocation.

3. Integration of well constraints with a dynamic data-driven model can improve the quality of history matching and yield feasible forecasting results.

1.4 Research Objectives

The main objective of this work is the development of a real-time steam allocation optimization workflow with a data-driven model for the ramp-up, normal, and wind-down stages of thermal recovery. The research-specific objectives that address the main goal to be answered are listed below:

1. Develop a real-time steam allocation optimization workflow with a data-driven predictive SAGD model. Limited steam availability and prioritization (i.e., adapting steam allocation range based on well-pair or pad performance) scenarios on SAGD operations performance are investigated for the ramp-up stage.

2. Integrate risk management into the workflow and investigate the workflow performance on mature SAGD reservoir for symmetric and asymmetric risk-adjusted objectives. Additionally, normalization of past data based on physical feature range, data-driven model training, and updating are incorporated in the workflow investigation. Using a modified Modigliani risk-adjusted performance approach to include expert opinion to select the optimum risk-adjusted control strategy.

3. Extend the real-time workflow to a single objective distributed optimization. Investigate the short-long term performance of single objective real-time multi-pad steam allocation with ADMM distributed optimization algorithm. A novel alternating cost minimization and steam chamber growth objective are also investigated.

4. Develop a multi-criteria distributed multi-pad real-time steam allocation optimization workflow. Investigate two, three, and four joint optimization goals that balance short-long term performance objectives. Using a compromise programming approach, incorporate expert opinion to select the best control strategy.

1.5 Thesis Structure

The paper-based thesis combines four articles (chapters 2–5). Each chapter gives a specific introduction, literature review, methodology, and conclusion. At the end of the thesis is a list of all the sources used. The thesis is made up of six chapters. Chapter 1 is the introduction; Chapters 2–5 are the main topics, and Chapter 6 is the conclusion. The thesis is organized as follows:

Chapter 1 presents a general introduction to this study, comprising the background on the impact of heavy oil on future economic development, applications of data-driven models and real-time optimization in SAGD recovery operations, decomposition optimization, problem statement, and research objectives.

Chapter 2 describes a novel steam prioritization and steam availability real-

time optimization workflow of SAGD operations with a dynamic data-driven model. In this chapter, the real-time steam allocation workflow is tested on a three-well-pair pad with different amounts of shale distribution, which affects steam chamber conformance.

Chapter 3 investigates the workflow application to mature SAGD operations. A nine-well-pair pad undergoing NCG steam co-injection is used to investigate the workflow performance at the wind-down stage. Several symmetric and asymmetric risk-adjusted goals are tested for real-time allocation of NCG steam when the oil price is uncertain. A novel modified Modigliani risk-adjusted performance is incorporated in selecting the optimum strategy from a set of risk-return trade-offs.

Chapter 4 investigates the single-objective short-long-term optimization of real-time steam allocation. Increasing well-pads as the SAGD process matures means a higher dimensional optimization problem. A multi-pad reservoir for steam allocation is developed to test the real-time short-long-term optimization workflow with high dimensions. Additionally, a novel alternating objective is investigated.

Chapter 5 explores different joint objectives for real-time optimization, which balances short-long term performance. A novel approach for a multi-criteria distributed optimization and selection of optimal control strategy with compromise programming is investigated using a multi-pad reservoir.

Chapter 6 summarizes the study's main findings, conclusions, original contributions, and recommendations for future work.

Chapter 2

Real-Time Steam Allocation Workflow Using Machine Learning for Digital Heavy Oil Reservoirs [1]

2.1 Introduction

Cost of thermal recovery techniques is affected significantly by steam supply and water recycling and treatment costs (Edmunds and Chhina, 2001). The operating expenses of injecting steam in thermal recovery techniques account for more than half of the recurrent cost. Traditionally, predetermined steam is allocated using the reservoir model to optimize the steam assisted gravity drainage (SAGD) process. Allocating steam using proration can lead to a suboptimal return on investment and hence optimization of steam allocation is required to maximize the net present value (NPV). Unexpected operational challenges or water availability for a steam generation are significant constraints on the amount of steam injected for SAGD operations. SAGD project life-cycle requires well-pairs or well-pads to be added to the production stream at different project stages. The addition of well-pairs or pads introduces an additional steam generation capacity requirement which affects the project performance in addition to reservoir heterogeneity. Hence, for optimal SAGD performance, identifying a well-pair or well pad for allocating excess steam be-

[1] A version has been published in Journal of Petroleum Science and Engineering and proceedings of SPE Western Regional Meeting 2019

comes essential. Moreover, the environmental concerns and low oil prices have triggered an urgent need to optimize overall SAGD performance. Therefore, a coordinated steam supply to each well-pair or well-pad with real-time steam allocation is necessary.

The formulation of an optimization problem requires two key features irrespective of the optimization algorithm: decision variables to be perturbed and the objective function to be minimized or maximized. Over the years, various researchers have formulated different approaches to optimize SAGD process using different decision variables and objective function. From simulation studies conducted by Edmunds and Chhina (2001), the economic operating pressure decision variable for typical McMurray formations could be as low as 400 kpa. Yang et al. (2009) used NPV as an objective function for optimizing the infill SAGD project. NPV was maximized using the steam injection rate and the liquid withdrawal rate as decision variables for designed exploration and controlled evolution algorithm. The results from their study showed significant improvement in NPV when a large amount of steam was allocated to the injector and high liquid production targets were set at an early stage. When the desired steam chamber growth was achieved, the steam and liquid rates were lowered to prevent steam breakthrough in the bottom water. Manchuk and Deutsch (2013) presented an optimization algorithm to optimize the placement of surface production pads and drainage-area of the SAGD project for maximizing economically recoverable bitumen. For SAGD projects with multiple steam generators, optimizing the efficiency of the generators presents an additional technical and operational challenge. To optimize the efficiency of numerous steam generators, Hao and Popa (2015) used a quantum particle swarm optimization algorithm. The optimization problem was formulated as a constrained optimization to determine the minimum and maximum steam contribution for each generator. Additionally, steam quality and the total steam for all generators were considered as decision variables. The sum of efficiency curves of the steam generators was the objective function to be maximized. Normal scheduled SAGD operations usually do not go as planned and face many interruptions. These interruptions have adverse

effects on the economics of SAGD projects. Nourozieh et al. (2017) performed optimization on the Athabasca type oil reservoirs to quantify the impact of interruptions on SAGD operations. The initial steam injection period, shut-in period, and steam injection rate after re-initiation were perturbed to maximize SAGD economics. The study concluded that there is an optimal shut-in period dependent on the initial steam injection period that maximizes the recovery of oil. Mohankumar et al. (2020) studied optimization of SAGD well pad scheduling. A nonlinear model predictive control was used to find the optimal development sequence and timing of multiple well-pads by finding the optimal steam injection profile. Patel and Trivedi (2020) presented a real-time SAGD production optimization workflow that ensures stable well operations by controlling subcool setpoint.

Improvement in real-time data acquisition and evolution of machine learning methods present an opportunity for a near real-time decision making in SAGD operations. Various researchers have presented workflows that demonstrate the improvement in key performance indicators (KPI) of SAGD real-time optimization. Mohajer et al. (2010) proposed a workflow that uses artificial intelligence and data mining algorithms to analyze real-time data from SAGD operations. The four staged (surveillance, analysis, optimization, and control) workflow was coupled with a thermal reservoir simulator for a real-time decision making. Gonzalez et al. (2012) proposed a real-time workflow to optimize SAGD well-pair's inflow performance. The workflow used fibre optic downhole array temperature measurements and pressure-temperature downhole gauges to guide updating of steam injection rates and pressures during start-up and production stages of the SAGD process in real-time. Kumar et al. (2018) proposed a workflow of machine learning coupled with numerical simulation to predict SAGD performance. The workflow used field surveillance data to determine the optimal field and well steam injection rate, duration of steam injection, and the rate of reduction of steam injection to mature wells for redistribution to newly developed regions.

However, the amount of data from the real-time acquisition and large computational cost of first principle models introduce a challenge of effectively

using them to make short to medium-term decisions. Updating and running first principle models are computationally expensive. Therefore, reservoir simulators are inappropriate as a tool for short term reservoir management. As a result, the use of data analytics to improve real-time intelligent field decision making in the petroleum industry has grown significantly. Popa et al. (2015) employed a data analytics model to improve the quality of heavy oil reservoir management decisions. To get solutions of critical questions such as steam breakthrough time and redistribution volumes during steam management operations, Jones and Dwivedi (2018) used diagnostic plots and data analytic workflow. The principal KPI analysis performed during the reservoir management decision-making process was economic analysis. Ockree et al. (2018) presented an economic analysis for the Marcellus Shale reservoir in which they used cognitive analytics to generate economic type curves for decision making. Reinforcement learning has shown to improve NPV by at least 30% and a decrease in the computational cost by 60% when used for optimizing SAGD operations (Guevara et al., 2018).

Over the years, various researchers have presented data analytics models as a proxy to this high fidelity first principle model to make real-time decisions. In SAGD, most popular techniques used to create proxy models included linear and non-linear regression (Kim and Shin, 2017), semi-analytical models (Dehdari et al., 2017; Vanegas et al., 2008), and neural networks (Fedutenko et al., 2014; Sun and Ertekin, 2015; Zheng et al., 2016). Ma and Leung (2020) studied the influence of the shale barrier on SAGD performance using convolutional neural network and data analytic techniques. System identification for data analytics has been applied over the years in the petroleum industry for SAGD (Patel et al., 2018; Patel and Trivedi, 2017; Yao et al., 2015), waterflooding design (Hourfar et al., 2016; Renard et al., 1998), oil PVT properties estimation (Salehinia et al., 2016) and production optimization (Elgsaeter et al., 2008).

Various SAGD optimization studies discussed earlier do not account for the impact of steam availability. Besides, the reported methods formulate the optimization problem as a life-cycle problem. Hence, the optimization problem does not account for daily, weekly, or quarterly steam availability

issues. Also, formulating the optimization problem as the life-cycle problem ignores the impact of planned activities such well workover operations, well testing, and low oil price, which interrupts SAGD operations. Excess steam injection in well-pairs or pad leads to lower KPIs due to reservoir heterogeneity or the maturity of the SAGD project. Mature SAGD projects require less amount of steam allocated to well-pairs or pad. The workflow presented in this study accounts for steam prioritization by allocating steam from low performing wells to high performing wells. Another contribution is the formulation of the optimization problem to simulate possible steam availability scenarios that may be encountered during SAGD operations. The steam allocation is optimized in real-time using data-driven predictive models. The workflow is used for the short-term NPV forecast of the SAGD heavy oil reservoir. The parameters of the model are continuously updated using a moving horizon approach for short-term forecasting to maximize NPV. A case study with high, medium, and low recovery well-pairs is presented in order to show applicability of the workflow for real-time optimal steam allocation in a SAGD facility under non-steady-state operating conditions where steam availability changes. Optimization under different scenarios of steam availability such as a) 100% steam availability, i.e., operations at full capacity, b) 100% or lower steam availability with continuous injection rates, and c) varying steam availability between 80 to 100% operating capacity with continuous injection rates, is performed.

2.2 SAGD Reservoir Model

In this study, a synthetic reservoir model representative of western Canadian oilfield with three horizontal well-pairs is used. Well-pair 1 is located in a high-quality reservoir (high permeability section). Well-pairs 2 and 3 are drilled in the moderate and low reservoir sections, respectively. The model properties are typical of the Athabasca oil sands reservoir (Robinson et al., 2005). The model is built with an average porosity, horizontal, and vertical permeabilities of 0.31, 2357 md, and 1768 md, respectively. The oil viscosity is modelled to be 414279 cP at 16^oC and 5.7 cP at 250^oC. Relative permeability curves are

adopted from Guo et al. (2018). Initial water saturation and injection steam quality of 0.2 and 0.9 respectively are used (Guo et al., 2018). The wells are pre-heated for four months before the production phase starts.

2.2.1 Data Analytics for SAGD Model

The use of observed data of a dynamic system to construct a representative mathematical model is referred to as system identification (Ljung, 1999). Petroleum reservoirs are dynamic systems since properties such as pressure and saturation change with time and space and hence can be modelled using system identification techniques. In system identification of the SAGD process, a mathematical model is built based on the historical injection and production data of a heavy oil reservoir. This data-driven mathematical model is then used in real-time steam allocation optimization. Steps followed to build a system identification model for the SAGD process are explained below:

1. The first step is data generation or gathering. Since a synthetic SAGD model is used in this work, an experiment was designed to generate the input and output data for the proxy model. The steam injection rate is created using a random binary signal (RBS) input with MATLAB system identification toolbox (MATLAB, 2018). The steam injection rate ranges from zero to 400 m^3/day to ensure that the model captures the dynamic reservoir state during optimization or deployment. The use of RBS is necessary to ensure that generated input sequence for which output data (oil rate) will be recorded is persistently exciting and leads to acceptable model performance. After that, the reservoir simulation model was run using the RBS signal to measure the response (or output) of the model. Fig. 2.1[a-c] shows the RBS signal (measured injection rate) and model response (measured production rate) for well-pairs $1-3$. The data was taken at one day sampling period and hence 360 data points (days). The first 90% (i.e. 324 data points) of the data was used for training and the last 10% (i.e. 36 data points).It is important to note that the steam injection rate does not follow the RBS sequence in the field. For

implementation in an oilfield, reservoir injection and production history should be used.

2. The next step after data generation or gathering is to find a model structure that gives an acceptable predictive performance for the SAGD process. A general model structure (Ljung, 1999) for dynamic systems can be represented as in Equation 2.1

$$y(t) = G_p\left(z^{-1}, \theta\right) u(t) + G_l\left(z^{-1}, \theta\right) e(t) \tag{2.1}$$

where $G_p(z^{-1}, \theta)$ is the process transfer function that relates the input ($u(t)$, steam injection rate) at any time (t) with the output ($y(t)$, oil or water rate). $G_l(z^{-1}, \theta)$ is the disturbance transfer function that relates the input noise ($e(t)$) with the output. z^{-1} is the backward shift operator; this allows the process and disturbance transfer functions to include the effects of the past inputs on the current output. θ represents the vector of parameters to be estimated. The prediction error model (PEM) is used for this work. The general PEM (Huang and Kadali, 2008) can be expressed as Equation 2.2

$$A\left(z^{-1}\right) y(t) = \frac{B(z^{-1})}{F(z^{-1})} u(t) + \frac{C(z^{-1})}{D(z^{-1})} e(t) \tag{2.2}$$

$$A(z^{-1}) = 1 + a_1 z^{-1} + \cdots + a_{na} z^{-na}$$
$$B(z^{-1}) = b_1 z^{-1} + \cdots + b_{nb} z^{-nb}$$
$$C(z^{-1}) = 1 + c_1 z^{-1} + \cdots + c_{nc} z^{-nc}$$
$$D(z^{-1}) = 1 + d z^{-1} + \cdots + d_{nd} z^{-nd}$$

The formulation now reduces to finding the optimal parameter

$\theta = [a_1, \ldots, a_{na}, b_1, \ldots, b_{nb}, c_1, \ldots, c_{nc}, d_1, \ldots, d_{nd}, f_1, \ldots, f_{nf}]$ which minimizes the error between the measured and predicted historical data (oil rate). The process (Equation 2.3) and disturbance (Equation 2.4) transfer functions are defined as the rational backward shift operator, respectively as

$$G_p\left(z^{-1}\right) = \frac{B\left(z^{-1}\right)}{A\left(z^{-1}\right)F\left(z^{-1}\right)} \tag{2.3}$$

$$G_l\left(z^{-1}\right) = \frac{C\left(z^{-1}\right)}{A\left(z^{-1}\right)D\left(z^{-1}\right)} \tag{2.4}$$

Three PEM-based model structures were tested to identify the model with the best fit for oil and water rate. Huang and Kadali (2008) defined the structures mathematically as

Autoregressive with Exogenous Input Model (ARX)

$$y\left(t\right) = \frac{B\left(z^{-1}\right)}{A\left(z^{-1}\right)}u\left(t\right) + \frac{1}{A\left(z^{-1}\right)}e\left(t\right) \tag{2.5}$$

Box-Jenkins Model (BJ)

$$y\left(t\right) = \frac{B\left(z^{-1}\right)}{F\left(z^{-1}\right)}u\left(t\right) + \frac{C\left(z^{-1}\right)}{D\left(z^{-1}\right)}e\left(t\right) \tag{2.6}$$

Output Error Model (OE)

$$y\left(t\right) = \frac{B\left(z^{-1}\right)}{F\left(z^{-1}\right)}u\left(t\right) + e\left(t\right) \tag{2.7}$$

After completing system identification using 350 different models and validation tests were conducted to identify the best representative model. The model fit (Equation 2.8) is estimated by (Ljung, 1999)

$$Model\ fit\left(\%\right) = \left(1 - \frac{|y - \hat{y}|}{|y - \overline{y}|}\right) \times 100 \tag{2.8}$$

where $y, \hat{y}$ and $\overline{y}$ are measured, predicted, and mean of measured outputs respectively.

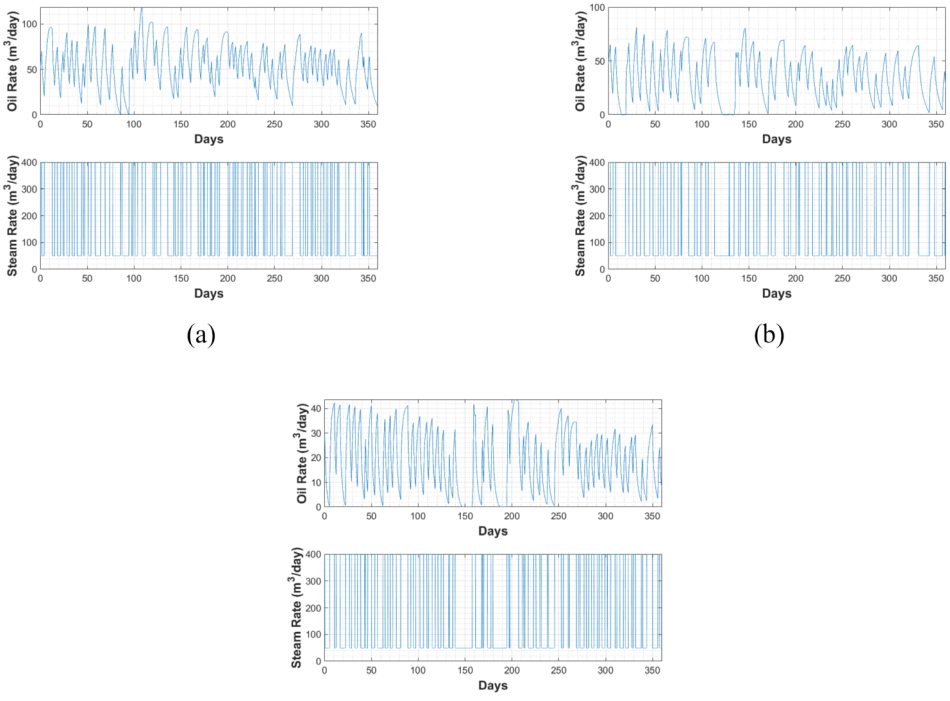

Figure 2.1: Historical production and injection rates for (a) Well-pair 1 (b) Well-pair 2 (c) Well-pair 3 in a synthetic SAGD model

2.3 Real-Time Non-linear Optimization

The overall idea is to investigate the future and decide the best course of action to be taken. As shown in Fig 2.2 and the detailed description in the Algorithm, the acquired real-time data from the heavy oil reservoir is used to build a data analytic predictive model based on system identification. The model is used for a short-term forecast of KPI (NPV in our case). As explained in the previous section, a predictive data-driven model is generated after recursively training and validation until the acceptance criteria are met. In this study, the minimum validation error of 40% is an acceptance criterion. The model that passes the validation test is then used to determine steam allocation rate for each well-pair which maximizes NPV. Typically, when an action is taken, a response from the system is measured for a specified period. In this work, the forecast period or prediction horizon (P) is seven days long. It means that

a constant steam injection rate is set for every seven days, and the heavy oil production rate is measured for the same period.

To determine the optimal steam to be allocated, non-linear constrained optimization is performed using the data-driven model. The objective here is to use the predictive model to take an action which optimizes NPV for the specified prediction horizon. An approximate NPV formulation was used as an objective function for optimization. Equation 2.9 shows the NPV objective maximized for each prediction horizon. The NPV is calculated for each well (j) at each time (t) by summing up the difference between the revenue (the price of oil [p_o] x oil production rate [$\hat{y}_j\,(t)$]) and production cost (steam processing cost [p_w] x steam injection [$u_j\,(t)$]) over the prediction horizon. The present value calculated over the prediction horizon is discounted and then summed over all wells (N_w) in the model. Various assumptions are made to approximate NPV. The water produced is recycled, and hence Equation 2.9 factors in the produced water as part of the steam processing cost. Also, an initial investment cost term in the NPV formulation is absent. The optimization starts after $200 days$ of the beginning of the production phase and the facilities are installed already. The oil price, steam processing cost and the discount factor (D) are considered as $60\$/bbl$, $12\$/bbl$ and 10% respectively. NPV optimization is constrained by minimum (u_j^{min}) and maximum (u_j^{max}) steam injection rate (Equation 2.10). Instabilities in the SAGD operations as a result of changes in steam injection are controlled by restricting the rate changes between subsequent prediction horizon to a minimum (Δu_j^{min}) and maximum (u_j^{max}) steam injection rate (Equation 2.11). In this case study, the value is set to 20 m^3. This value is chosen arbitrarily, and an appropriate range based on operating experience should be used in a field application. The maximum rate change can be set as a percentage of the previous allocation rate.

After performing non-linear optimization with the predictive model, the optimally allocated steam is assigned to the heavy oil reservoir. The response from the reservoir is recorded using a data acquisition system. The predictive model is then updated with the newly recorded response from the reservoir to improve its prediction performance. The workflow breaks out of the recursive

loop when it is not profitable to continue production using SAGD.

$$\sum_{j=1}^{N_w}\sum_{t=1}^{P}\frac{\left(p_o\hat{y}_j\left(t\right)-p_w u_j\left(t\right)\right)}{\left(1+D\right)^{\Delta t}} \tag{2.9}$$

$$\text{s.t.} u_j^{min} \leq u_j \leq u_j^{max} \tag{2.10}$$

$$\Delta u_j^{min} \leq \Delta u_j \leq \Delta u_j^{max} \tag{2.11}$$

$$\sum_{j=1}^{N_w} u_j\left(t\right) = \overline{U} \tag{2.12}$$

$$\sum_{j=1}^{N_w} u_j\left(t\right) \leq \overline{U} \tag{2.13}$$

$$0.8\overline{U} \leq \sum_{j=1}^{N_w} u_j\left(t\right) \leq \overline{U} \tag{2.14}$$

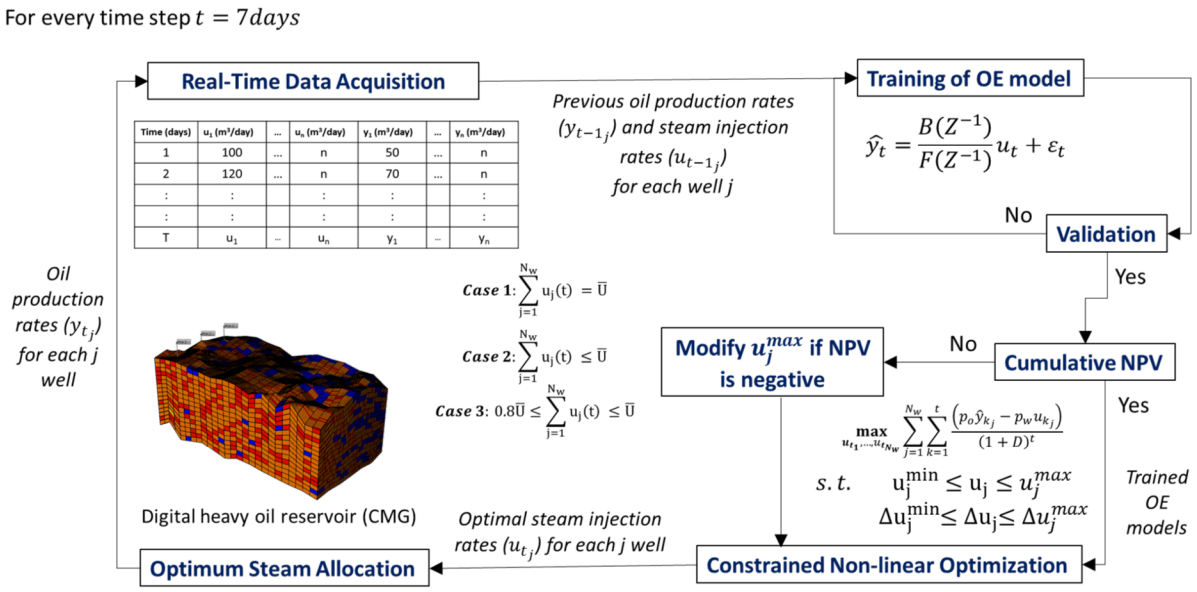

Figure 2.2: Real-Time steam allocation workflow for digital heavy oil reservoirs

Algorithm: Steam Allocation Optimization

For every time step $\boldsymbol{t = 7\ days}$

1. Set scenario
   - Zero (no steam prioritization)
   - One (steam prioritization)
2. Set global constraint
   - Zero (utilize all available steam)
   - One (utilize a fraction or all available steam)
   - Two (random steam generator capacity)
3. Read the previous oil production and steam injection rates
4. Identify the structure and parameters of the OE model Equation 2.7
5. If the model passes the validation test continue, else change the model order (step 2)
6. Set $\boldsymbol{u_j^{min}}$ and $\boldsymbol{u_j^{max}}$
7. Find steam injection rates that will maximize NPV for the prediction horizon 2.9
   - If the global constraint equals zero Equation 2.12
   - Else If the global constraint equals one Equation 2.13
   - Else If the global constraint equals two Equation 2.14
   - End If $\boldsymbol{\Delta u_j^{min} \leq \Delta u_j \leq \Delta u_j^{max}}$ $\boldsymbol{u_j^{min} \leq u_j \leq u_j^{max}}$
8. If scenario equals to zero, skip 8 and go to step 9 else
9. Check NPV of individual wells $\sum_{k=1}^{t} \frac{\left(p_o \widehat{y}_{k_j} - p_w u_{k_j}\right)}{(1+D)^t}$
10. If a well records negative NPV, set new $\boldsymbol{u_j^{max}}$ (increase $\boldsymbol{u_j^{max}}$ for the wells with positive NPV and decrease for the well or wells with negative NPV) else repeat 8
11. Apply optimal steam injection rates to the digital heavy oil reservoir
12. Obtain new oil production rates
13. $\boldsymbol{t = t + 1}$
14. Repeat steps 2-10 until operating period ends

2.3.1 Base case

The base was designed to have a constant steam injection rate in each well-pair (well-pair 1 = 150 m^3/day, well-pair 2 = 150 m^3/day, well-pair 3 = 100 m^3/day) which sums up to total steam generation capacity ($\overline{U}$) of 400 m^3/day. This generation capacity was selected to ensure positive NPV for the base case. The producers were constrained by a minimum bottom hole flowing pressure of 600 kpa as a primary constraint and a maximum liquid rate of 900 m^3/day as a secondary constraint. Also, each producer was constrained by the steam production rate of 1 m^3/day to mimic steam trap control.

2.3.2 Case 1: Utilization of full steam generation capacity

In this case, the total steam supply for all the well pairs in the pad is constant for the optimization period. The total steam generation capacity is considered same as the base case. An additional constraint (Equation 2.12) is added to Equations 2.9 and 2.11 to model this operating strategy. The optimizer determines the optimal steam allocation for each well-pair in the pad. Case 1 assumes that it is economically and environmentally safe to inject all available steam. Moreover, this formulation is effective at ramp-up and plateau stage of SAGD. The lower steam allocation bound is set to 0 m^3/day i.e. no steam injection). The upper steam allocation bound is set at 170 m^3/day for well-pair 1 and 2 and 120 m^3/day for well-pair 3.

2.3.3 Case 2: Underutilization of steam generation capacity

In this case, the total steam injected into all the well pairs in the pad can be equal or less than the available steam. Equation 2.12 in Case 1 is replaced with Equation 2.13 to reformulate the optimization problem for Case 2. This case models a situation in the field when it is not economically or environmentally safe to inject all available steam. Technical issues in the well pad such as failure of downhole equipment is one such scenario. Besides, when SAGD projects

mature or reach decline stage, steam injection is reduced gradually to avoid overheating (blowdown phase).

2.3.4 Case 3: Random utilization of steam between 80% and full steam generation capacity

The total steam supply to wells in the pad at each control interval randomly changes between 80% to 2.9 of the maximum steam generator capacity in Case 3. Equation 2.14 is used to model the variable steam supply constraint. Case 3 models an unstable steam generator or irregular water supply to a steam generator. The lower bound for steam generating capacity is 2.9 of its maximum operating capacity.

2.3.5 Steam Prioritization

The optimization problem was formulated to let an algorithm maximizes pad NPV. The optimization algorithm tends to ignore well-pairs with low KPI if the cumulative well-pair NPV is positive. The optimization problem formulation does not change; however, the search range of decision variables is adjusted based on KPI to mimic steam prioritization. After optimizing for each prediction horizon, the individual well NPV is checked. If it is negative, the optimization for the prediction horizon is repeated with upper bound of steam allocation reduced to 10 m^3/day for that particular well-pair and increased to 200 m^3/day for well-pairs that recorded positive NPV. The upper steam allocation bound is set based on the maturity of the steam chamber, well productivity, heterogeneity around the well, etc., from expert opinion. For RTO, this upper bound is dynamic. Defining simultaneous optimization with multiple upper steam allocation bounds in RTO is computationally expensive. For this study, a check is performed at each prediction horizon if it is required to adjust the upper steam allocation bound to re-run the optimization. In field operations, steam is allocated to the whole pad at each control horizon. The operator prorates the steam among the wells-pairs based on their injection capacity. Excess steam from low KPI well-pairs (i.e. high Cumulative Steam-Oil ratio (cSOR), negative NPV) is re-allocated to high performing (low cSOR,

positive NPV) well-pairs/pads. Since data-driven predictive reservoir models cannot allocate excess steam from low to high performing wells or pads, steam prioritization is used in this workflow to model such behaviour. Also, in the field, it is natural to allocate less steam to low performing well-pairs. The steam prioritization option in this workflow may also be used to detect well-pairs that require workover operations. In the event workover operations are planned, it allows predicting the optimal allocation of steam for operating the other well-pairs. For conventional oil reservoirs, wells can be shut and open at any time during exploitation. Heavy oil wells will require pre-heating to mobilize oil around the well before production can be initiated. Events such as low oil prices, high water cut, and steam production in thermal oil recovery may require wells to be shut and opened when conditions are favourable. Instead of shutting the injection wells, the proposed steam prioritization workflow allows the setting of the steam injection rate at a constant value. The injection well is heated to keep the oil around it mobile. The opened production well is expected to produce mobile oil from neighbouring well-pairs. The proposed steam prioritization can model mature SAGD recovery techniques such as wedge well technique (Delamaide, 2018). However, the only difference here is that the injection well is not shut.

2.4 Results and Discussion

In this section, training and validation results of the models and three different case studies are presented. All predictions are for seven days prediction horizon and the workflow is implemented for 535 days in total. Note that the final NPV reported as KPI for the performance of the workflow is calculated using the field response (first principle reservoir model in this work). In addition to NPV, other KPIs such as cSOR and oil production rate are also presented.

2.4.1 SAGD Model Training and Validation

After testing different model structures, the OE model structure was observed to model the SAGD process with best accuracy. An OE model after train-

ing and validation is shown for well-pairs 1, 2, and 3 in Equations 2.15, 2.16, and 2.17 respectively. These models are designed for a specific reservoir and updated to reflect the dynamic state of the reservoir as new data from the reservoir are recorded. The challenge with the first principle models is that the data acquisition and model updating is computationally and financially expensive. The developed predictive models are resourceful in optimizing production operations. Accurate predictive models can practically be used in lieu of first principle models for weekly, monthly, and quarterly planning and production optimization to meet annual goals.

$$y(t) = \left[\frac{0.0434\ z^{-1} - \ 0.07476\ z^{-2} + \ 0.03134\ z^{-3}}{1\ -\ 2.129\ z^{-1} + \ 1.239\ z^{-2} - \ 0.04967\ z^{-3} - \ 0.06029\ z^{-4}}\right] u(t) + \varepsilon(t) \tag{2.15}$$

$$y(t) = \left[\frac{0.03467\ z^{-1} - \ 0.08471\ z^{-2} + \ 0.06699\ z^{-3} - \ 0.01696\ z^{-4}}{1\ -\ 2.871\ z^{-1} + \ 2.815\ z^{-2} - \ 1.01\ z^{-3} + \ 0.06622\ z^{-4}}\right] u(t) + \varepsilon(t) \tag{2.16}$$

$$y(t) = \left[\frac{0.02918\ z^{-1} - \ 0.04268\ z^{-2} + \ 0.008716\ z^{-3} + \ 0.004852\ z^{-4}}{1\ -\ 1.904\ z^{-1} + \ 0.9046\ z^{-2}}\right] u(t) + \varepsilon(t) \tag{2.17}$$

Fig 2.3 shows the result of system identification after training and cross-validation for the three well pairs. The red line is the measured data, and the blue is the prediction from the system identification model during the training phase. A green dashed line which represents the model fit on the validation dataset showed a satisfactory trend when compared to the measured data. Table 2.1 shows the orders of the polynomials and model fit of all three models. The OE models of the three well-pairs were validated for 35 days future prediction horizon. In this work, the prediction horizon for real-time optimization is seven days long. Hence, these models can be used with minimum uncertainty in their predictions.

Table 2.1: System Identification Models for All Well Pairs

Well-Pair	Orders	Fit (%)	
		Training	Validation
1	[3 4]	76.98	75.36
2	[4 4]	80.43	78.49
3	[4 2]	78.37	62

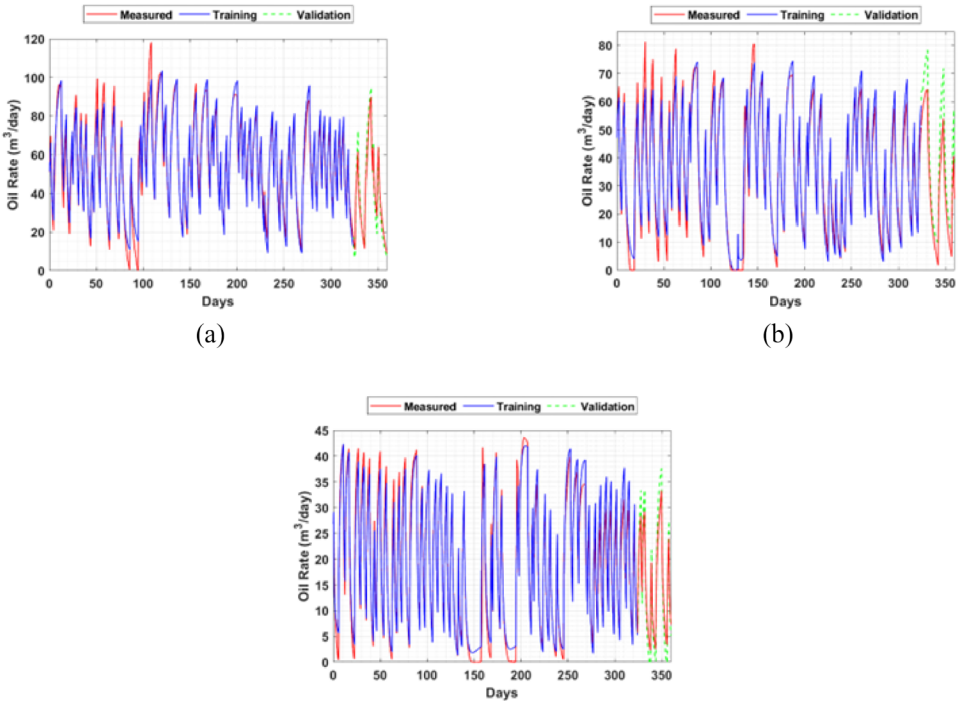

Figure 2.3: fig:Validation of the OE model for (a) Well-pair-1 (b) Well-pair-2 (c) Well-pair-3

2.4.2 Case 1: Utilization of Full Steam Generation Capacity

In this case, the total steam supply to the entire pad is fixed throughout the period for SAGD optimization. Fig 2.4 (a – d) in the appendix shows the evolution of steam allocation for no steam prioritization and steam prioritization scenarios. The approach of no steam prioritization is similar to the one used by commercial software like CMOST (CMG, 2018) for optimization.

The formulation of the optimization problem, as presented by most researchers and commercial software, is based on the cumulative pad NPV and not the individual well-pair (Shahandeh et al., 2016). It avoids complications of using multi-objective optimization. For example, a well pad consists of six well-pairs with one of them performing good can lead to positive pad NPV. If the optimization algorithm gets stuck in a local optimum, it returns this feasible sub-optimal solution. As seen from Fig 2.4 (a-b), the steam prioritization scenario (pink dashed line) resulted in high steam allocation to well-pair 1 and 2 as compared to the no prioritization (continuous blue line). The extra allocated steam came from well-pair 3 (Fig 2.4 (c)). Also, Fig 2.4 (a-c) shows that maximum injection rate change constraint (maximum allowable change is $\pm 20\ m^3$ between the prediction horizons) was honoured between subsequent prediction horizons (Equation 2.11). It ensures the stability of the well operations and wellbeing of the downhole equipments. Unstable operation can lead to an inefficient steam chamber growth and the poor displacement of bitumen towards production wells. Honouring this constraint in SAGD optimization formulation is a critical technical parameter that results in high KPI. Constant steam allocation to the pad (Equation 2.12) was also honoured in Fig 2.4 (d). Fig 2.4 (a-c) demonstrates the effectiveness of the steam prioritization scenario over no steam prioritization in allocating steam to high KPI well-pairs.

As a result of optimal steam allocation to well-pairs, an increase in well-pair as well as pad oil production rates for both no steam prioritization and prioritization can be observed when compared with the base case. Fig 2.5 (a-b) indicates steady increase in oil production rates of well-pair 1 and 2 from 40 m^3/day to 75 m^3/day and 47 m^3/day respectively for steam prioritization scenario. Steam prioritization ultimately resulted in a higher pad oil production rate than no steam prioritization scenario (see Fig 2.5 (d)). The economics of SAGD operations depends on maintaining low cSOR. From Fig 2.6 (a-d), it can be said that steam prioritization scenarios resulted in lower cSOR as compared to no steam prioritization. Typically, higher cSOR (Fig 2.6 (a-b)) results in lower NPV, but the steam prioritization scenario still had a higher NPV than no steam prioritization scenario. The case with no steam

prioritization and the base case yielded a low cSOR but at the cost of lower oil production rate. Hence, the overall oil volume recovered was lower. The NPV for well-pair 1 (Fig 2.7 (a)) showed 2.11 and 24.71% increase for steam prioritization and no steam prioritization case, respectively, compared to the base case. It can be inferred that the steam prioritization helped to attain an optimal cSOR that balances between a low cSOR requirement for SAGD operations and an optimal bitumen production rate that maximizes NPV. It also implies that low cSOR may not always lead to higher economic benefits if the oil production rate is sacrificed to attain it. This observation has been reported in the literature (Guo et al., 2018). The authors observed a 16% reduction in cSOR, but oil recovery also dropped by 20%. Fig 2.7 (a, c, d) further demonstrates the better performance of steam prioritization over no steam prioritization.

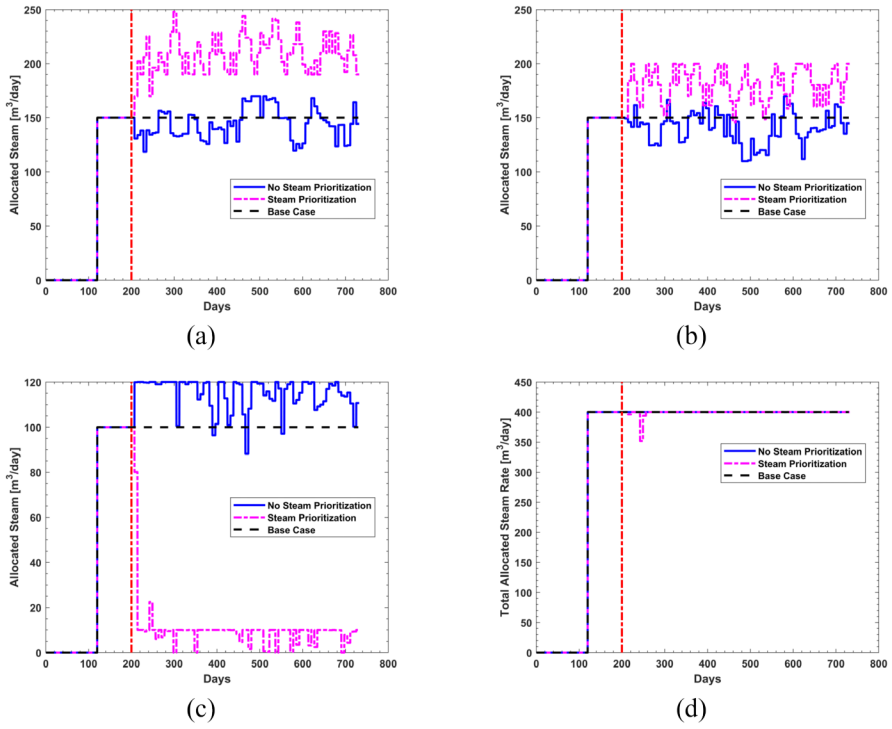

Figure 2.4: Case-1 Steam rate performance evolution (a) Well-pair-1 (b) Well-pair-2 (c) Well-pair-3 (d) Well-pad

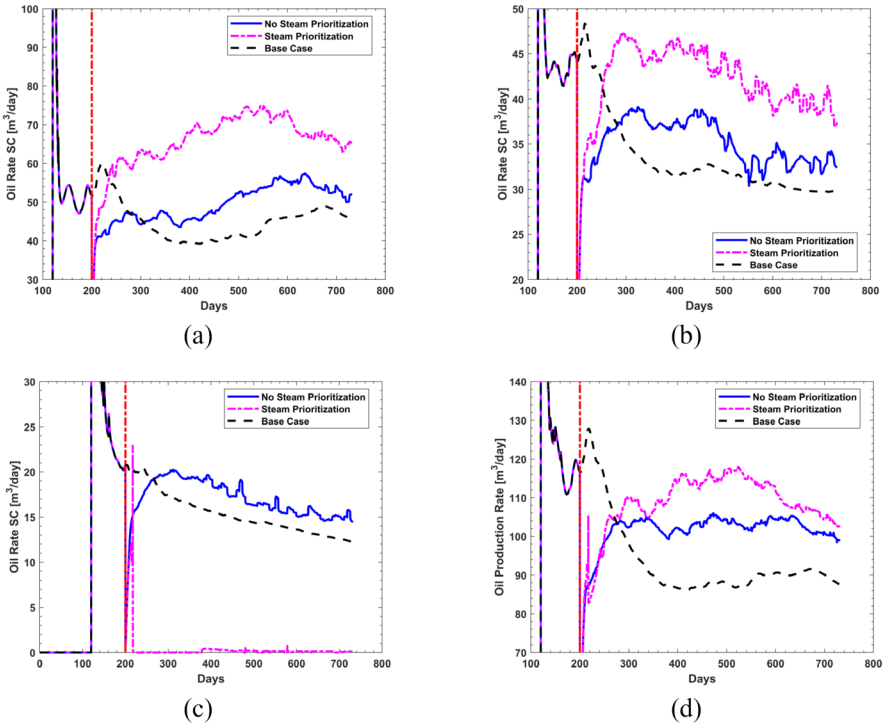

Figure 2.5: Case-1 Oil rate performance evolution (a) Well-pair-1 (b) Well-pair-2 (c) Well-pair-3 (d) Well-pad

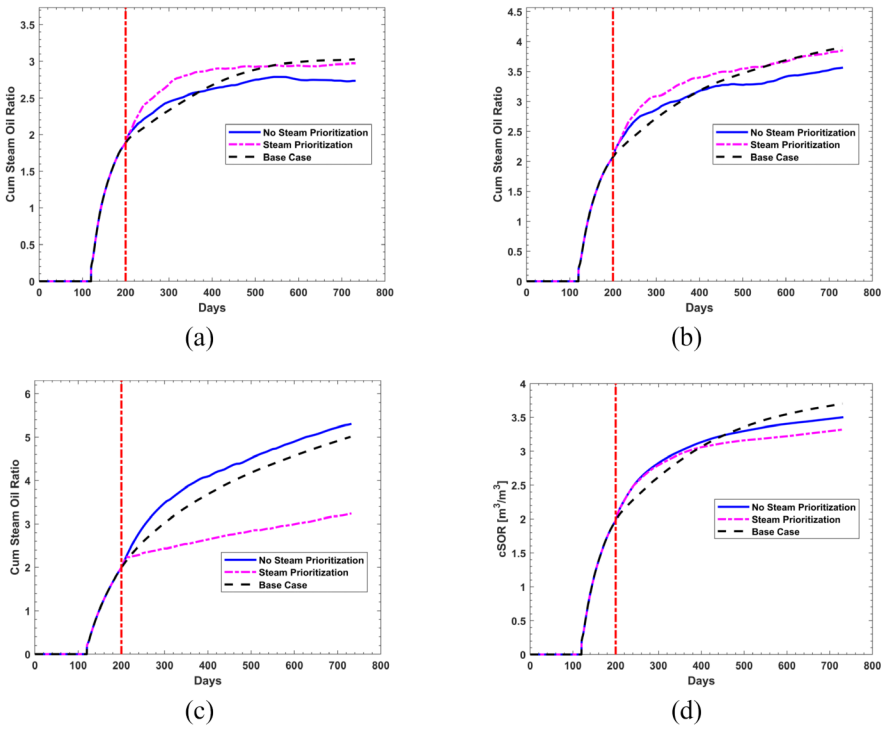

Figure 2.6: Case-1 cSOR performance evolution (a) Well-pair-1 (b) Well-pair-2 (c) Well-pair-3 (d) Well-pad

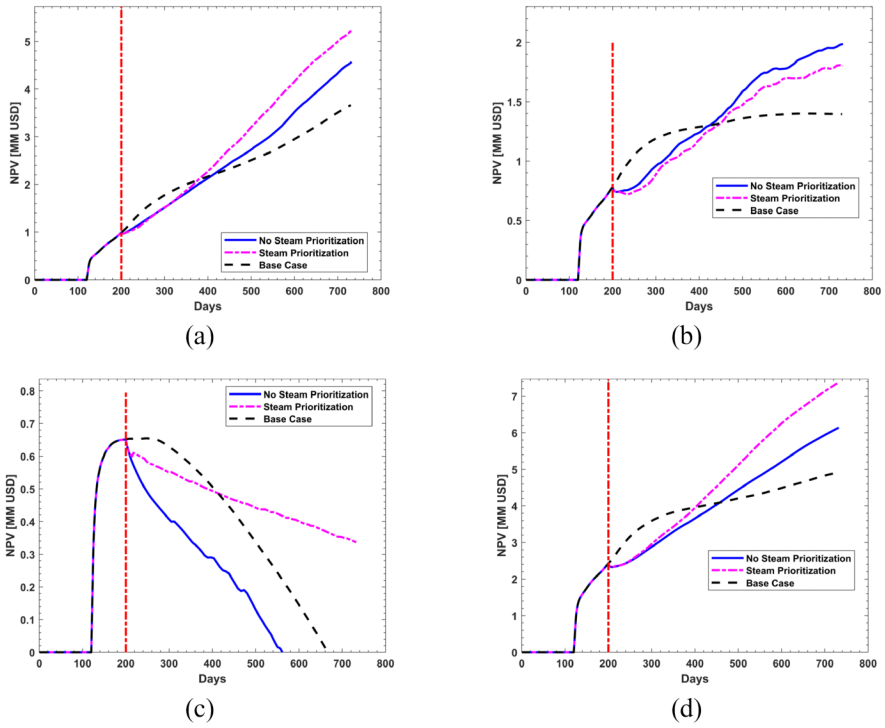

Figure 2.7: Case-1 NPV performance evolution (a) Well-pair-1 (b) Well-pair-2 (c) Well-pair-3 (d) Well-pad

2.4.3 Case 2: Utilization of Full or Less Steam Generation Capacity

Case 2 was designed to find the optimal amount of total steam to be injected at each prediction horizon. The full steam to be generated or injected is not an explicit decision variable. In case of steam prioritization (Fig 2.8 (c)), steam is injected at a small and almost constant allocation to well-pair 3. The expectation for the optimization algorithm was to allocate high amount of steam to high-quality reservoir areas. While defining the optimization problem, bounds for the decision variable of the wells were set based on the quality of permeability around the wells. As shown in Fig 2.8 (c), if the optimization algorithm finds a feasible solution based on the constraints, it terminates the run given that no improvement in NPV is observed. Fig 2.9 (a-d) shows the evolution of the oil rate for well-pairs and pad. For well-pair 2 (Fig 52.9 (b)), there was an average increment of about 10 m^3/day and 15 m^3/day for no steam prioritization and steam prioritization scenarios, respectively.

In case of cSOR, Fig 2.10 (a – d) shows that steam prioritization eventually results in better pad performance. The NPV Fig 2.11 (b) shows better performance of no steam prioritization compared to steam prioritization for well-pair 2. It could be due to the higher than required steam allocation from excess steam available which did not result into higher oil production due to moderate reservoir quality around that well-pair. However, NPV of the pad (Fig 2.11 (d)) demonstrates a better pad performance for steam prioritization case over no steam prioritization.

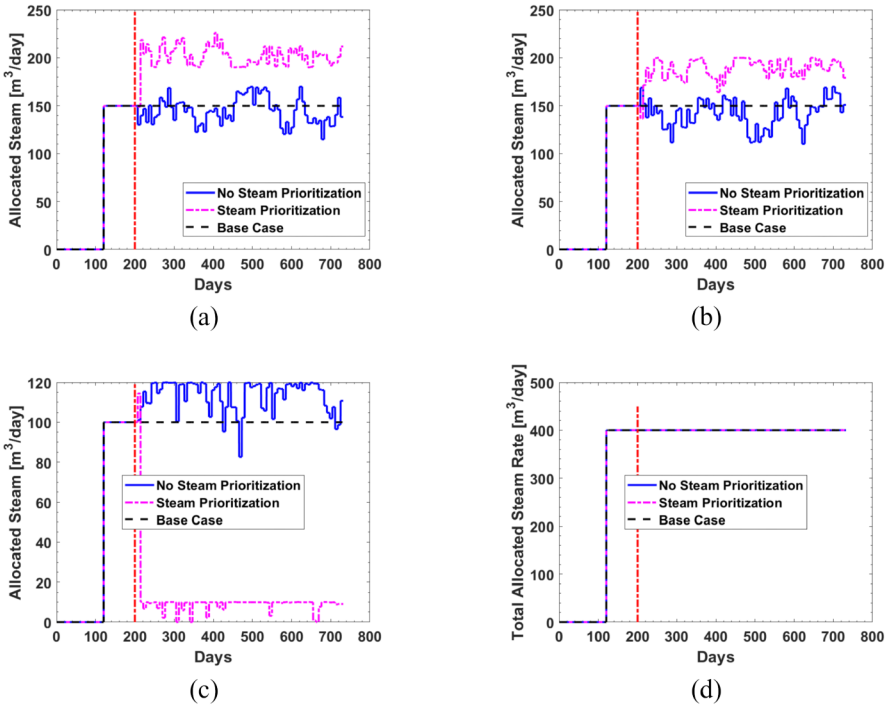

Figure 2.8: Case-2 Steam rate performance evolution (a) Well-pair-1 (b) Well-pair-2 (c) Well-pair-3 (d) Well-pad

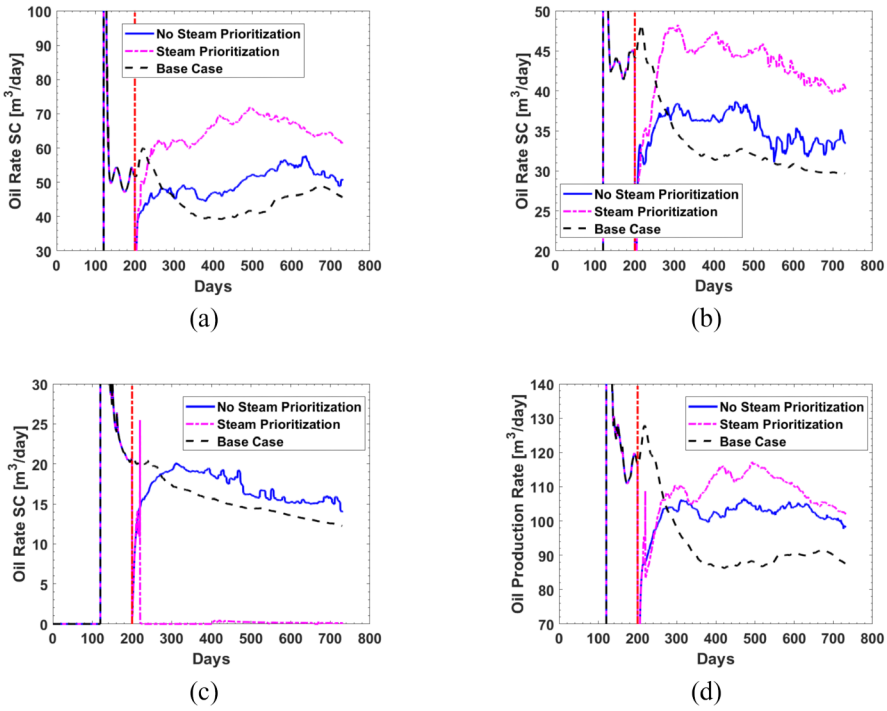

Figure 2.9: Case-2 Oil rate performance evolution (a) Well-pair-1 (b) Well-pair-2 (c) Well-pair-3 (d) Well-pad

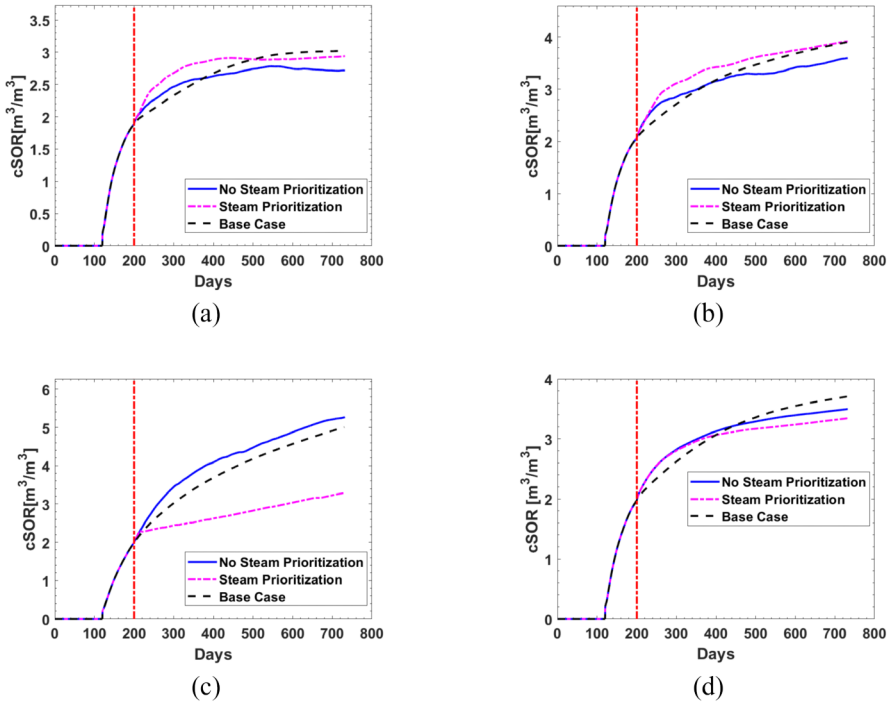

Figure 2.10: Case-2 cSOR performance evolution (a) Well-pair-1 (b) Well-pair-2 (c) Well-pair-3 (d) Well-pad

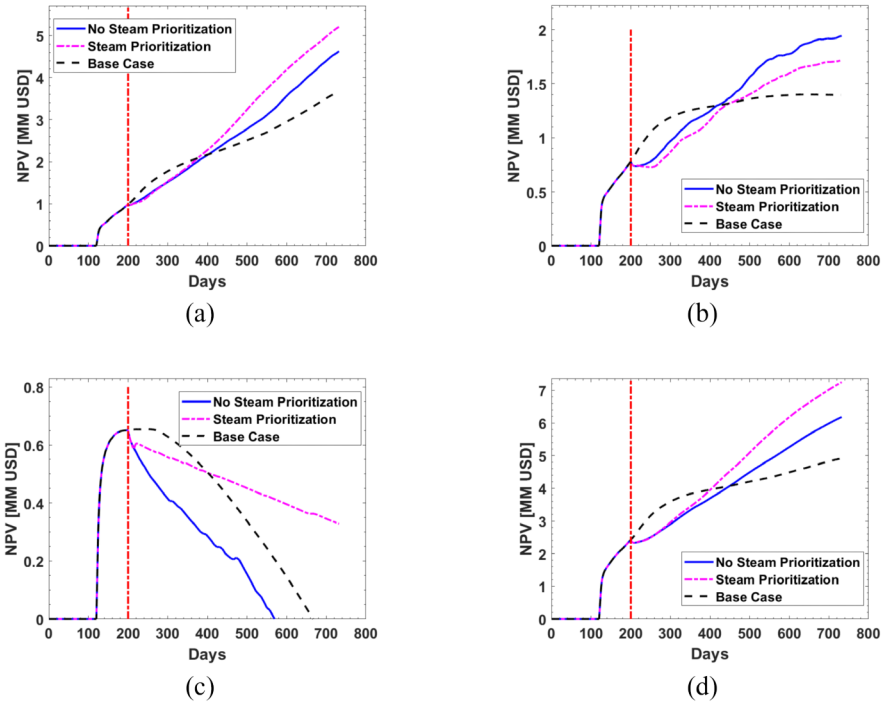

Figure 2.11: Case-2 NPV performance evolution (a) Well-pair-1 (b) Well-pair-2 (c) Well-pair-3 (d) Well-pad

2.4.4 Case 3: Random Utilization of Between 80% and Full Steam Generation Capacity

In this case, the optimization problem was formulated to model variability in maximum available steam. Technical issues with the boiler, water source and pumps can result in changing steam availability. Case 3 is modelled to simulate the variable nature of steam generation process. The available steam ranges between 80 to 100% of maximum steam generator capacity. Steam injection rate for the entire pad is below 400 m^3/day unlike other cases (Fig 2.12(d)). Fig 62.13 (a–d) shows the evolution of the oil rate after optimization. The pad oil production rate (Fig 2.13 (d)) displays no significant difference between no steam prioritization and steam prioritization cases. The changing steam availability might be the reason for such close results.

The pad cSOR (Fig 2.14 (d)) is the lowest for steam prioritization because of the significant drop in cSOR of well-pair 3 which had minimal steam allo-

cated. The NPV for pad (Fig 2.15 [d]) increased by approximately 31% and 46% for no steam prioritization and steam prioritization scenarios, respectively compared to the base case. Case 3 also demonstrates an improved performance of steam prioritization over no steam prioritization through all the KPIs.

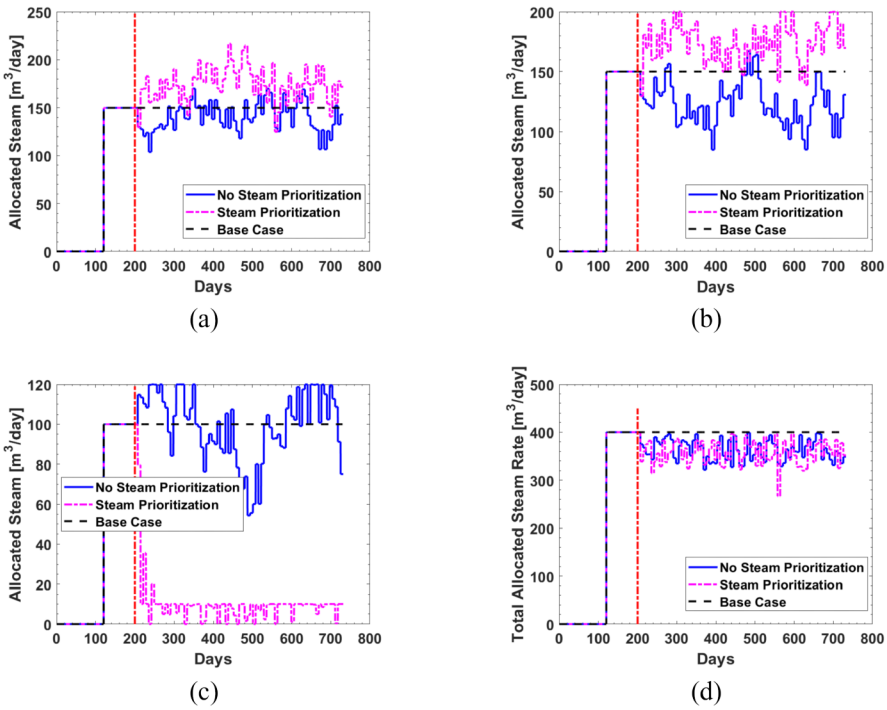

Figure 2.12: Case-3 Steam rate performance evolution (a) Well-pair-1 (b) Well-pair-2 (c) Well-pair-3 (d) Well-pad

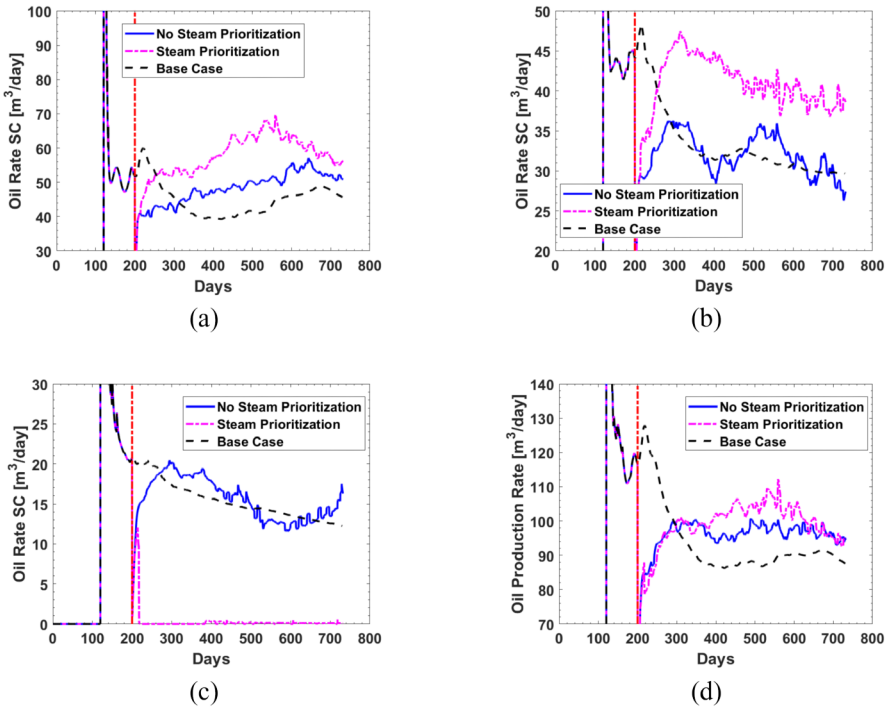

Figure 2.13: Case-3 Oil rate performance evolution (a) Well-pair-1 (b) Well-pair-2 (c) Well-pair-3 (d) Well-pad

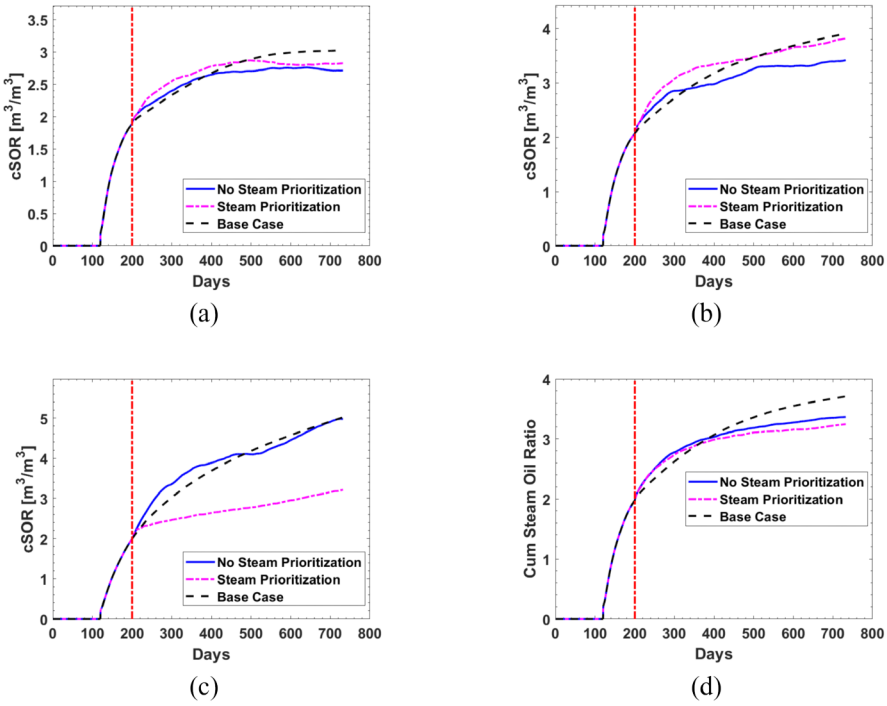

Figure 2.14: Case-3 cSOR performance evolution (a) Well-pair-1 (b) Well-pair-2 (c) Well-pair-3 (d) Well-pad

Table 2.2: Change in NPV for Cases 1, 2, and 3 compared to the base case

Cases	Change in NPV (%)					
	Well-pair 1		Well-pair 2		Pad	
	No steam prioritization	Steam prioritization	No steam prioritization	Steam prioritization	No steam prioritization	Steam prioritization
1	24.71	42.85	42.04	29.24	25.03	50.12
2	26.24	42.04	38.83	22.91	25.89	47.67
3	23.59	36.78	46.69	30.18	31.4	46.11

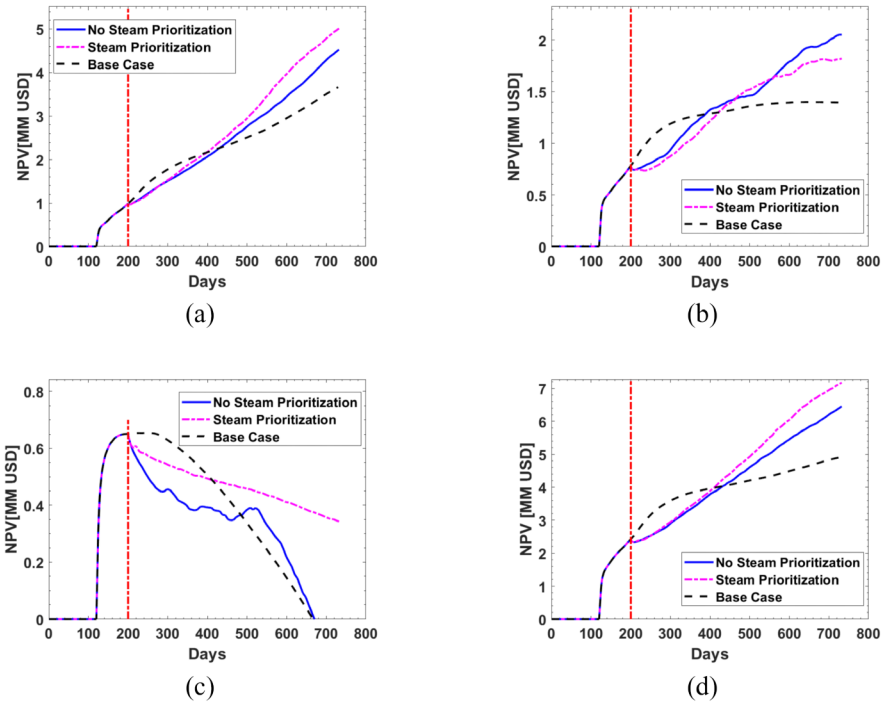

Figure 2.15: Case-3 NPV performance evolution (a) Well-pair-1 (b) Well-pair-2 (c) Well-pair-3 (d) Well-pad

Table 2.2 summarizes the performances of all cases in terms of change in NPV relative to the base case. In all cases, steam prioritization outperforms its counterpart if pad NPV is considered. The proposed workflow optimizes NPV, however, it can be updated to account for other engineering and environmental performance indicators of the heavy oil production process. The workflow is currently designed to work for a single pad and assumes other scheduled activities such as drilling of new wells/pads does not affect the current operations.

2.5 Conclusions

A workflow for real-time steam allocation under uncertainty for SAGD multilateral well pad operations is developed and presented in this study. The workflow comprises of model that continuously updates in real-time for the short-term prediction horizon which is then used in the nonlinear optimization to determine the best steam injection sequence for well-pairs. This workflow was assessed using a field scale model from which following conclusions can be drawn:

1. After assessing the workflow on different case studies, field NPV increased between 22% to 50% and field cSOR decreased between 5% to 15% for the steam prioritization scenario when compared to the base case.

2. Considering all KPIs, it can be said that the ultimate pad performance of steam prioritization outperforms no steam prioritization scenarios.

3. The computational time for real-time steam allocation reduces significantly with the replacement of first principle models with data analytic models.

4. Another advantage of this proposed workflow is the real-time update of the reservoir predictive model for quick short-term decision-making process. Unlike the first principle models which are computationally intensive, the proposed workflow can be easily integrated with the daily decision-making process in field operations.

The proposed workflow demonstrates significant potential in daily, weekly, or short-term operational decision-making for heavy oil production. Proposed data analytic predictive model that uses only steam injection and heavy oil production rates could be improved to integrate more data attributes that are recorded daily in the field. The workflow also can be expanded to incorporate activities such as new well-pair or pad scheduling, uncertainty in steam supply, and oil price.

Chapter 3

Risk Management and Optimization in Real-Time Non-condensable Gas Co-Injection Under Economic Uncertainty[1]

3.1 Introduction

Despite the successful implementation of SAGD in western Canadian oil reservoirs, significant potential research goals remain for improving bitumen recovery, lowering steam injection cost, and improving energy efficiency to reduce carbon footprint. Non-condensable gas (NCG) injection has been shown in experimental (Butler, 1999; Mendoza and Kantzas, 2020), numerical simulation (Austin-Adigio and Gates, 2019; Mendoza and Kantzas, 2020), and field application (MEG, 2017) to alleviate the SAGD drawback of high-water demand and its associated negative environmental repercussions. NCG injection improves the SAGD process by lowering heat losses to the overburden (Butler, 1999), lowering steam-oil-ratio (MEG, 2017), thereby reducing water and fuel requirements and greenhouse gas emissions. In addition to lowering greenhouse gas emissions, sequestration of NCG such as CO_2 or methane positively impacts the environment. Therefore, one of the vital considerations in the design of NCG co-injection is the stage of SAGD maturity to start co-injection.

[1] A version has been published in SPE Reservoir Evaluation & Engineering

Mendoza and Kantzas (2020) simulation study showed NCG co-injection is beneficial after three-quarters of the reservoir is swept. A simulation study of MEG Energy Christina Lake reservoir by Austin-Adigio and Gates Austin-Adigio and Gates (2019) beginning NCG co-injection at mid to late stages of SAGD. From the study, an increase in oil rates was observed in the first two years of NCG co-injection, which displaced already mobilized oil by SAGD but decreased as the NCG gas accumulates. Therefore, the mole fraction of NCG co-injection is another critical design parameter considered during the optimization of the scheme. Petro-Canada's phase B of the Dover field simulation study showed 0.8 mole % as the optimum (Yee and Stroich, 2004). Hangistone Demonstration project by JACOS targeted 1 mole % of NCG, resulting in a 15% reduction in steam requirements and an average instantaneous steam-oil-ratio (ISOR) of 3.7 m^3/m^3 (Doan et al., 2014). In the Devon Jackfish SAGD project, NCG injection targeted 1 - 4 mole % , which successfully maintained steam chamber pressure and reduced ISOR without negatively impacting oil recovery (Devon, 2017). Detpunyawat (2017) performed an optimization study of NCG co-injection with injection pressure design parameters, the injection fluid volume fraction of solvent, methane, and steam. The optimized case returned the injection pressure of 1682 kPa and the injection volume fraction of 0, 0.59, and 0.41 for solvent, methane, and steam. An optimal mole fraction of 1 mole % was observed in the simulation study of NCG. (Mendoza and Kantzas, 2020). The proposed real-time workflow optimizes NCG co-injection total injection phase rate and mole fraction in a synthetic matured SAGD reservoir under oil price uncertainty.

Additionally, advancements in intelligent field technology enable real-time SAGD process decision-making optimization. Closed loop reservoir management (CLRM) is a concept that leverages advances in smart field technology to improve real-time decision-making by perturbing control setpoints (i.e., injection rates, bottom hole pressure) to maximize the recovery process KPIs (Jansen et al., 2005; Wang et al., 2009). The optimal control setpoints for each prediction horizon are determined using a dynamic predictive model of the recovery process, the inputs perturbed by a constrained nonlinear opti-

mizer. The CLRM concepts have been an effective tool in the development of SAGD reservoirs over the years. Subcooling of SAGD well-pairs is a critical control parameter of SAGD development for steam conformance. CLRM has been shown in the literature to be an effective tool for managing subcool control in SAGD real-time optimization (RTO).(Mohajer et al., 2010; Patel et al., 2014, 2019; Patel and Trivedi, 2020). Purkayastha et al. (2018) demonstrated that when compared to the SAGD RTO's multi-input single-output control structure (MISO), a multi-input multi-output (MIMO) control structure for steam trap control and oil rate control significantly improves both oil production rate and cumulative steam-oil ratio (cSOR). A MIMO control structure for NCG co-injection will be adopted in this work. Sibaweihi et al. (2019) also presented RTO workflow for SAGD steam prioritization with varying steam generation. One of the critical advantages of RTO is the reduction of computational cost and higher chances of optimal objective function results. The computational cost reduction is achieved due to the decomposition of life-cycle optimization into small-scale control horizon (predictive horizon) optimization sub-problems. Due to the uncertain nature of the economics of SAGD because of oil price uncertainty, the risk of losing RTO returning sub-optimal objective is high.

Two main approaches have been shown to handle uncertainty. A probabilistic-based method (Hanssen et al., 2015; Vembadi et al., 2018) of handling uncertainty known as stochastic optimization (SO) and a deterministic-based (Capolei et al., 2015; Siraj et al., 2015; Yang et al., 2011) set of scenarios of the uncertain variables known as robust optimization (RO). In this work, the RO approach will be implemented to handle oil price uncertainty. The main aim of economic uncertainty optimization is to mitigate the risk of oil price uncertainty. In real-time RO, a bi-objective approach is employed to minimize risk whiles return is maximized. In the petroleum industry, risk measures include mean-variance (Capolei et al., 2015; Siraj et al., 2015), max-min (Chen et al., 2017; Siraj et al., 2015), semi-variance (Santos et al., 2017; Siraj, 2017), and conditional variance-at-risk (Chen et al., 2017; Siraj et al., 2015) have been reported. The tradeoff factor of risk-return is an essential

selection tool for real-time RO solutions. Typically, a set of tradeoff factors in RO and decision-makers use their judgment to select the best control strategy (Siraj et al., 2015). Chen et al. (2017) suggested a two-stage lexicographic risk mitigation approach. First, maximize the expected NPV and set the maximized expected NPV as a constraint in the second stage of risk minimization. Capolei et al. (2015) suggested using the Sharpe ratio to select the optimal tradeoff factor between risk-return in a CLRM. The market solution is considered the tradeoff factor with maximum Sharpe ratio and the best outcome for the control horizon. Sharpe ratio does not account for non-normally distributed returns. The project's financial performance cannot be compared to a benchmark for investors. The Anderson-Darling test is used to check if the returns are non-normally distributed. For non-normally-distributed returns, a modified Modigliani's risk-adjusted performance is used for optimal tradeoff selection.

Multi-criteria (NPV, recovery factor, water balance, steam chamber conformance) optimization of SAGD operations can be challenging with conflicting objectives. Single objective economic optimization of SAGD projects may not account for negative environmental impact (i.e. greenhouse gas emissions) or meet safe engineering standards (steam chamber pressure above fracture gradient). NPV is the main criterion that has been mainly used for real-time SAGD optimization (Mohajer et al., 2010; Patel et al., 2014; Vembadi et al., 2018). Implementing multi-objective optimization in real-time SAGD operations comes with the challenge of the non-uniqueness of the optimal solutions (non-dominated solutions) to be executed in the current prediction horizon. SAGD RTO with uncertainty is complicated, and the optimization problem complexity grows with multi-criteria optimization. In the literature, multi-criteria decision making (MCDM) optimization problems are formulated as a weighted sum of criteria (Awotunde and Sibaweihi, 2014), goal programming (Maremi et al., 2020), Pareto-front optimization (Farahi et al., 2021; Ma and Leung, 2020) or a single objective with other objectives as constraints. In this work, the optimization problem is formulated as a financial risk mitigation problem. A scenario-based approach that characterizes the NCG co-injection

oil price uncertainty is implemented. In this study the following are proposed to improve on real-time production optimization workflow:

1. Modigliani risk-adjusted (M^2) performance (Modigliani and Leah, 1997) as an optimal trade-off risk-return contrary to Sharpe ratio in Capolei et al. (2015).

2. Anderson-Darling normality test is used to determine the normality of the returns distribution and to adjust M^2 performance of non-normally distributed returns.

3. Normalization of previously recorded data based on the physical or operating range instead of max-min data (Prakash et al., 2020) adds an advantage of automatic outlier detection and elimination of train-test split contamination. In addition, defining well constraints for each control horizon used in MPC (Purkayastha et al., 2018) is eliminated.

4. A compromise online-offline model training based on the concept of forgetting factor compared to the adaptive scheme using residual analysis (Siraj et al., 2017).

5. The decision variables and constraints are normalized to each physical or operating range to give them equal importance, unlike previously reported (Capolei et al., 2015; Patel and Trivedi, 2020)

The paper deals with uncertainty using four different risk measures: (i) Mean-Variance optimization (m-VO): mean of the NPV realizations as return and variance as the risk, (ii) Max-Min Optimization (MMO): risk is defined as the minimum of NPV realizations, (iii) Mean-Semi-Variance Optimization (m-SVO): downside risk or variance of NPV realizations below the mean value and (iv) Mean-Conditional Value-at-Risk (m-cVaR): risk is measured as a weighted tail end of the NPV realizations below the mean value.

3.2 Methodology

In this section, a description of the proposed real-time risk mitigation divisions under uncertainty is presented in detail. Fig 3.1 shows a flowchart of the real-time workflow. The previously recorded input-output history is normalized at each prediction horizon based on the physical feature range and not the max-min recorded. In the initial horizon, the data-driven model is trained based on the forgetting factor for online parameter estimation to identify the input-output lags and their coefficients. Robust optimization is then performed with the identified data-driven model to find the optimal control inputs. The trade-off with the highest market value is implemented as controller setpoints. The response from the reservoir is then recorded for data-driven model updating in the next prediction horizon. In the subsequent steps, the data-driven model with known lags is updated with the new recorded input-output data to update the lag coefficients. If the adapted model passes a pre-defined best-fit-ratio, robust optimization, market-selected controller setpoints and reading of input-output data are repeated in a recursive loop. Finally, training based on the forgetting factor concept is implemented if the updated data-driven model does not pass the pre-defined best-fit ratio to identify a model with new lags and their coefficients adapting to the current state of the reservoir. The workflow improves our previous work on SAGD real-time optimization (Sibaweihi et al., 2019) to account for economic uncertainty and data-driven model training and validation. Modigliani's risk adjustment factor is used to select the optimal risk-return tradeoff as opposed Sharpe ratio used in the work of Capolei et al. (2015). A detailed description of the proposed real-time workflow is presented in the following subsections.

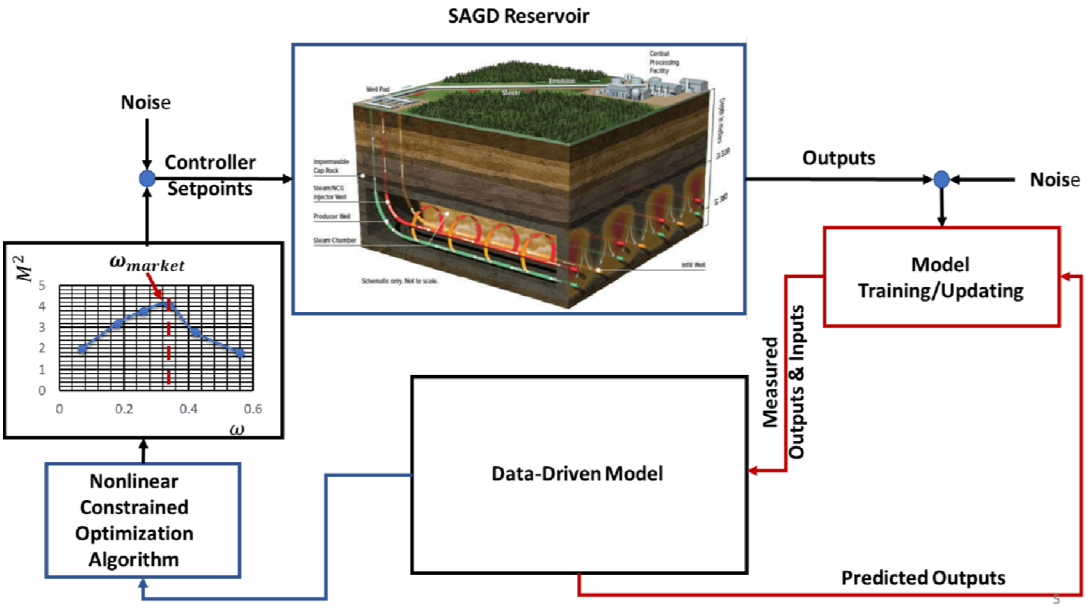

Figure 3.1: Real-Time risk mitigation steam allocation workflow

3.2.1 SAGD Data-Driven Model Development.

The first step is data gathering from the SAGD reservoir. A reservoir simulator will be used as a data generator or a proxy to an actual field for this work. Zero mean noise is then added to the recorded data before the data is normalized for the data-driven model development. Min-max (Equation 3.1) normalization is then used to transform the observed time-series data between 0 and 100. The proposed normalization approach does not use the observed min-max of the feature, but min-max based on engineering, environmental, and equipment limitations. For the SAGD process, the min-max of features is selected, as shown in Table 3.1. The proposed normalization approach offers the following advantages compared to the current approach while keeping the benefits of normalization or standardization.

1. Reservoir simulators use well constraints to bound the forward model forecast, and if there is a violation, a set of actions is taken. Data-driven models lack the option of imposing well constraints. By selecting the min-max based on the proposed approach, data-driven forecasting is bound within a feasible range. Thus, defining well constraints as used in

MPC (Purkayastha et al., 2018) is eliminated and reduces computational time.

2. Normalizing using the min-max of the previously recorded data or standardizing with the mean and standard deviation does not offer the options for prescriptive analysis. The second advantage is automatic outlier detection, which can be used for prescriptive analytics (suggest a course of action based analysis of the normalized past recorded data) . For example, after normalization, if the temperature is below zero for a continuous period, this indicates possible conning and requires further attention. If the pressure is greater than 100 for a continuous period, that shows requirement for lowering the injection pressure to avoid possible formation fracture.

3. The third advantage the proposed approach offers is interpretability for both linear and nonlinear data-driven models. For example, a percentage change of an input can be correlated to the corresponding percentage change of the outputs.

$$x_{norm} = \frac{x(t) - min(x)}{max(x) - min(x)} \times 100 \tag{3.1}$$

Table 3.1: Feature range for max-min normalization

Feature	**Min**	**Max**
Temperature	Initial reservoir temperature	Maximum well equipment design temperature
Pressure	Bubble point	80% of fracturing pressure
Rate	No injection or production	Maximum allowable choke rate
Steam Chamber Volume	Zero	Reservoir or pad pore volume

A Box-Jenkins model structure for dynamic systems can be represented as in Equation 3.2. Where the input ($u\,(t)$: total phase injection rate or mole fraction) at any time(t) to the output ($\hat{y}\,(t)$: Liquid or water cut). z^{-1} is the backward shift operator; this allows the process and disturbance transfer functions to include the effects of the past inputs on the current output. Model identification is then performed after the pre-processing step (Fig 3.2). The proposed

identification approach uses an adaptive offline one-step ahead prediction error minimization approach that estimates the outputs of the SAGD process model or minimizes the difference between model predictions and recorded reservoir history. The best fitness is selected based on normalized root mean square error. First, small-scale optimization is performed to select the best fit model order. Cross-validation is then performed to determine a regularization parameter that gives the best fit. If the identified model does not pass a set threshold training and validation fitness, one percent of the early time dataset is eliminated from the training dataset. The optimization, cross-validation, and elimination of the first part of the training dataset are repeated until fitness criteria are met, or 50% of the training dataset is eliminated. As shown in Fig 3.1, the model is updated to adapt to the current state of the reservoir after optimized controller setpoints are implemented. The data-driven model is updated with the previous validation data set and the response of the data-driven model compared recorded reservoir response of the optimal controller setpoints. Suppose the data-driven model passes the validation test. In that case, it is used for the current horizon optimization, and if it fails, model identification is initiated, as shown in Fig. 3.2, to account for the new reservoir state.

Box-Jenkins Model (BJ)

$$\hat{y}(t) = \frac{B(z^{-1})}{F(z^{-1})}u(t) + \frac{C(z^{-1})}{D(z^{-1})}e(t) \tag{3.2}$$

$$B(z^{-1}) = b_1 z^{-1} + \cdots + b_{nb} z^{-nb}$$
$$C(z^{-1}) = 1 + c_1 z^{-1} + \cdots + c_{nc} z^{-nc}$$
$$D(z^{-1}) = 1 + d z^{-1} + \cdots + d_{nd} z^{-nd}$$
$$F(z^{-1}) = 1 + f_1 z^{-1} + \cdots + f_{nf} z^{-nf}$$

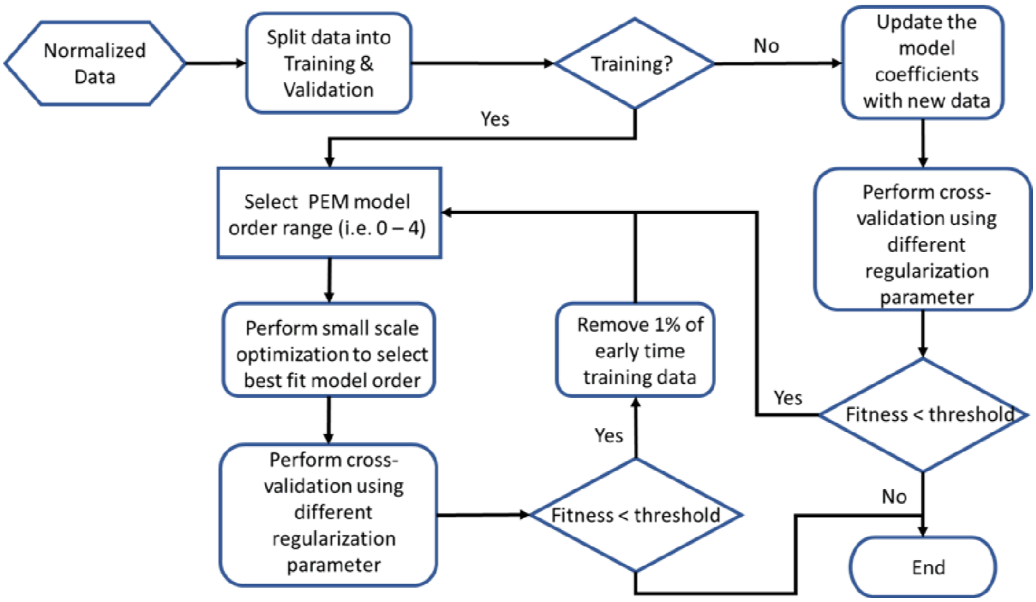

Figure 3.2: Workflow for model identification and updating of the data-driven model

3.2.2 SAGD Data-Driven Model Forecast Validation.

In Fig. 3.2, the validation step selects the recursively optimal model structures and parameters. The best fit model to past recorded data is used for optimal decision-making. After the optimization study, the model's forecast and reservoir response performance are compared in this validation section. The term prediction is used in this study refers to utilization of the model to estimate output within previously recorded data. Forecasting, on the other hand, entails estimating future outcomes using the best fit model. Modified Kling-Gupta (Kling et al., 2012) efficiency will be used to validate the data-driven model forecast outputs (Equation 3.3 – 3.4). Where y_i and $\hat{y}_i$ are the measured and forecasted outputs at the time (t). $\overline{y}$ and $\overline{\hat{y}}$ are the measured and forecasted mean outputs. A perfect positive correlation is indicated by 1, no correlation by zero and a perfect negative correlation by -1 for Pearson correlation (Equation 3.3). The drawbacks of Pearson correlation, as noted by Legates and McCabe (1999), are sensitive to outliers, not suitable for offset error evaluation and when y_i and $\hat{y}_i$ are proportional Pearson Correlation $(r = 1)$. In temporal dynamics modelling, the goal is to reproduce the system

dynamics measured by r while flow distribution is preserved through measuring bias (β) and the variability (γ) ratios. The r in modified Kling-Gupta Efficiency (KGE') represent the Pearson's r correlation between y and $\hat{y}$, while μ and σ are the mean and standard deviation of the forecast (f) and measured (m) outputs. The optimum value for each term $r,\ \beta,\ \gamma$ and KGE' is equal to one. With the performance of the model decomposed with KGE, the relative contribution of each term can be estimated to understand which term is contributing to poor or good model performance. The terms under the square root in Equation 3.4 represent the Euclidean distance, and each term can be re-scale during model training to improve upon its performance. Using the mean of the previous recorded data to forecast as a benchmark data-driven model, the $KGE' = -0.41$. Hence any data driven model with $KGE' > -0.41$ is better forecaster than the mean forecaster model. $KGE' = -0.41$ for the mean forecaster is derived by assuming $\mu_f = \mu_m,\ \sigma_m \neq 0$ and $\sigma_f = 0$ (Knoben et al., 2019). To asses the adequacy of the data-driven model, skill score (ss) metric is used (Equation 3.5) as performance of the data-driven model relative to benchmark model. Positive ss indicates improvement over benchmark and negative ss indicates model is worse than benchmark. As noted by Knoben et al. (2019), if the benchmark has $KGE' = 0.99$, then $ss = 0.5$ might not indicate a real practical improvement because of the scaled KGE' since the room for improvement is 0.01.

Pearson Correlation

$$r = \frac{\sum_{t=1}^{N_p} (y_t - \overline{y}) \left(\hat{y}_t - \overline{\hat{y}}\right)}{\sqrt{\sum_{t=1}^{N_p} (y_i - \overline{y})^2} \sqrt{\sum_{t=1}^{N_p} \left(\hat{y}_t - \overline{\hat{y}}\right)^2}}, \qquad -1 \leq r \leq 1 \tag{3.3}$$

Modified Kling-Gupta Efficiency (Kling et al., 2012)

$$KGE' = 1 - \sqrt{(r-1)^2 + (\beta - 1)^2 + (\gamma - 1)^2}, \tag{3.4}$$

$$-0.41 < KGE' \leq 1$$

$$\beta = \frac{\mu_f}{\mu_m}$$

$$\gamma = \frac{\sigma_f / \mu_f}{\sigma_m / \mu_m}$$

Skill score (Knoben et al., 2019)

$$ss = \frac{KGE'_{model} - KGE'_{benchmark}}{1 - KGE'_{benchmark}} \tag{3.5}$$

3.3 Real-time Robust Optimization: NCG Coinjection with Steam

In-situ recovery using SAGD techniques goes through three stages (ramp-up, normal and wind-down). During the wind-down phase, non-condensible gas such as methane is co-injected with steam to maintain steam chamber pressure while steam chamber temperature is utilized in bitumen production. The main KPI for SAGD process optimization is net-present-value (NPV). The NPV for this work is defined as in Equation 3.6. The optimization algorithm iteratively perturbs the total injection rate (u) and the mole fraction (ϑ) of the NCG at each control horizon. The NPV is calculated for each well (j) at each time (t) by summing up the difference between the revenue (the oil production rate $[\hat{y}_{o,j}(t)]$) and cost (steam injection $[u_{s,j}(t)]$, gas injection $[u_{g,j}(t)]$, produced water $[\hat{y}_{w,j}(t)]$, transportation and blending of oil, royalty rate) over the prediction horizon. The present value calculated over the prediction horizon (P) is discounted and then sum over total wells (N_w) in the model.

$$J(u,\vartheta) = \sum_{j=1}^{N_w}\sum_{t=1}^{P} \frac{(p_o\hat{y}_{o,j}(t) - p_w\hat{y}_{w,j}(t) - p_r p_o\hat{y}_{o,j}(t) - p_s u_{s,j}(t) - p_g u_{g,j}(t) - p_{otbc}\hat{y}_{o,j}(t))}{(1+D)^{\Delta t}} \tag{3.6}$$

Table 3.2 shows the input of the NPV parameters used in the optimization. They are based on major SAGD projects operating costs in Canada (Alexey, 2018). SAGD co-injection economic uncertainty is accounted for using a finite set of oil price scenarios ($\theta_i, i = 1, \ldots, N_\theta$) by maximizing the expected returns while minimizing the risk simultaneously.

The expected returns, which are maximized, are approximated over a set of oil price scenarios as defined in Equation 3.7. Where J_{MO} is the expected return, θ_i is oil price realization and N_θ is the total realization.

Table 3.2: Economic input parameters

Description	Value
Price of oil $[p_o]$	Uncertain parameter
Steam processing cost $[p_s]$	$6\$/bbl$
Gas processing cost $[p_g]$	$320\$/liqm^3$
Produced water processing cost $[p_w]$	$1.96\$/bbl$
the transportation and blending cost of oil $[p_o tbc]$	$4.95\$/bbl$
Royalty rate $[\ p_r]$	2%
Discount factor (D)	10%

$$J_{MO} = \frac{1}{N_\theta} \sum_{i=1}^{N_\theta} J\left(u, , \vartheta, \theta_i\right) \tag{3.7}$$

For each control horizon, the real-time robust optimization problem is formulated as shown in Equation 3.8. Robust optimization is constrained subject to $(s.t.)$ minimum $(u_j^{min}, \vartheta_j^{min}\ )$, and maximum $(u_j^{max},\ \vartheta_j^{max})$ total phase (steam + methane) and mole fraction injection rate. Because of the normalization approach proposed, the minimum and maximum design variables and constraints cannot be less than zero and greater than 100. The normalization ensures equal importance be given to each design variable and constraint by the optimization algorithm. Instabilities in the SAGD operations as a result of changes in steam injection were controlled by restricting the rate changes between subsequent prediction horizons to a minimum $(\Delta u_j^{mina}\ )$ and maximum (u_j^{max}) total phase injection rate. In this case study, the value was set to a 10% maximum rate change of the previous week's allocation rate. A constraint violation of 5%or less in addition to the maximum is accepted. The maximum rate is field-dependent and highly advised to be observed as a function of prior behaviour or an optimization variable.

$$\max_{u,\vartheta} J_{MO} = \frac{1}{N_\theta} \sum_{i=1}^{N_\theta} J\left(u, , \vartheta, \theta_i\right) \tag{3.8}$$

$$s.t.\ \ u_j^{min} \leq u_j \leq u_j^{max}$$
$$\vartheta_j^{min} \leq \vartheta_j \leq \vartheta_j^{max}$$
$$\Delta u_j^{min} \leq \Delta u_j \leq \Delta u_j^{max}$$

$$\sum_{j=1}^{N_w} u_j(t) \leq \overline{U}$$

Due to uncertain oil prices, the deviation from the expected return can be largely resulting in uneconomic returns or high-risk optimal controls. Therefore, mitigating the risk while maximizing the expected returns deserves attention. Maximizing return while minimizing risk means reformulating Equation 3.8 into a bi-objective optimization problem, increasing the computational cost. Hence a risk-return tradeoff $\omega_r \in [0, 1]$ is introduced, and the optimization problem is reformulated as a single objective. The optimization is then performed on a pre-defined set of risk-return tradeoff parameters, and the optimal tradeoff control setpoints based on risk-adjusted criteria are selected. Essentially, the goal is to maximize the expected return while ensuring the defined risk measure does not deviates significantly from the expected returns or avoid fat-tail return distribution. The following subsection discussed strategies employed to handle risk-return tradeoffs using symmetric and asymmetric risk management schemes (Aackermann, 2015; Capolei et al., 2015; Siraj et al., 2015) .

3.3.1 Mean-Variance Optimization (m-VO).

Markowitz (1952) risk-return portfolio selection optimization is employed under this case study. As shown in Equation 3.9, $\boldsymbol{\omega_r}$ is the risk-return tradeoff parameter. At each control strategy, an odd-numbered pre-defined set of the parameter is used. The parameter with the highest risk-adjusted return ($\boldsymbol{M^2}$) is selected as the optimal control strategy. The motivation for implementing this approach is to reduce the sampled returns' variance, hence reducing the risk of low returns. The use of the m-VO method gives equal preference to both tails of the return's distribution.

$$J_{MVO} = \omega_r J_{MO} - \ (1 - \omega_r) \frac{1}{N_\theta - 1} \sum_{i=1}^{N_\theta} \left(J\left(u_{stf}, \theta_i\right) - J_{MO}\right)^2 \tag{3.9}$$

3.3.2 Max-Min Optimization (MMO).

In this method, the MMO represents the risk of uncertain returns. Equation 3.10 shows the formulation of the tradeoff, maximizing the expectation and the minimum of the uncertain returns. Thus, MMO is an asymmetric approach that maximizes the worst cases of returns without penalizing the best returns. Conservative solutions are generated when the uncertain parameter has a wide variability (Siraj, 2017).

$$J_{WCO} = \omega_r J_{MO} - \ (1 - \omega_r)\, min\left\{J_1, \ldots, J_{N_\theta}\right\} \tag{3.10}$$

3.3.3 Mean-Semi-Variance Optimization (m-SVO).

m-SVO was proposed by (Markowitz, 1952) as a measure of the deviation of the squared dispersion of returns falling above and below the expectation of uncertain returns. Equation 3.11 (Siraj, 2017) defines the risk-return tradeoff optimization. The second term of Equation 3.11 is the risk term which is the lower tail of the returns mathematically to estimate the downside risk of the objective function. The objective here is to ignore desirable risk and maximize the worst returns (returns lower than the mean).

$$J_{m-SVO} = \omega_r J_{MO} - (1 - \omega_r)\, \frac{1}{N_\theta - 1} \sum_{i=1}^{N_\theta} min\{J_{MO} - J\left(u, , \vartheta, \theta_i\right), 0\}^2 \tag{3.11}$$

3.3.4 Mean-Conditional Value-at-Risk Optimization (m-CVaR).

The m-CVaR approach was introduced by Rockafellar and Uryasev (2002) as a risk management approach that focuses on $\boldsymbol{\alpha}$ of the worst cases. The method is asymmetric risk management for focuses on the lower tail of the distribution, unlike mean-variance, which treats the lower and the upper tail equally. Aackermann (2015) defines CVaR as the average return given that the return is smaller than VaR with a certain level of confidence. Hence the objective function for risk-return optimization is defined mathematically as in

Equation 3.12.

$$J_{m-SVO} = \omega_r J_{MO} - (1 - \omega_r) \frac{1}{\alpha} \sum_{i=1}^{N_\theta} NPV_i b \tag{3.12}$$

3.3.5 Simulating Oil Price Uncertainty

. Oil price uncertainty is modelled using geometric Brownian motion. The model is defined as in Equation 3.13. Where $P(t)$ is the future oil price at the time (t, month), $P(0)$ is the initial oil price, σ is the oil price volatility, μ is the drift in oil price, and Δt is the period selected as monthly in this work. A finite set of oil price scenarios $\theta_i, i = 1, \ldots, N_\theta$ of 100 realizations is used in this study. Fig 3.3 shows the realizations of oil price uncertainty based on Equation 3.13. The thick brown, black and red line represents the maximum, mean and minimum of all realizations at each month. This workflow's RTO control horizon is set to a weekly optimization period. Generally, significant oil price uncertainty is not recorded over such a short period. As a result, monthly average oil price uncertainty is used in this study, as illustrated in Fig 3.3. Due to the four-week length of each month, the uncertain pricing range for four consecutive weeks is identical.

$$P(t) = P(0)\, exp\left[\left(\mu - \frac{\sigma^2}{2}\right)\Delta t + \sigma * \sqrt[2]{\Delta t}\varepsilon\right] \tag{3.13}$$

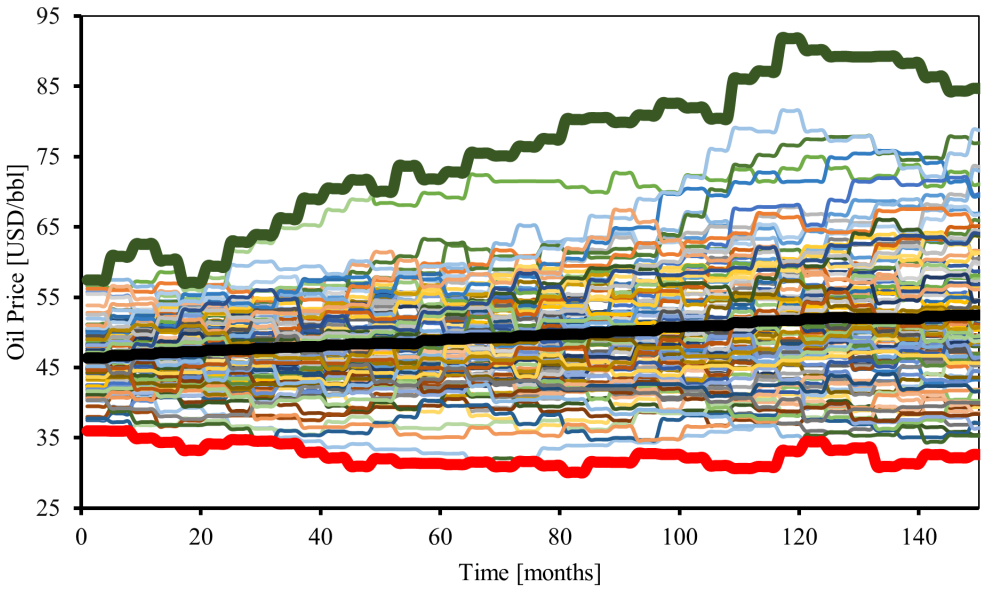

Figure 3.3: Oil price uncertainty realizations

3.3.6 Risk-Return Trade-off Selection.

After the robust optimization, the optimal risk-return tradeoff is selected using Modigliani risk-adjusted (M^2) performance (Modigliani and Leah, 1997). Motivation is to find the tradeoff parameter that gives the highest expected return with lower risk. The Sharpe ratio (Equation 3.14) suggested by Capolei et al. (2015) as an optimal tradeoff risk-returns compares the uncertainty scenarios among themselves. The ratio of the expected returns $\left(\mathbb{E}\left[J\left(\theta_i\right)_{i=1}^{N_\theta}\right]\right)$ to the standard deviation $\left(\sigma\left[J\left(\theta_i\right)_{\mathrm{i=1}}^{\mathrm{N}_\theta}\right]\right)$ is the Sharpe ratio. However, M^2 compares the uncertainty scenarios and a benchmark index.

Based on Capolei et al. (2015) definition for Sharpe ratio (S_h), M^2 for this proposed work would be defined in Equation 3.15. σ_M is the standard deviation of a benchmark (any broad index, possibly S&P 500 energy index), and r_f is the risk-free ratio (3-month treasury bill or Libor rate can be used). The drawback of S_h as an optimal risk-return tradeoff is the assumption the $\mathbb{E}\left[\theta_{\mathrm{i=1}}^{\mathrm{N}_\theta}\right]$ will always be symmetric. To ensure the correct optimal tradeoff of risk-return is selected at each control horizon, the Anderson and Darling (1952) is used to test the normality of the return's distribution. If the distribution is

not normally distributed, M^2 is modified using adjusted Sharpe ratio (AS_h) proposed by Pezier and White (2006) to penalize negative skewness and excess kurtosis. Hence Equation 3.16 is used to calculate the modified Modigliani risk-adjusted $\left(mM^2\right)$ performance. If the returns are normally distributed, the skewness (s) is zero, and the kurtosis (k) will be three else the penalization is applied to the S_h.

$$S_h = \frac{\mathbb{E}\left[J\ \ (\theta_i)_{\mathrm{i=1}}^{\mathrm{N}_\theta}\right]}{\sigma\left[J\ \ (\theta_i)_{\mathrm{i=1}}^{\mathrm{N}_\theta}\right]} \tag{3.14}$$

$$M^2 = \frac{\mathbb{E}\left[J\ \ (\theta_i)_{\mathrm{i=1}}^{\mathrm{N}_\theta}\right]}{\sigma\left[J\ \ (\theta_i)_{\mathrm{i=1}}^{\mathrm{N}_\theta}\right]}\sigma_M + r_f \tag{3.15}$$

$$mM^2 = \left[S_h \times \left\{1 + \left(\frac{s}{6}\right) \times S_h - \left(\frac{k-3}{24}\right) \times {S_h}^2\right\}\right]\sigma_M + r_f \tag{3.16}$$

The proposed real-time optimization workflow is summarized as shown in the Algorithm below.

Algorithm: Real-Time NCG Optimization

For every time step $\boldsymbol{t = 7\ days}$.

1. Set risk measure.

   - The standard deviation of returns: $\frac{1}{N_\theta - 1} \sum_{i=1}^{N_\theta} \left(J\left(u, , \vartheta, \theta_i\right) - J_{MO}\right)^2$.
   - Minimum of returns: $J_1, ..., J_{N_\theta}$.
   - Covariance at Risk of returns: $\frac{1}{N_\theta (1-\beta)} \sum_{i=1}^{N_\theta} min\left\{J_i\left(u, , \vartheta, \theta_i\right) - \alpha, 0\right\}$.
   - Semi-variance of returns: $\frac{1}{(N_\theta - 1)} \sum_{i=1}^{N_\theta} max\left\{J_{MO} - J_i\left(u, , \vartheta, \theta_i\right), 0\right\}^2$.

2. Set risk-return trade-off parameters (ω_r).

3. Read the previous production and injection rates.

4. Normalize the previously recorded data based on each parameter's physical or operating constraint (range).

5. Identify the structure and parameters of the data-driven model [**Fig. 2**].

6. Estimate the recoverable oil.
   If the produced oil is less than recoverable oil Go to step seven. Else Go to step 14.

7. Check the status of all wells in the pad. If $max\left(u_s\left(t\right) + u_g\left(t\right)\right) < U_{min}\ \forall\ \left(t\right) < 28$ The injection well is shut. Else if $max\left(u_s\left(t\right) + u_g\left(t\right)\right) < U_{min}\ \forall\ \left(t\right) \geq 28$ Open injection well Else The injection well is open.

8. For each tradeoff parameter ($\omega_r \in \Omega$). Normalize the decision variable and constraint-based on each parameter physical or operating constraint (range). Find $u_{steam}\left(k\right) \in U_{steam},\ u_{gas}\left(k\right) \in U_{gas}$ that maximizes expected returns $\left(E\left[\theta_{i=1}^{N_\theta}\right]\right)$.
   If the well model's prediction is out of the physical range or operating range, use the previous week's prediction for the well and adjust the forecast by a factor. Test for normality of returns distribution using Anderson-Darling test. If returns are normally distributed, Estimate risk-adjusted performance $M^2 = \frac{\mathbb{E}\left[J\ (\theta_i)_{\mathrm{i=1}}^{\mathrm{N}_\theta}\right]}{\sigma\left[J\ (\theta_i)_{\mathrm{i=1}}^{\mathrm{N}_\theta}\right]} \sigma_M + r_f$
   Else Estimate $mM^2 = \left[S_h \times \left\{1 + \left(\frac{s}{6}\right) \times S_h - \left(\frac{k-3}{24}\right) \times {S_h}^2\right\}\right] \sigma_M + r_f$

9. Select the tradeoff parameters ($\omega_r \in \Omega$) that have the maximum risk-adjusted performance (M^2)

10. Set the total optimal control setpoints (steam + gas rate) to a specified steam rate if the total optimal control setpoints are below or equal to a pre-defined value.

11. Apply optimal injection controls of the selected maximum risk-adjusted performance to the digital heavy oil reservoir

12. Record the response (production and injection rates) of the reservoir to the optimal control setpoints

13. $t = t + 1$

14. Repeat steps $4 - 13$ until it is not profitable or the end of field life.

3.4 Case Study

3.4.1 SAGD Reservoir Model.

A synthetic reservoir of the Western Canada oilfield is used in this study and consists of nine horizontal well-pairs. It was based on available publications with an average porosity of 0.31 and average horizontal and vertical permeabilities of 4495 mD and 3596 mD. Fig 3.4 displays the permeability (Fig 3.4a) and shale barrier distribution (Fig 3.4b) of the well-pad. In addition, rock-liquid properties of CMG SAGD training for NCG were used in fluid reservoir behaviour (CMG, 2020). With 128000 grid cells, the pad is 800 m x800 m in size. The cell grid size of the grid is 10 m on average laterally and 2.5 m vertically.

There are three different SAGD scenarios. The well-pairs for each model were initially heated for four months. Each injection well was operated at a maximum steam rate of 750 m^3/day (cold water equivalent, CWE) and a maximum injection pressure of 2500 kPa. The injection steam quality of 0.9 and temperature of 223.7^oC. The production wells have a primary constraint of 2000 kPa bottom hole pressure and a secondary constraint of 1000m^3/day surface liquid rate. In addition, a maximum steam production rate of 10 m^3/day is set to mimic steam trap control. Conventional SAGD operating strategy was implemented for 14 years for each model. The differences in the models were based on the operating plan for the last two years and four months. Model 1 (Base SAGD) is the conventional SAGD where steam is continuously injected at a constant pressure for the rest of the two years. Model 2 (Base SAGD-NCG) steam and NCG of 2 $moles\%$ were co-injected at a constant total phase rate of 2500 m^3/day. Model 3 (SAGD-NCG optimized) an experiment was designed to generate an initial input and output data to train a data-driven model using a sinusoidal signal. The training and validation period was the first four months, and the remaining two years were then optimized. The control setpoints optimized in real-time at each control horizon are the total injection phase rate (u) and NCG mole fraction (ϑ) for each injection well.

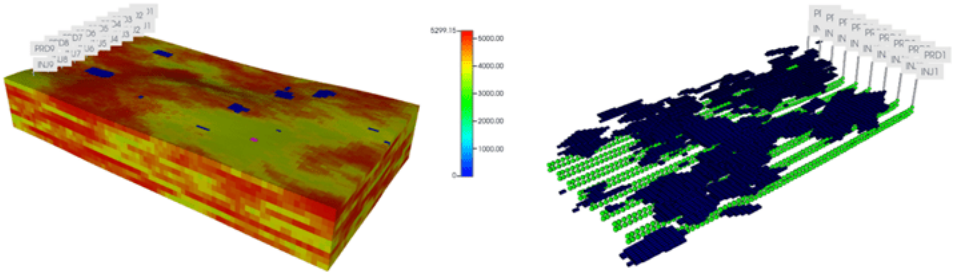

Figure 3.4: Permeability and shale barriers distribution

3.5 Results and Discussion

NCG co-injection aims to enhance SAGD economics by lowering water and fuel consumption, which will lead to a reduction in greenhouse gas emissions through reducing SOR. Additionally, by decreasing steam losses to overburden and maintaining the reservoir pressure of a matured SAGD process, the ultimate recovery can be improved. Furthermore, if methane or CO_2 gas is employed as the injection fluid, sequestration provides an extra benefit to the environment. The section presents the performance of the proposed workflow in forecasting reservoir response and the risk-return objective function formulations for NCG co-injection.

3.5.1 Data-Driven SAGD Reservoir Model Validation.

The calibrated model used during optimization periods for forecasting performance statistics is presented for the NCG co-injection process outputs (Table 3.3 through 3.6) in the appendix. The data-driven model is for each unique well-pair, therefore, there are no substantial local heterogeneities that would cause poor forecast performance. For all four case studies, the highest performing well model is highlited as green, medium with yellow, and least performance with red in Table 3.3. In addition, the performance metric ss is used to rank the best well-pair data-driven model for forecasting, which is split into correlation (r), bias (β), and variability factors (γ). The third, fourth and fifth columns are the correlation (r), bias (β), and variability respectively for each

well-pair. The sixth column is the KGE' which represent the composite metric while the seventh is the relative contribution for r, β, and γ. Skill score (ss) is the last column which shows the KGE' of the data-driven model relative mean benchmark forecaster. From Table 3.3 - 3.6 higher bias relative contribution leads to higher ss and hence comparing with mean benchmark forecaster. The data-driven NCG co-injection model has three outputs (Liquid rate, water-cut and Gas-Oil-Ratio). Figs 3.5 through 3.8 show the evolution of the model forecasted performance and system response (numerical or digital reservoir) for the (a) best (b) median and (c) least performance for the duration of the optimization period, which were highlighted in Table 3.3 through 3.6. The oil rate is a derived output of the data-driven model of liquid rate and water-cut.

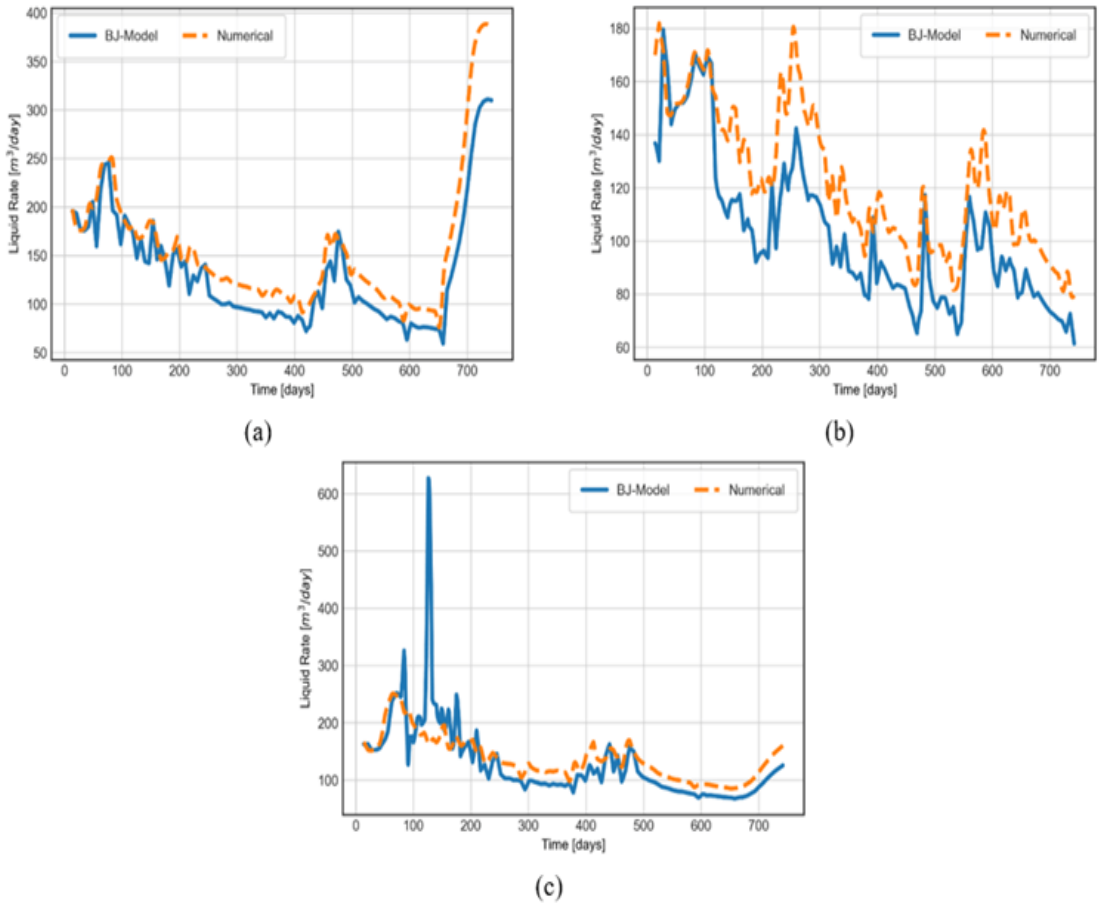

Figure 3.5: Forecasted (BJ-Model) and response (Numerical) liquid rate during the optimization period (a) Best (green) (b) Median (yellow) and (c) least (red) highlighted in Table 3 for all four cases studied.

Table 3.3: Liquid rate model forecast dimensionless validation performance.

		r	β	γ	KGE'	**rc**	**ss**
	Well 1	0.78	0.86	1.17	0.69	[0.5, 0.2, 0.3]	0.78
	Well 2	0.82	0.83	1.18	0.69	[0.35, 0.31, 0.34]	0.78
	Well 3	0.91	0.83	1.26	0.68	[0.08, 0.26, 0.66]	0.77
	Well 4	0.76	0.86	1.53	0.4	[0.17, 0.05, 0.78]	0.58
m-cVaR	Well 5	0.85	0.83	1.25	0.66	[0.19, 0.25, 0.56]	0.76
	Well 6	0.76	0.87	1.34	0.56	[0.31, 0.09, 0.6]	0.69
	Well 7	0.91	0.84	1.29	0.66	[0.06, 0.22, 0.71]	0.76
	Well 8	0.86	0.83	1.29	0.63	[0.16, 0.22, 0.62]	0.74
	Well 9	0.88	0.84	1.3	0.64	[0.11, 0.19, 0.7]	0.74
	Well 1	0.87	0.84	1.29	0.64	[0.13, 0.19, 0.68]	0.75
	Well 2	0.9	0.84	1.25	0.69	[0.11, 0.26, 0.64]	0.78
	Well 3	0.88	0.84	1.4	0.56	[0.08, 0.13, 0.8]	0.69
	Well 4	0.75	0.85	1.57	0.37	[0.15, 0.05, 0.8]	0.55
m-VO	Well 5	0.37	0.88	1.91	-0.11	[0.32, 0.01, 0.67]	0.21
	Well 6	0.86	0.86	1.36	0.59	[0.12, 0.12, 0.76]	0.71
	Well 7	0.83	0.84	1.23	0.68	[0.27, 0.24, 0.49]	0.77
	Well 8	0.87	0.85	1.36	0.58	[0.1, 0.13, 0.76]	0.71
	Well 9	0.93	0.85	1.32	0.64	[0.04, 0.18, 0.78]	0.74
	Well 1	0.96	0.86	1.2	0.76	[0.03, 0.32, 0.65]	0.83
	Well 2	0.61	0.93	2.15	-0.22	[0.1, 0.0, 0.9]	0.13
	Well 3	0.93	0.85	1	0.83	[0.16, 0.84, 0.0]	0.88
	Well 4	0.93	0.86	1.34	0.63	[0.04, 0.14, 0.83]	0.74
m-SVO	Well 5	0.83	0.86	1.25	0.67	[0.26, 0.18, 0.56]	0.77
	Well 6	0.85	0.85	1.19	0.71	[0.28, 0.27, 0.45]	0.8
	Well 7	0.79	0.86	1.15	0.71	[0.53, 0.23, 0.24]	0.79
	Well 8	0.86	0.85	1.21	0.71	[0.22, 0.27, 0.51]	0.8
	Well 9	0.95	0.85	1	0.84	[0.08, 0.92, 0.0]	0.89
	Well 1	0.94	0.84	1.19	0.75	[0.06, 0.4, 0.54]	0.82
	Well 2	0.91	0.84	1.13	0.77	[0.15, 0.52, 0.33]	0.84
	Well 3	0.89	0.84	1.2	0.72	[0.16, 0.34, 0.5]	0.8
	Well 4	0.95	0.84	1.16	0.77	[0.05, 0.48, 0.47]	0.84
mmo	Well 5	0.86	0.83	1.11	0.75	[0.33, 0.46, 0.21]	0.82
	Well 6	0.91	0.84	1.23	0.7	[0.09, 0.3, 0.61]	0.79
	Well 7	0.92	0.85	1.16	0.77	[0.12, 0.42, 0.46]	0.84
	Well 8	0.9	0.84	1.2	0.73	[0.12, 0.32, 0.55]	0.81
	Well 9	0.95	0.85	1.17	0.77	[0.04, 0.43, 0.53]	0.83

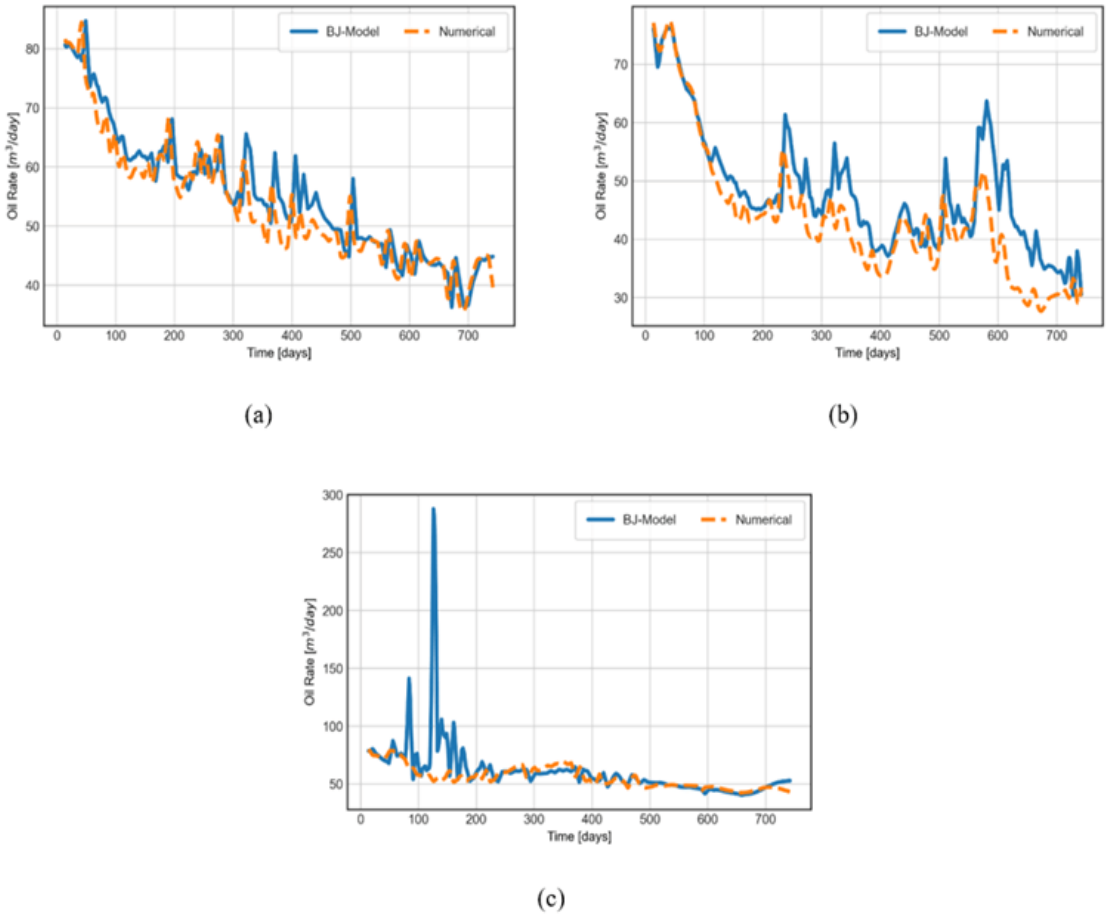

Figure 3.6: Forecasted (BJ-Model) and response (Numerical) oil rate during the optimization period (a) Best (green) (b) Median (yellow) and (c) least (red) highlighted in Table 4 for all four cases studied.

Table 3.4: Oil rate model forecast dimensionless validation performance.

		r	β	γ	KGE'	**rc**	**ss**
	Well 1	0.66	1.13	1.15	0.61	[0.74, 0.11, 0.14]	0.72
	Well 2	0.85	1.13	0.78	0.7	[0.25, 0.2, 0.55]	0.79
	Well 3	0.9	1.07	0.89	0.84	[0.4, 0.19, 0.41]	0.88
	Well 4	0.76	1.09	1.21	0.67	[0.51, 0.08, 0.42]	0.76
m-cVaR	Well 5	0.9	1.13	0.84	0.77	[0.21, 0.31, 0.48]	0.84
	Well 6	0.65	1.18	0.91	0.59	[0.75, 0.2, 0.05]	0.71
	Well 7	0.93	1.08	0.97	0.89	[0.38, 0.54, 0.08]	0.92
	Well 8	0.95	1.06	0.85	0.83	[0.09, 0.15, 0.76]	0.88
	Well 9	0.84	1.06	1.1	0.8	[0.64, 0.1, 0.26]	0.86
	Well 1	0.92	1.03	0.95	0.9	[0.69, 0.06, 0.24]	0.93
	Well 2	0.92	1.04	0.91	0.87	[0.43, 0.09, 0.48]	0.91
	Well 3	0.95	1.02	0.89	0.88	[0.2, 0.04, 0.76]	0.91
	Well 4	0.78	1.08	1.03	0.77	[0.88, 0.11, 0.02]	0.84
m-VO	Well 5	0.31	1.16	1.65	0.04	[0.51, 0.03, 0.46]	0.32
	Well 6	0.91	1.06	0.85	0.81	[0.23, 0.11, 0.66]	0.86
	Well 7	0.9	1.1	0.83	0.78	[0.2, 0.18, 0.62]	0.84
	Well 8	0.9	1.11	0.84	0.78	[0.22, 0.26, 0.51]	0.84
	Well 9	0.92	1.03	0.98	0.92	[0.82, 0.1, 0.08]	0.94
	Well 1	0.96	0.96	1.09	0.89	[0.13, 0.13, 0.74]	0.92
	Well 2	0.25	1.09	2.88	-1.02	[0.14, 0.0, 0.86]	-0.43
	Well 3	0.69	1.04	0.97	0.69	[0.98, 0.01, 0.01]	0.78
	Well 4	0.94	1	0.92	0.9	[0.38, 0.0, 0.62]	0.93
m-SVO	Well 5	0.72	1.07	0.79	0.65	[0.63, 0.03, 0.34]	0.75
	Well 6	0.47	1.08	1.27	0.4	[0.79, 0.02, 0.2]	0.57
	Well 7	0.67	1.15	0.73	0.54	[0.53, 0.11, 0.36]	0.67
	Well 8	0.78	1.05	0.81	0.71	[0.56, 0.03, 0.41]	0.79
	Well 9	0.54	1.03	1.08	0.54	[0.96, 0.0, 0.03]	0.67
	Well 1	0.95	0.97	1.14	0.85	[0.14, 0.03, 0.83]	0.89
	Well 2	0.88	1.02	1.02	0.88	[0.92, 0.04, 0.04]	0.91
	Well 3	0.92	1.03	0.99	0.92	[0.85, 0.15, 0.01]	0.94
	Well 4	0.92	0.99	1.19	0.8	[0.14, 0.0, 0.86]	0.85
mmo	Well 5	0.82	1.06	0.86	0.76	[0.59, 0.06, 0.35]	0.83
	Well 6	0.92	1.02	0.94	0.9	[0.6, 0.03, 0.37]	0.93
	Well 7	0.85	1.03	1.2	0.75	[0.35, 0.02, 0.63]	0.82
	Well 8	0.85	1.04	1.22	0.74	[0.31, 0.02, 0.67]	0.81
	Well 9	0.92	0.98	1.06	0.9	[0.6, 0.04, 0.35]	0.93

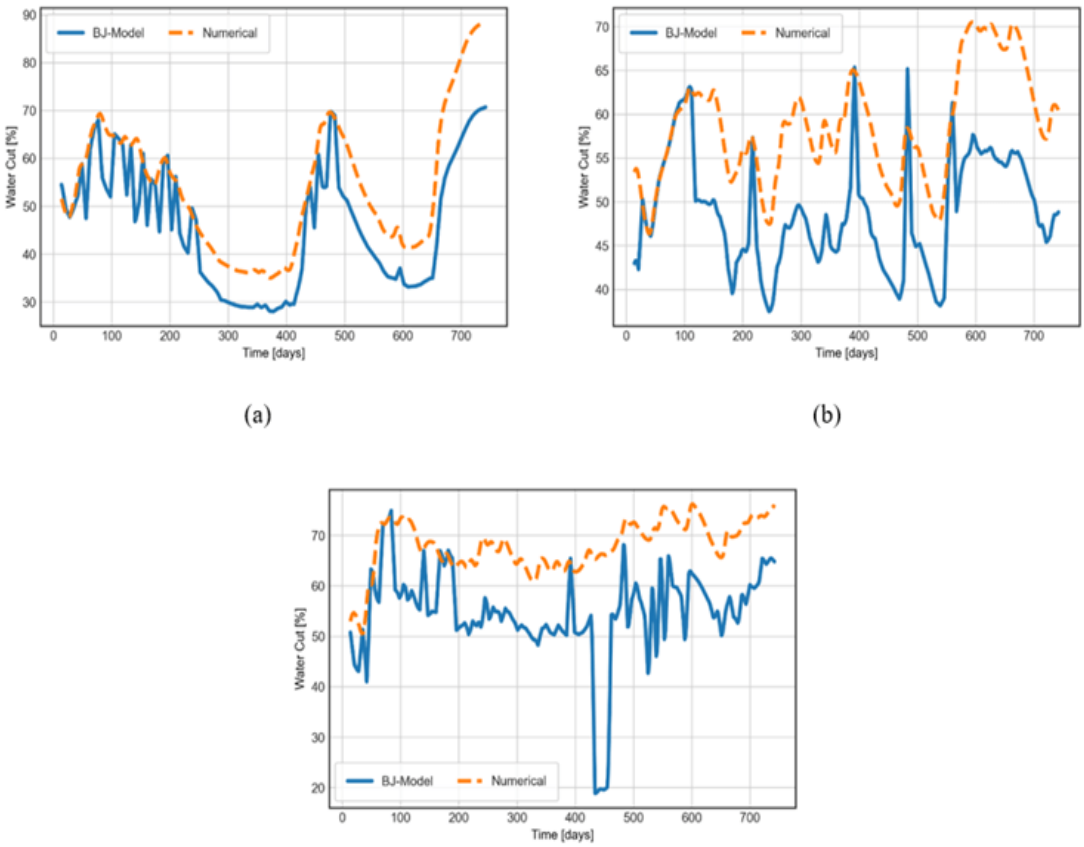

Figure 3.7: Forecasted (BJ-*Model) and* response (Numerical) water cut during the optimization period (a) Best (green) (b) Median (yellow) and (c) least (red) highlighted in Table 5 for all four cases studied.

Table 3.5: Water cut model forecast dimensionless validation performance.

		r	β	KGE'	γ	**rc**	**ss**
	Well 1	0.59	0.81	0.31	1.52	[0.36, 0.07, 0.57]	0.51
	Well 2	0.71	0.82	0.63	1.13	[0.64, 0.24, 0.12]	0.74
	Well 3	0.71	0.82	0.53	1.33	[0.38, 0.14, 0.47]	0.66
	Well 4	0.64	0.83	-0.08	2.01	[0.11, 0.03, 0.87]	0.23
m-cVaR	Well 5	0.6	0.82	0.52	1.21	[0.68, 0.14, 0.19]	0.66
	Well 6	0.42	0.81	-0.48	2.35	[0.16, 0.02, 0.83]	-0.05
	Well 7	0.51	0.82	0.15	1.67	[0.34, 0.04, 0.62]	0.4
	Well 8	0.62	0.82	0.44	1.36	[0.47, 0.11, 0.43]	0.61
	Well 9	0.74	0.82	0.32	1.6	[0.14, 0.07, 0.79]	0.52
	Well 1	0.72	0.83	0.64	1.15	[0.62, 0.21, 0.17]	0.74
	Well 2	0.72	0.83	0.59	1.25	[0.45, 0.17, 0.38]	0.71
	Well 3	0.71	0.83	0.59	1.23	[0.51, 0.17, 0.32]	0.71
	Well 4	0.7	0.83	0.64	1.11	[0.69, 0.22, 0.1]	0.74
m-VO	Well 5	0.64	0.83	0.53	1.24	[0.6, 0.13, 0.27]	0.67
	Well 6	0.72	0.84	0.63	1.19	[0.56, 0.19, 0.26]	0.74
	Well 7	0.67	0.83	0.63	1	[0.79, 0.21, 0.0]	0.73
	Well 8	0.62	0.83	0.25	1.62	[0.26, 0.05, 0.69]	0.47
	Well 9	0.73	0.83	0.49	1.39	[0.29, 0.11, 0.6]	0.64
	Well 1	0.91	0.86	0.54	1.42	[0.04, 0.1, 0.86]	0.68
	Well 2	0.87	0.85	0.56	1.39	[0.08, 0.11, 0.81]	0.69
	Well 3	0.86	0.85	0.78	1.05	[0.44, 0.51, 0.05]	0.85
	Well 4	0.87	0.85	0.72	1.2	[0.22, 0.29, 0.49]	0.8
m-SVO	Well 5	0.81	0.85	0.7	1.17	[0.41, 0.26, 0.33]	0.79
	Well 6	0.88	0.85	0.78	1.1	[0.28, 0.5, 0.22]	0.85
	Well 7	0.77	0.85	0.72	1.04	[0.67, 0.31, 0.02]	0.8
	Well 8	0.81	0.85	0.7	1.17	[0.4, 0.26, 0.34]	0.79
	Well 9	0.92	0.85	0.8	1.1	[0.18, 0.58, 0.24]	0.86
	Well 1	0.9	0.83	0.65	1.29	[0.09, 0.23, 0.68]	0.75
	Well 2	0.85	0.83	0.73	1.14	[0.32, 0.4, 0.27]	0.81
	Well 3	0.57	0.83	0.37	1.42	[0.47, 0.07, 0.46]	0.55
	Well 4	0.85	0.83	0.68	1.23	[0.21, 0.28, 0.5]	0.77
mmo	Well 5	0.82	0.83	0.74	1.07	[0.49, 0.44, 0.07]	0.81
	Well 6	0.74	0.83	0.54	1.34	[0.31, 0.14, 0.55]	0.67
	Well 7	0.91	0.83	0.72	1.21	[0.11, 0.35, 0.54]	0.8
	Well 8	0.77	0.83	0.5	1.4	[0.22, 0.12, 0.66]	0.65
	Well 9	0.89	0.83	0.69	1.24	[0.12, 0.29, 0.59]	0.78

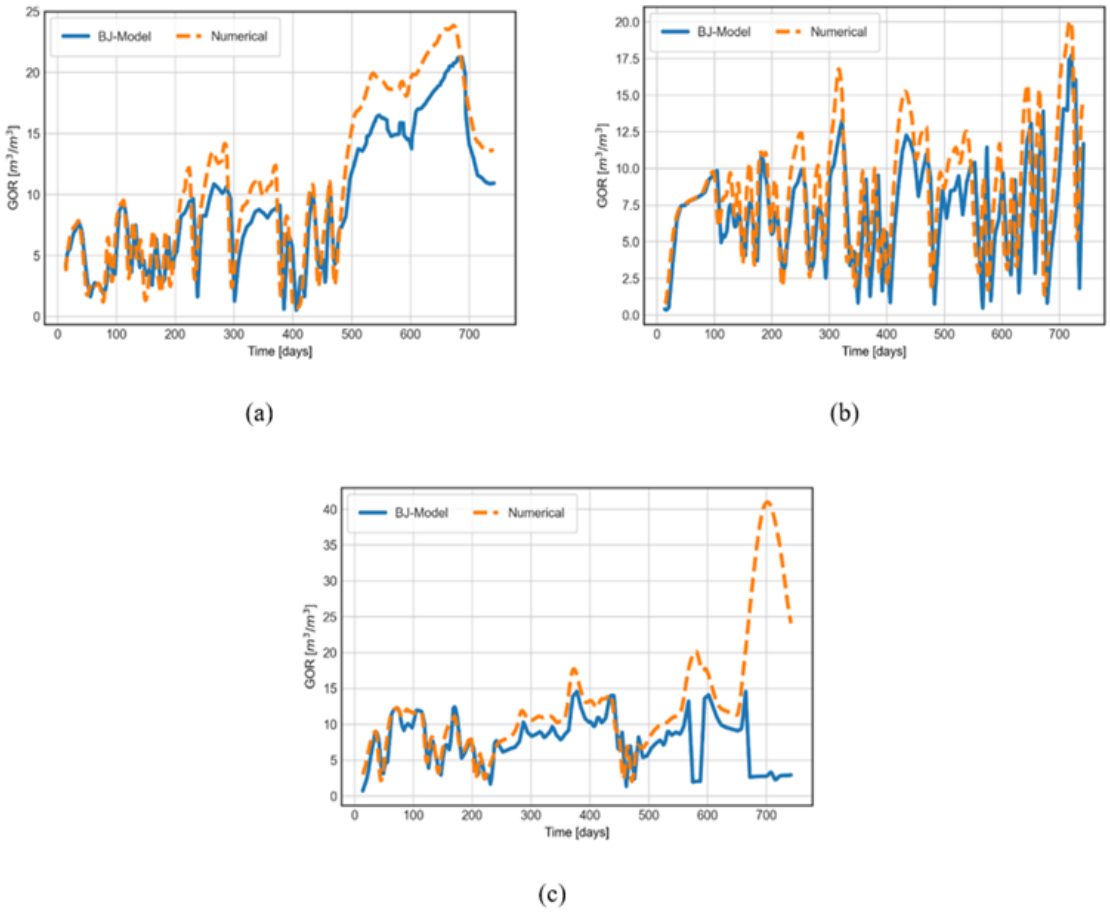

Figure 3.8: Forecasted (BJ-Model) and response (Numerical) GOR during the optimization period (a) Best (green) (b) Median (yellow) and (c) least (red) highlighted in Table 6 for all four cases studied.

3.5.2 Key Performance Indicators.

Fig 3.9 shows the evolution of cumulative NPV at the end of the two years of real-time optimization with an uncertain oil price using the various risk-return objective function. The risk-return objective function formulations are compared against two unoptimized base cases (i.e. For a field application, it recommended to optimize the base cases). The first case is continuous conventional SAGD, and the second is constant mole fraction NCG injection. An average of the oil price realizations was used to estimate the NPV for the two unoptimized cases. The results show that the risk-return formulation of

Table 3.6: Gas-oil-ratio model forecast dimensionless validation performance.

		r	β	γ	KGE'	**rc**	**ss**
	Well 1	0.54	0.82	1.08	0.5	[0.85, 0.12, 0.03]	0.64
	Well 2	0.55	0.81	1.05	0.51	[0.84, 0.15, 0.01]	0.65
	Well 3	0.72	0.81	0.94	0.65	[0.65, 0.32, 0.03]	0.75
	Well 4	0.76	0.83	0.93	0.7	[0.62, 0.32, 0.06]	0.79
m-cVaR	Well 5	0.62	0.75	0.87	0.53	[0.66, 0.27, 0.07]	0.66
	Well 6	0.3	0.75	0.85	0.24	[0.85, 0.11, 0.04]	0.46
	Well 7	0.54	0.78	1.05	0.49	[0.81, 0.18, 0.01]	0.64
	Well 8	0.79	0.82	1.11	0.7	[0.48, 0.37, 0.15]	0.79
	Well 9	0.71	0.68	0.79	0.52	[0.37, 0.44, 0.19]	0.66
	Well 1	0.82	0.82	0.95	0.74	[0.48, 0.47, 0.05]	0.82
	Well 2	0.8	0.78	0.92	0.69	[0.42, 0.51, 0.07]	0.78
	Well 3	0.83	0.85	1.03	0.77	[0.55, 0.43, 0.02]	0.84
	Well 4	0.59	0.84	1.03	0.56	[0.87, 0.12, 0.0]	0.69
m-VO	Well 5	0.62	0.86	1.03	0.59	[0.87, 0.13, 0.01]	0.71
	Well 6	0.37	0.63	0.91	0.26	[0.73, 0.25, 0.01]	0.48
	Well 7	0.73	0.91	1.17	0.66	[0.66, 0.07, 0.27]	0.76
	Well 8	0.79	0.8	0.94	0.71	[0.51, 0.45, 0.04]	0.79
	Well 9	0.45	0.49	0.69	0.19	[0.46, 0.4, 0.14]	0.43
	Well 1	0.99	0.8	0.94	0.79	[0.0, 0.91, 0.09]	0.85
	Well 2	0.91	0.85	0.98	0.82	[0.28, 0.7, 0.02]	0.88
	Well 3	0.74	0.87	0.94	0.7	[0.76, 0.19, 0.04]	0.79
	Well 4	0.58	0.77	0.87	0.51	[0.72, 0.21, 0.07]	0.65
m-SVO	Well 5	0.83	0.8	0.93	0.73	[0.39, 0.54, 0.07]	0.81
	Well 6	0.56	0.77	0.89	0.49	[0.75, 0.2, 0.05]	0.64
	Well 7	0.52	0.93	1.11	0.5	[0.93, 0.02, 0.05]	0.64
	Well 8	-0.16	0.6	0.7	-0.26	[0.84, 0.1, 0.06]	0.11
	Well 9	0.47	0.51	0.62	0.19	[0.42, 0.37, 0.21]	0.42
	Well 1	0.81	0.81	0.94	0.73	[0.46, 0.48, 0.06]	0.81
	Well 2	0.76	0.81	0.92	0.68	[0.58, 0.36, 0.06]	0.77
	Well 3	0.82	0.84	0.8	0.68	[0.33, 0.25, 0.42]	0.78
	Well 4	0.64	0.84	0.94	0.6	[0.81, 0.16, 0.02]	0.72
mmo	Well 5	0.68	0.89	0.96	0.66	[0.89, 0.09, 0.02]	0.76
	Well 6	0.59	0.75	0.96	0.52	[0.72, 0.27, 0.01]	0.66
	Well 7	0.33	0.89	1.16	0.3	[0.93, 0.02, 0.05]	0.5
	Well 8	0.83	0.83	0.97	0.76	[0.52, 0.47, 0.02]	0.83
	Well 9	0.07	0.38	0.57	-0.2	[0.6, 0.27, 0.13]	0.15

MMO outperform all formulations. For example, in Fig 3.9, the best NPV obtained was 59 $MMUSD$ which is 78.26% higher than the base case continuous conventional SAGD. The order of performance is ranked as MMO > m-VO > m-SVO > m-cVaR > Base-NCG (2.0% *mole*) in terms of final cumulative NPV.

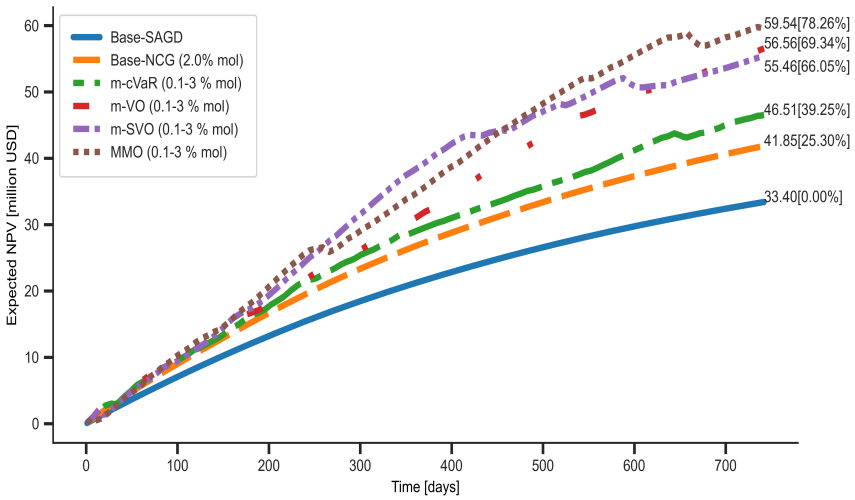

Figure 3.9: Cumulative NPV comparison for risk-return cases and base SAGD and NCG.

In addition, as shown in Fig 3.10a, the low economic performance of the two base cases can be attributed to the probability density function (PDF's) likelihood of getting the expected NPV of 0.4 $MMUSD$ or less. Confirming from the cumulative density function (CDF) plot Fig 3.10b, there is a 20% and 42% probability that the weekly expected NPV is higher than 0.4 $MMUSD$ for SAGD and NCG base cases. The optimized cases all have a higher PDF likelihood of a weekly expected NPV of 0.4 $MMUSD$ (Fig 3.10a). From the CDF plot (Fig 3.10b), the final cumulative NPV performance can be attributed to the fact that there is an 80% probability of the weekly expected NPV of MMO exceeding 0.4 $MMUSD$. Similarly, the likelihood of the weekly expected NPV performance exceeding 0.4 $MMUSD$ is ranked as in the order of cumulative NPV performance as 80% > 70% > 60% > 50% > 42% > 20%. Hence, the higher likelihood of high expected weekly NPV, the higher the

cumulative NPV performance.

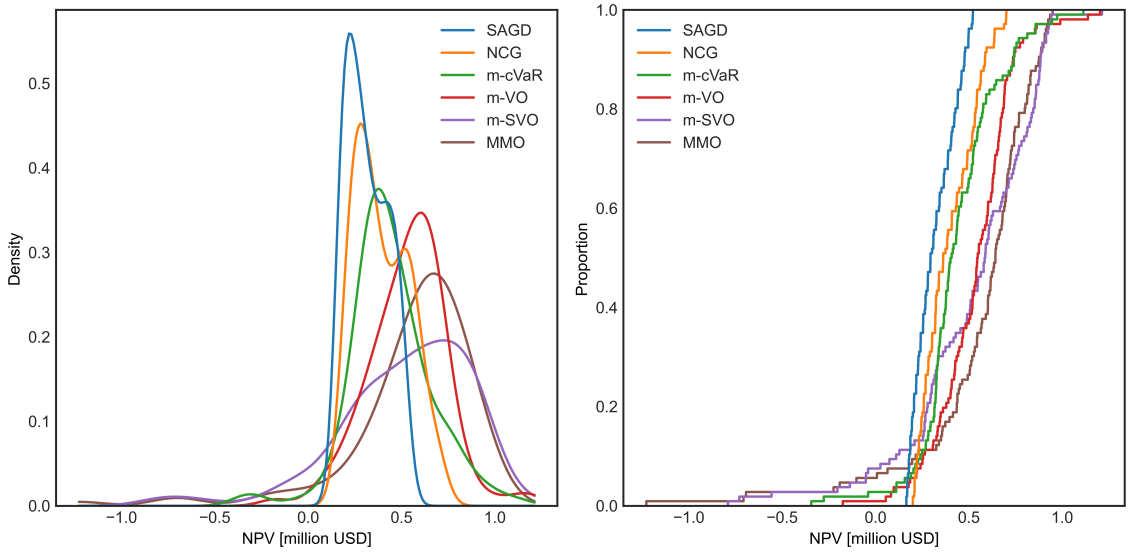

Figure 3.10: Weekly expected NPV PDF and CDF distribution for different under oil price uncertainty.

A higher expected NPV is associated with a higher probability of failure. Thus, the risk is minimized using a tradeoff objective formulation while maximizing NPV for each control sequence (week) in the real-time optimization. The objective is to determine the optimal tradeoff parameter for the current control sequence that maximizes the expected NPV while minimizing risk. As shown in Fig 3.11, it can be inferred the MMO optimal tradeoff is disproportionately skewed towards emphasizing maximizing the expected NPV than the risk. The PDF plot (Fig. 3.11a) shows that the tradeoffs are distributed around 1 and 0.75. Tradeoff values of 0.6 and above have 80% and above the probability of being selected as the optimal control strategy (Fig 3.11b). The opposite of such behaviour is observed with the m-VO, favouring low tradeoffs or emphasizing minimizing the risk. Thus, optimal tradeoffs of m-SVO tend to be equiprobable with the m-cVaR compromise between MMO and m-VO.

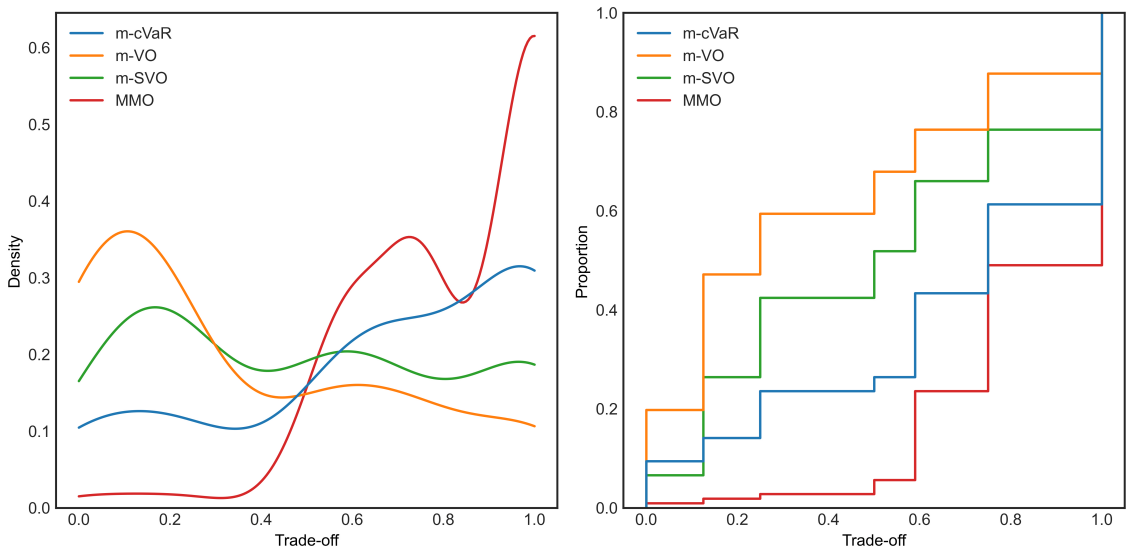

Figure 3.11: Optimal weekly tradeoff for each risk-return formulation.

Petroleum recovery operations are high risk investment. However, investors weigh options on the returns as compared to other investment portfolios. As noted earlier , the Sharpe ratio was used as an optimal tradeoff for risk-return (Capolei et al., 2015). Using M^2 as an optimal tradeoff for risk-return allows for the NPV's uncertain oil price adjusted for the risk of the NPV realizations to a benchmark (i.e. S&P 500 energy index). This approach makes it easier for engineers to present their decision to management in language easily understood by non-technical members. From Fig 3.12, the PDF or density shows all the risk-return objective function formulation with a high likelihood of $8-10\%$ percent higher performance compared to the benchmark S&P 500 energy index performance for the same period. There is a sharp decrease in the likelihood exceeding 10%, as shown in Fig. 3.12b. The PDF or density curves show a right-skewed distribution; performance beyond 10% are rare occurrences, and eliminating them leads to a normally distributed performance. The adjusted M^2 (Equation 3.16), which is proposed in this work, ensured the correction of non-normally distributed performance.

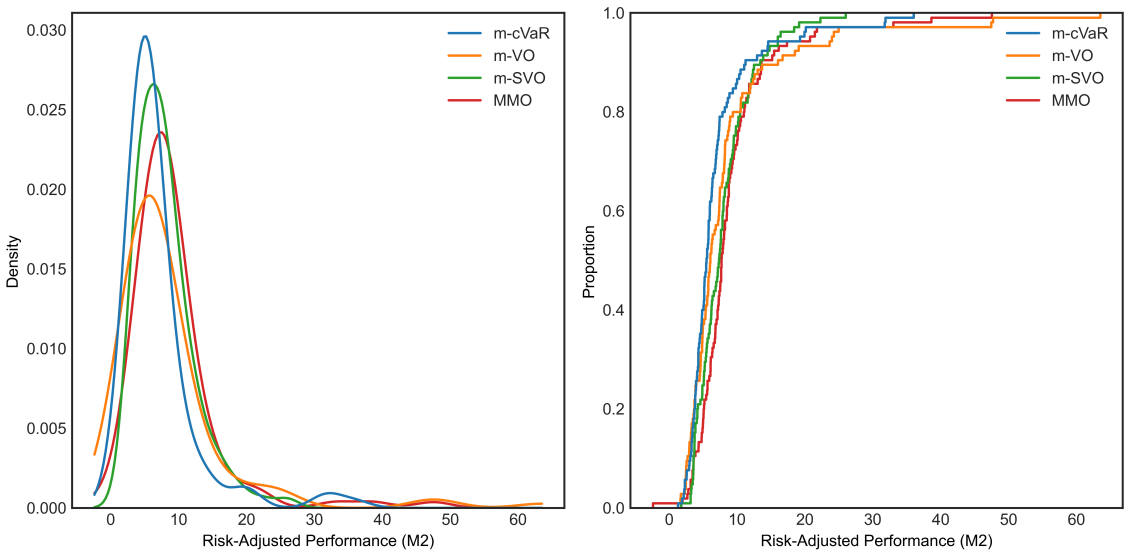

Figure 3.12: Risk-adjusted performance distribution.

Besides the economic performance, cSOR measures the economic and environmental performance of the SAGD recovery process. Lowering cSOR leads to less fuel and greenhouse gas emission and reduce capital and operating cost. Fig. 3.13 compares the performance of conventional SAGD to NCG co-injection for two years and four months. The cSOR (Fig. 3.13a) decreased as the NCG injection was initiated. The drop was from cSOR of 2.21 m^3/m^3 to $\sim$ 2.06 m^3/m^3. The reduction in cSOR is consistent with the high expected NPV performance when compared to conventional SAGD. In terms of the cSOR performance, m-VO had the highest decrease of 6.65% after two years four months. The ranking in terms of cSOR performance follows m-VO [-6.65%] $>$ MMO [-6.11%] $>$ m-SVO [-5.05%] $>$ Base-NCG (2.0%$mole$) [-5.4%]$>$ m-cVaR [-4.53%] as compared to conventional SAGD. In addition, the decline is consistent with SAGD NCG co-injection cSOR goals of reducing steam requirements to improve economics and reduce greenhouse gas footprints. The ranking does not follow NPV because pore volume of fluid injected and the processing cost of produced fluids. Since the higher the injection, the higher the operating cost, which reduces the NPV. The decline in cSOR is consistent with field reports (Doan et al., 2014) and published worked (Austin-Adigio and Gates, 2019)

At the initiation of NCG co-injection as seen from the average reservoir plot (Fig. 3.13b), there is a lowering of average reservoir pressure; as a result, average reservoir temperature (Fig. 3.13c) decreased as less steam is injected. Reduced steam chamber temperature results in less heat lose to overburden formation due to the injected NCG forming an insulated zone at the steam chamber's edges. Figs 3.13 (b and c) show increases in pressure and temperature after an initial decline as the injection volume increases before the optimization, which started after 127 *days* of NCG injection. The increases in temperature and pressure continued in the early days of the optimization and then stabilized for some months afterwards the drop begun again. The base constant NCG co-injection and m-CVaR saw an initial average reservoir pressure drop, then pressure increased and stabilized as the conventional SAGD. This behaviour is typical of NCG co-injection, which maintains reservoir pressure while mobilizing the oil via the excess steam chamber temperature.

Interestingly, constant NCG co-injection and m-CvaR had the lowest NPV and lowest decrease in cSOR to SAGD performance for the NCG co-injection cases. This demonstrates that lowering the reservoir pressure towards the initial reservoir pressure leads to an additional increase in recovery, which improves NPV. The results are consistent with Detpunyawat (2017) workon optimization of the NCG co-injection volume fraction. The best NPV case was obtained in his work when steam injection pressure is slightly higher than the original reservoir pressure. The final oil recovery (Fig. 3.13d) is and incremental is ranked as MMO [3.13] = m-SVO [4.7082%] > m-VO [4.4632%] > m-cVaR [] > Base SAGD [4.1911%] $\sim$ Base-NCG (2.0% *mole*) [3.7033%]. The oil recovery (Fig 3.13d) performance further supports NPV performance ranking. As can be observed, the total liquid phase pore volume injected for conventional SAGD is the highest. The pore volume injected for Base-NCG (2.0%*mole*) is lower than m-CVaR, explaining the approximate performance for both cases even though m-cVaR was optimized. The two best performing cases (MMO and m-SVO), though they have higher pore volume injected, performance can be attributed to final high steam chamber volume (Fig. 3.13e). The trend shows that as the NCG accumulates, the average temperature (Fig

3.13c) and steam chamber volume (Fig 3.13e) decreases, and the previous mobilized oil is displaced towards the producers and translates into an increased oil production rate initially.

Fig. 3.13f confirms the increase in recovery due to the NCG rising and displacing mobilized oil. The behaviour is consistent with experiments by Butler et al. (2000) and numerical work by worked (Austin-Adigio and Gates, 2019). As the NCG accumulates, the relative permeability of oil decreases, leading to reduced oil production. In Fig. 3.13f, all the NCG co-injection experienced an initial increase in oil production before lowering. As a result of optimization effects kick in, the oil production rate was kept mostly above the conventional SAGD rate, the additional oil recovered. Since the Base-NCG ($2.0\%mole$) was not optimized, the trend oil production rate became lower than Base SAGD, similar to observation by Austin-Adigio and Gates (2019). It can be inferred that proposed workflow was able to balance the steam and NCG requirement without significantly impeding relative permeability to oil.

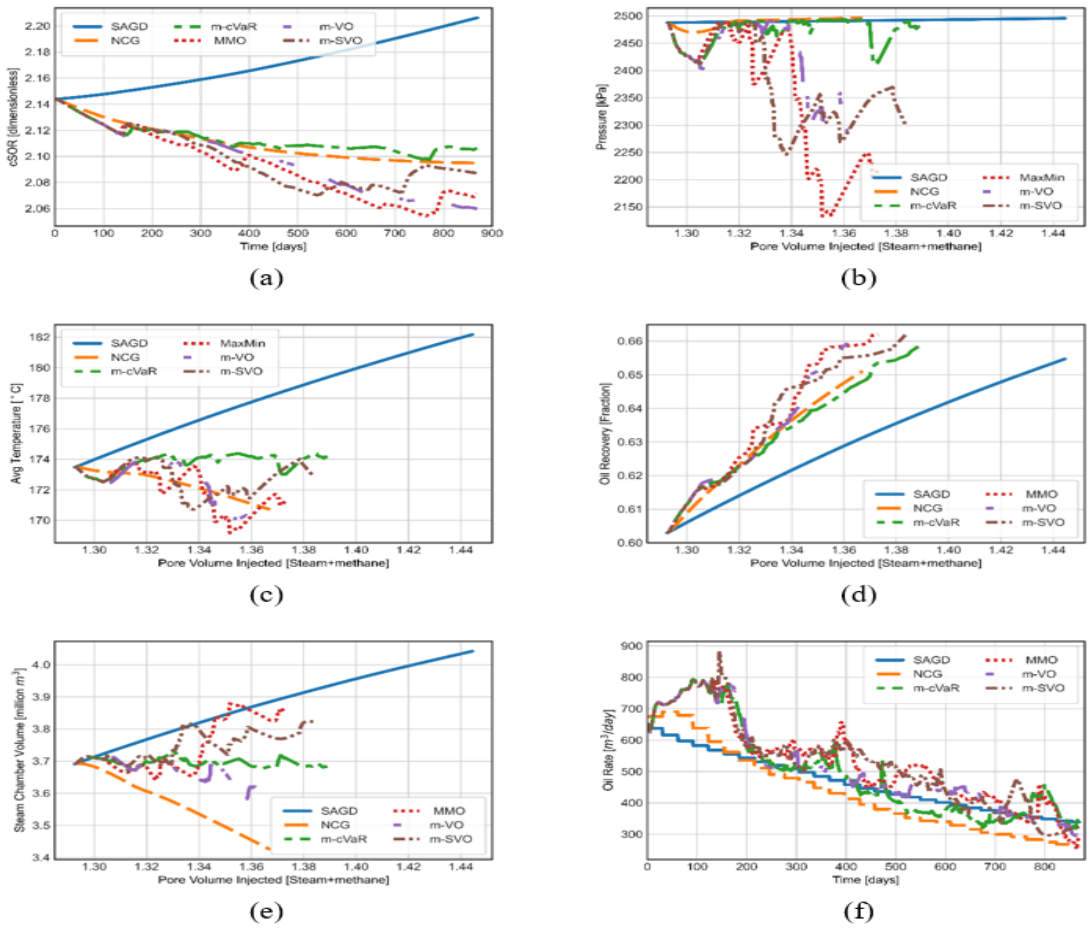

Figure 3.13: Comparison of SAGD and NCG performance (a)decreasing cSOR for SAGD while NCG decreases (b) average reservoir pressure constant for SAGD and unoptimized NCG but changes overtime for optimized SAGD because of changing injection ratio (c) average reservoir temperature following the changing injection ratio (d) oil recovery changing with injection ratio and shows higher recovery for optimized NCG (e) steam chamber development and (f) Oil rate generally higher for SAGD and unoptimized NCG evolution over time.

One of the significant drawbacks of SAGD is the high-water usage which can lead to higher feed water requirements and increased capital and operating costs. Additionally, this leads to high greenhouse gas emissions and possible competition for water resources for community use. SAGD NCG co-injection motivation is to mitigate these drawbacks. Two performance criteria are used to assess the environmental impact of NCG co-injection, as illustrated in Fig 3.14. The water (Equation 3.17) and gas (Eq 3.18) loss defined mathematically

as:

$$WaterBalance = \frac{Cum.SteamInjected_{CWE} - Cum.WaterProduced}{Cum.SteamInjected_{CWE}} \quad (3.17)$$

$$GasBalance = \frac{Cum.GasInjected - Cum.GasProduced}{Cum.GasInjected} \quad (3.18)$$

Doan et al. (2014) used the water loss to explain the performance of NCG co-injection at the Hangingstone Demonstration Project. Zero, almost zero water loss was achieved, meaning steam injection was balanced against water production. When NCG co-injection was switched to SAGD, that lead to an increase in the instantaneous cSOR. The results from Fig 3.14a show a similar trend as observed in the Hanginstone Demonstration Project of water balance of almost zero. In addition, no adverse effects on oil rate was also observed. In this study we are adopting the concept of water balance to gas balance. A zero loss means of produced water or gas is recycled and re-injected, which complies with environmental requirements of recycling 80% of the water produced. A positive water or gas loss means sequestration of injected fluids. In the case of methane or CO_2, it results in net carbon stored. *Fig 3.14*b shows a positive effect of NCG co-injection on methane sequestration after $130 days$ of initiation. On the other hand, negative balance leads to a negative impact on the environment because of water disposal and methane flaring impact. The results show water balance deacrease over time for all scenarios but the decrease was higher for the optimized cases (Fig. 3.14a). That indicates lowering of water make-up from other sources for steam injection as the produced water is completely recycled. For Fig. 3.14b the gas balance started as negative which means methane production was higher than produced (no sequestration) eventually became positive (sequestration). The optimized cases had lower positive balance compared to unoptimized NCG co-injection because of changing mole fraction. The workflow maintain a balanced between economics and sequestration of methane. The results further demonstrate the proposed workflow improves the economics of the SAGD recovery process while minimizing the environmental impact.

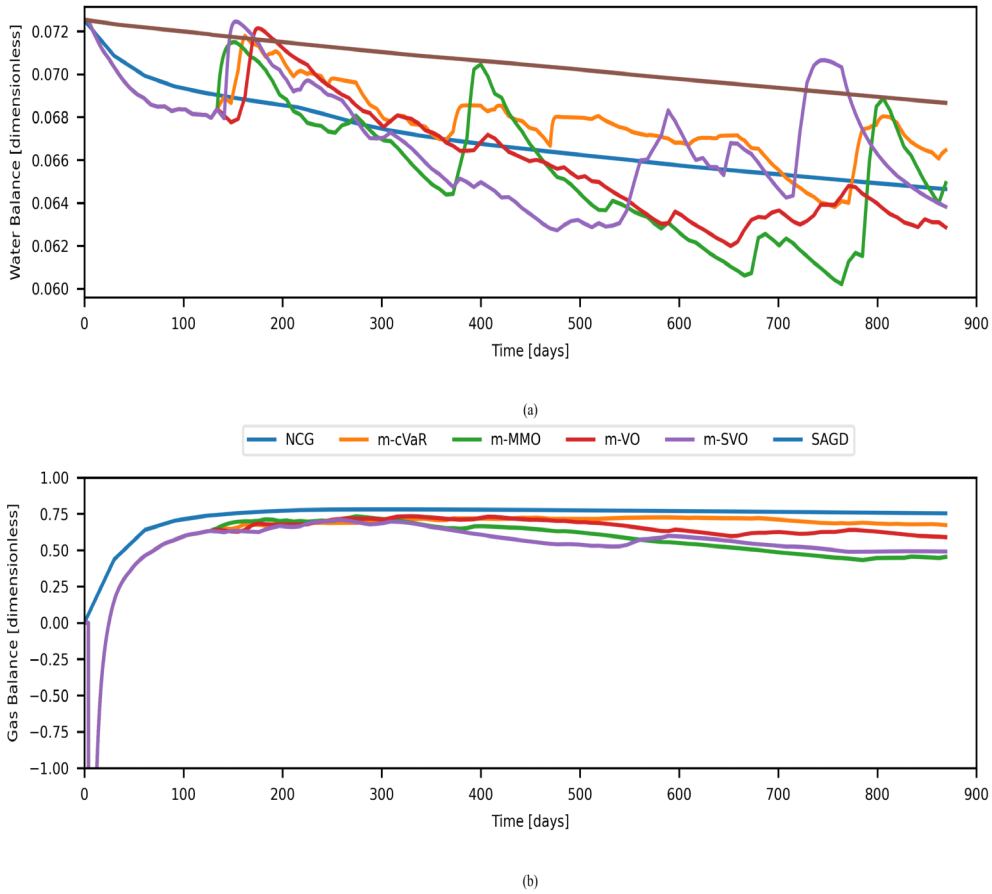

Figure 3.14: Injected fluid balance performance (a) decreasing water requirement as injection rate getting closer to production (b) gas (methane) sequestration overtime as the gas injection rate higher than produced.

3.6 Conclusion

The study describes a real-time workflow for risk mitigation in the SAGD NCG co-injection scheme in the presence of oil price uncertainty. The recursive workflow used to update the data-driven model during real-time production optimization demonstrates an approach to risk management that is computationally tractable. The risk management strategies considered in this study resulted in improved economic performance while minimizing adverse environmental impact. The following conclusions were drawn from the workflow assessment.

1. After assessing the workflow on different case studies, field NPV increased between $25\% - 77\%$. Field Cumulative SOR decreased between $4.5\% - 6.65\%$ of the steam optimized NCG co-injection than the base conventional SAGD case.

2. In all KPI metrics considered, the ultimate pad performance of NCG co-injection outperforms the base conventional SAGD case.

3. As shown in the NCG base case, NCG co-injection improves SAGD economics without requiring optimization. The proposed real-time optimization workflow improved the economics by an additional 1% incremental oil recovery, keeping oil production rates mostly above SAGD over a two-year four-month period, while the base NCG case initially increased and dropped.

4. The results from the optimization studies show that the risk-return formulation of MMO outperform all formulations.

The proposed workflow, in our opinion, has significant potential in daily, weekly, or short-term operational decision-making for heavy oil production.

Chapter 4

Distributed Real-Time Optimization of Multi-Pad Steam Allocation[1]

4.1 Introduction

Long-term SAGD performance is challenging to achieve. To achieve long-term aims and goals in a SAGD recovery life cycle, daily decisions such as steam chamber compliance, pressure, fluid balance, and subcool control are made. In addition, it is common for multiple pads with limited steam generating capacity to be physically linked via pipeline networks in SAGD development. For example, Fig 4.1 shows a multi-pad sharing a limited steam availability through a commonly connected flow line. As a result, optimizing operational decisions is critical if long-term goals are met.

Several SAGD RTO studies have been presented over the years. Vembadi et al. (2018) applied RTO to optimize steam chamber growth and NPV of the SAGD process using model predictive control to find the optimum rates and subcool temperature at each control horizon. Multi-input multi-output model predictive control of steam trap and oil rate has been shown to outperform multi-input single output stream trap control in the RTO of the SAGD process (Purkayastha et al., 2018). Sibaweihi et al. (2019) presented the SAGD RTO workflow with varying reservoir quality for each well-pair in

[1]A version has been submitted to SPE Reservoir Evaluation & Engineering and accepted for proceedings of SPE Canadian Energy Technology Conference and Exhibition 2023

the well-pad and variable steam availability. RTO workflow using linear and nonlinear model predictive control has been shown to ensure steam chamber conformance by optimizing subcool setpoints (Patel and Trivedi, 2020). In the above-reported studies, the SAGD process is represented by a data-driven proxy model to speed up computation. Although the data-driven models reported have a short-term prediction accuracy, (Guevara et al., 2021) proposed a reinforcement learning approach for long-term production optimization of the SAGD process. With RTO, the decision-making horizon is typically between days to weeks (Foss et al., 2009). Our recent work shows excellent performance when a multi-input multi-output Box-Jenkins data-driven model in RTO compared with the out-of-train-test response from the first-principle model (Sibaweihi and Trivedi, 2022). The Box-Jenkins data-driven model for short-term decision-making will be used in this work.

The RTO method decomposes long-term operational decisions to meet long-term goals and aims. In addition, the RTO approach reduces the computation cost needed for optimization; through decomposition in time and data-driven proxy models. However, as the SAGD process progresses, new well-pads come online with limited steam availability. As a result, the optimization problem complexity grows because of new wells added (optimization variable) competing for limited steam, increasing computational time. Most works on SAGD optimization are constrained to a maximum of a single pad (Guo et al., 2018; Sibaweihi and Trivedi, 2022). Few studies have tried to work on multi-pad optimization of the SAGD process. Card et al. (2014) presented a workflow for numerical tuning a multi-pad, multi-million grid cell SAGD model that reduced the computational time from over a month to seven days. Kumar et al. (2020) presented an entire field of 15 pads (96 well pairs) of SAGD steam allocation aided by artificial intelligence and machine learning algorithms to automate numerical tuning and dynamic gridding of a numerical model which runs in less than 24 hours for a ten-year simulation. The above workflows focused on long-term optimization. Multi-pad SAGD operations have a decentralized structure with a limited steam availability of coupled well-pads is suited for decomposition-based optimization approaches. Dantzig-Wolfe de-

composition approach (Gunnerud et al., 2009) and Lagrangian decomposition (Foss et al., 2009; Krishnamoorthy et al., 2018,?) are efficient in RTO by decomposing the original optimization problem into subproblems. Knudsen et al. (2014) presented a Lagrangian relaxation-based scheme to shut off multi-pad shale-gas systems. This work will implement the ADMM (Boyd et al., 2010) inequality constraints version of Maxeiner and Engell (2017).

Optimal ultimate recovery of SAGD operations is achieved by targeting the strategies of steam chamber growth, conductive heating, and infill wells production (Strobl et al., 2016). After the pre-heating stage of SAGD, steam is continuously injected to grow the chamber vertically and horizontally. At this stage, a low steam injection rate will stall steam chamber growth, which will affect SAGD performance because of a drop in reservoir pressure and temperature. RTO optimization decomposes long-term optimization into a series of short-term prediction horizons, treating each prediction horizon as a life-cycle optimization of the SAGD process. The economic performance of SAGD relies heavily on the cost of steam; hence, economic performance optimization will minimize the required steam to inject. In multi-pad steam allocation, the steam supply is limited, and if the steam allocation is not managed correctly, the steam chamber growth will stall and lead to deficient performance. A stalled steam chamber between a temperature of $80°C$ and $100°C$ at a barrier enables conductive heating underneath and adjacent to the steam chamber, resulting in residual oil saturation between 10% and 40% (Strobl et al., 2016). As a result, it is critical to define the RTO problem that accounts for the three strategies so that the long-term performance of SAGD is not jeopardized.

The RTO approach is a short-term technique that dictates the daily to weekly strategies of reservoir management, which in the medium to long-term results in a significant decline in recovery technique performance. In a study by van Essen et al. (2011), bi-objective hierarchical short and long-term performances were optimized as secondary and primary objectives while constraining the short-term performance to the optimal long-term performance. Chen et al. (2012) used uncertainty in the reservoir description to improve both long-term

and short-term NPV performance. They did this by optimizing short-term NPV performance over one or two years while ensuring that the long-term NPV performance stayed relatively high. Hasan et al. (2013) presented an approach that optimizes the long and short-term goals based on the prior ranking of the preference of the long and short-term goal performances using a multi-objective approach and introducing upper and lower bounds on the objectives. Shirangi et al. (2017) proposed a bi-objective long- and short-term NPV optimization alternative based on hierarchical joint optimization of long-term NPV performance and time-varying well control. The outer loop optimizes NPV while being limited by the modified internal rate of return, keeping cash flows from decreasing over time to the amount of capital invested. The inner loop optimizes the well controls. In the studies presented above, the long-short optimization problem does not apply to the RTO workflow because the decisions are based on the expected short-term response. The fact that the formulation is set up in a hierarchy also adds an extra cost to computing. Finally, Al-Aghbari et al. (2022) investigated different multi-objective function combinations to optimize waterflood management's short- and long-term performance. This study proposed using a single objective approach in RTO workflow, a short-term operations strategy optimization workflow that achieves both short- and long-term performance goals. The studies that came before are long-term optimization workflows made to meet short-term and long-term performance goals.

The contribution of this study is the multi-pad steam allocation distributed RTO with limited steam availability that maximizes short-long-term economic performance, lowering cumulative steam-oil-ratio (cSOR), stabilizing production, and leading to longer SAGD production life. The pads are drilled with all required wells from day one of the start of the operation to account for the infill production strategy. Six different case studies are presented to implement the above contribution. In addition, NPV, cSOR, recovery factor (RF), average temperature, and alternating NPV-RF based on time and temperature KPI optimization problem formulation that maximizes steam chamber growth and maximize economic returns are investigated. The formulations are tested on a

field with four pads with average pad temperature after two years of operation between 70 to 90^oC to mimic the impact of RTO KPI on balancing steam chamber growth while maximizing long-term economic performance. The rest of the paper is organized: (1) Data-driven model development, (2) Distributed real-time multiped steam allocation, (3) reservoir model, (4) results and discussion (5) conclusion.

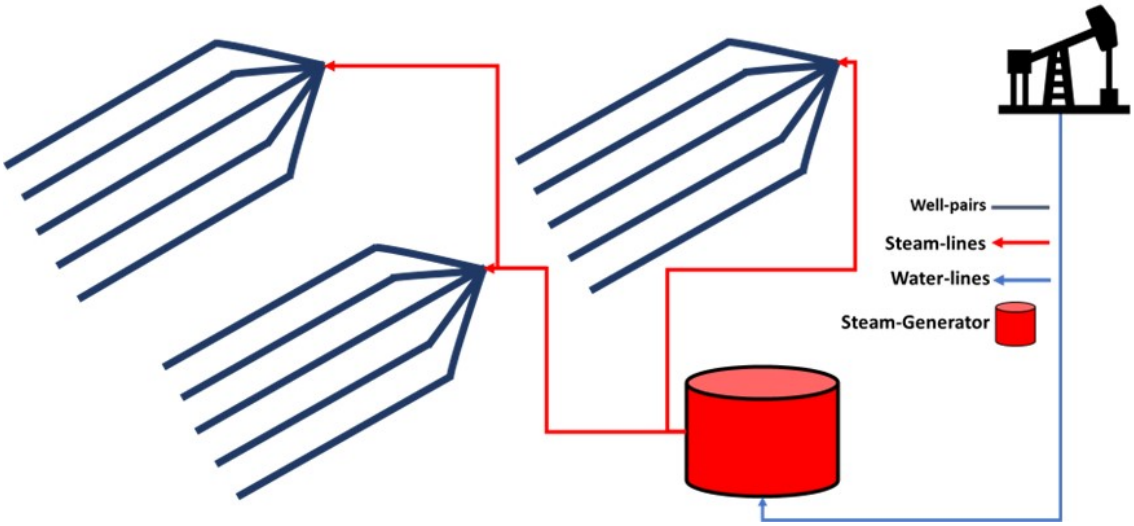

Figure 4.1: Schematic topology of multi-pad SAGD production system

4.2 Data-Driven Model Development

The first stage is to collect data from the SAGD reservoir. Next, a reservoir simulator will be employed as a data generator or surrogate for an actual field. Next, zero-mean noise is applied to the recorded data before the data is normalized for data-driven model building. Finally, the observed time-series data is transformed between 0 and 100 using min-max normalization, depending on the feature min-max engineering, environmental, and equipment limits. After the data-preprocessing, prediction error minimization is performed to train the data-driven model using the Box-Jenkins approach. MATLAB system identification toolbox (MATLAB, 2021) is used to build the data-driven model for the SAGD process.

Equation 4.1 stands for a Box-Jenkins model structure for dynamic sys-

tems. Here, the input ($u\,(t)$: steam injection rate) at any time (t) is related to the output ($\widehat{y}\,(t)$: Liquid rate or water cut). The backward shift operator (z^{-1}) enables the process and disturbance transfer functions to consider the impact of the previous inputs on the current output. Finally, Sibaweihi and Trivedi (2022) outline the process of training and validating. This work employs two data-driven models: a multi-input multi-output pad model for forecasting well-pairs in pad production parameters like liquid rate, water-cut, gas-oil-ratio, and a single-input single-output pad average temperature forecasting data-driven model.

Box-Jenkins Model (BJ)

$$\hat{y}\,(t) = \frac{B\,(z^{-1})}{F\,(z^{-1})}u\,(t) + \frac{C\,(z^{-1})}{D\,(z^{-1})}e\,(t) \tag{4.1}$$

$$B\,(z^{-1}) = b_1 z^{-1} + \cdots + b_{nb} z^{-nb}$$
$$C\,(z^{-1}) = 1 + c_1 z^{-1} + \cdots + c_{nc} z^{-nc}$$
$$D\,(z^{-1}) = 1 + d z^{-1} + \cdots + d_{nd} z^{-nd}$$
$$F\,(z^{-1}) = 1 + f_1 z^{-1} + \cdots + f_{nf} z^{-nf}$$

4.2.1 Data-Driven Model Forecast Validation.

Data-driven model forecast outputs will be validated using modified Kling-Gupta efficiency (Equation 4.2–4.3). The first term of the equation uses Pearson Correlation (Equation 4.2) with a range between 1 to -1. The data-driven forecasts ($\widehat{y}_i$) and the mean of the forecast $\left(\overline{\widehat{y}}\right)$ at each time (t) is correlated with the measured ($\overline{y}$) and mean of the measured outputs ($\overline{y}$) to determine the data-driven model performance. The Pearson correlation is sensitive to outliers (Legates and McCabe, 1999) which requires to be factored in model performance evaluation. The objective of temporal dynamics modeling is to mimic the system dynamics measured by r while preserving the flow distribution. The goal is achieved by assessing the bias (β) and the variability (γ) ratios, with optimum values of each term being 1. The μ and σ are the mean and standard deviation of the forecast (f) and measured (m) outputs. With the performance of the data-driven model decomposed with KGE, the relative contribution of each term can be estimated to understand which term is

contributing to poor or good model performance. A skill score (ss) metric, as defined in Equation 4, is used in this work to evaluate the performance of the data-driven model skill score (ss) metric is used (Equation 4.4). Using a mean forecaster model as a benchmark with a $\mathrm{KGE}^{'} = -0.41$ derived by assuming $\mu_f = \mu_m,\ \sigma_m \neq 0$ and $\sigma_f = 0$ (Knoben et al., 2019). Positive ss indicates a data-driven model preferred to benchmark and negative ss indicates a benchmark preferred to a data-driven model.

Pearson Correlation

$$r = \frac{\sum_{t=1}^{N_p} (y_t - \overline{y}) \left(\widehat{y}_t - \overline{\widehat{y}}\right)}{\sqrt{\sum_{t=1}^{N_p} (y_i - \overline{y})^2} \sqrt{\sum_{t=1}^{N_p} \left(\widehat{y}_t - \overline{\widehat{y}}\right)^2}}, \qquad -1 \leq r \leq 1 \tag{4.2}$$

Modified Kling-Gupta Efficiency (Kling et al., 2012)

$$KGE\prime = 1 - \sqrt{(r-1)^2 + (\beta - 1)^2 + (\gamma - 1)^2}, \tag{4.3}$$

$$-0.41 < KGE\prime \leq 1$$

$$\beta = \frac{\mu_f}{\mu_m}$$

$$\gamma = \frac{\sigma_f / \mu_f}{\sigma_m / \mu_m}$$

Skill score (Knoben et al., 2019)

$$ss = \frac{\mathrm{KGE}^{'}_{\text{model}} - \mathrm{KGE}^{'}_{\text{benchmark}}}{1 - \mathrm{KGE}^{'}_{\text{benchmark}}} \tag{4.4}$$

4.3 Distributed Real-time Multi-Pad Steam Allocation

4.3.1 Optimization Problem.

Managing a single pad within a multi-pad SAGD operation involves finding the optimum steam allocation to individual well-pairs in the pad that maximizes the return on investment. The main KPI for SAGD process optimization is net-present-value (NPV), defined in Equation 4.5. Where the steam injection rate (u) is the manipulated variable at each control horizon. For each well (j) at the time (t), the sum of the difference between the revenue (the oil production rate $[\widehat{y}_{o,j}(t)]$) and cost (steam injection $[u_{s,j}(t)]$, produced water $[\widehat{y}_{w,j}(t)]$, transportation and blending of oil, royalty rate) over the prediction horizon (P) is discounted and then summed over total wells (N_w) in the model. The allocation of steam to each well-pair is constrained subject to ($s.t.$) minimum ($u_j^{\min}$), and maximum ($u_j^{\max}$) steam injection rate. Instabilities in the SAGD steam allocation changes (Δu_j) are constrained between the next prediction horizons to a minimum ($\Delta u_j^{\min}$) and maximum ($u_j^{\max}$) steam injection rate for each well-pair in the pad. The steam available $u_j^{\max}$ is limited, which is denoted by $\overline{u}$. Table 4.1(Alexey, 2018).

$$J(\mathbf{u}) = \sum_{j=1}^{N_w} \sum_{t=1}^{P} \frac{(p_o \widehat{y}_{o,j}(t) - p_w \widehat{y}_{w,j}(t) - p_r p_o \widehat{y}_{o,j}(t) - p_s u_{s,j}(t) - p_{\text{otbc}} \widehat{y}_{o,j}(t))}{(1+D)^{\Delta t}} \tag{4.5}$$

$$\begin{gathered} \text{s.t.} \quad u_j^{\min} \leq u_j \leq u_j^{\max} \\ \Delta u_j^{\min} \leq \Delta u_j \leq \Delta u_j^{\max} \\ \textstyle\sum_{j=1}^{N_w} \mathbf{u}_j \leq \overline{u} \end{gathered}$$

Field-wide multi-pad optimization of the SAGD process considers all pads currently in operation and share the same steam generator through the connectivity of a flow line. Therefore, the RTO for a multi-pad is reformulated as Equation 4.6. Feasibility is achieved with RTO if the complicating constraint is honored. The sum of all steam allocations to each pad ($\overline{\mathbf{u}}_i$) should be equal

Table 4.1: Economic input parameters

Description	Value
Price of oil [p_o]	60 USD/bbl.
Steam processing cost [p_s]	6 USD/bbl.
Produced water processing cost [p_w]	1.96 USD/bbl.
the transportation and blending cost of oil [p_{otbc}]	4.95 USD/bbl.
Royalty rate [p_r]	2%
Discount factor (D)	10%

to or less than the maximum available steam ($\overline{U}$). A centralized optimization structure is recommended to solve multi-pad optimization, as shown in earlier works with CMG-CMOST (Card et al., 2014; Kumar et al., 2020). The challenge with the centralized approach is that as the number of well-pads to allocate steam increases, the optimization problem becomes too large for a single computer to handle. Another issue arises with competing demand for steam because of various stages of SAGD maturity and reservoir heterogeneity, complicating the optimization problem. A requirement for distributed optimization is communication between a coordinator and the sub-systems with the aim of the coordinator exchanging information between the sub-systems to steer the optimization problem toward a feasible solution.

$$\max_{u_i \in U_i \forall_i} \sum_{i=1}^{N_p} J_i\left(\mathbf{u}_i\right) \tag{4.6}$$

$$\text{s.t.} \quad \textstyle\sum_{i=1}^{N_p} \overline{\mathbf{u}}_i \leq \overline{U}$$

Besides NPV, three other KPIs were used in this study. The recovery factor, cumulative steam-oil ratio (cSOR), and average temperature. The optimization problem formulation follows the same as NPV. In the following subsections, J_i represents any of the KPI for each pad.

4.3.2 Distributed Optimization.

The iterative ADMM coordination algorithm used in this work for multi-pad RTO is based on Maxeiner and Engell (2017). For Eqn 3 to be separable, a slack variable ($z|\sum_{i=1}^{N_p} z_i = \overline{U}$) or globally feasible solutions is introduced as additional constraint. Reformulation of the centralized optimization problem into a distributed problem is achieved by Lagrangian relaxation (dual decomposition) of Equation 4.6 complemented with a quadratic penalty term as mathematically described in Equation 4.7. The complicating constraint function is multiplied by the dual variable ($\lambda^{k,T}$) which is the marginal cost to relax the constraint at each iteration (k). In addition, a penalty term (ρ^k) is added to the distributed reformulation to ensure each pad uses allocated resource and steer the solution toward global feasibility. Each pad (i) receives a vector of globally feasible solutions ($\mathbf{z}_i^k$) as a reference for the individual pads in addition to the dual vector ($\lambda^{k,T}$) and solves the optimization problem in parallel (Equation 4.8). The procedure for multi-pad real-time optimization workflow is described in Algorithm 1.

$$\max_{u_i \in U_i \forall_i} \sum_{i=1}^{N_p} J_i\left(\overline{\mathbf{u}}_i\right) + \lambda^{k,T} \sum_{i=1}^{N_p} \left(\overline{\mathbf{u}}_i - \mathbf{z}_i^k\right) + \frac{\rho^k}{2} \sum_{i=1}^{N_p} \left\|\overline{\mathbf{u}}_i - \mathbf{z}_i^k\right\|_2^2 \tag{4.7}$$

$$\max_{u_i \in U_i} J_i\left(\overline{\mathbf{u}}_i\right) + \lambda^{k,T} \left(\overline{\mathbf{u}}_i - \mathbf{z}_i^k\right) + \frac{\rho^k}{2} \left\|\overline{\mathbf{u}}_i - \mathbf{z}_i^k\right\|_2^2 \ \forall_i \tag{4.8}$$

ADMM iterates between the coordinator and pad after initializing user-defined convergence thresholds, price vectors, or dual variables. As shown in Fig 4.2, the coordinator sends the dual variables ($\lambda^{k,T}$), penalty (ρ^k) and feasible global solutions ($\mathbf{z}_i^k$) to each pad to optimize KPI. After optimization of all pads is done, the coordinator compares the sum of the optimal pad steam allocations ($\overline{\mathbf{u}}_i$) returned by each pad to available steam ($\overline{U}$). The difference between the available steam and the sum of optimal steam allocations (Equation 4.9) or primal feasibility from optimization is used to check global constraint violation at iteration (k). If the primal infeasibility ($\phi_{\text{primal}}^{k+1}$) is less than a pre-defined constraint violation tolerance (eps), then feasible steam allocation has been achieved. The dual infeasibility (ϕ_{dual}^{k+1}) which is a product

of the last penalty, and the absolute difference of means of steam allocated to pads between the next prediction horizons, measures convergence of prediction horizons. Maxeiner and Engell (2017) study used primal and dual feasibility to check global constraint satisfaction in Equation 4.6. The Equation 4.5 constraint for allowable steam allocation changes (Δu_j) performs the same role as the ϕ_{dual}^{k+1} . If primal infeasibility is higher than *eps*, update ($\lambda^{k,T}$, ρ^k, $\mathbf{z}_i^k$) to improve on the convergence. Equation 4.11-4.13 are used in updating $\lambda^{k,T}$, ρ^k, $\mathbf{z}_i^k$ for the next iteration. Since in this study, only the $\phi_{\text{primal}}^{k+1}$ is used as the check on steam availability violation; only the first condition must be honored. The study implemented an inequality constraint as in Maxeiner and Engell (2017) hence λ^{k+1} and $\mathbf{z}_i^k$ have to be positive for feasibility to be achieved. Table 4.2 shows the ADMM coordination parameters in this study. Algorithm 1 shows the steps to solve the multi-pad coordination optimization with ADMM.

$$\phi_{\text{primal}}^{k+1} = \sum_{i=1}^{N_p} \overline{\mathbf{u}}_i{}^{k+1} - \overline{U} \tag{4.9}$$

$$\phi_{\text{dual}}^{k+1} = \rho^k \left| \overline{u}^{k+1} - \overline{u}^k \right| \tag{4.10}$$

$$\lambda^{k+\frac{1}{2}} = \begin{cases} \lambda^k + \nu\rho^k \phi_{primal}^{k+1} & if \phi_{primal}^{k+1} \geq 0 \\ \lambda^k + \rho^k \phi_{primal}^{k+1} & if \phi_{primal}^{k+1} < 0 \end{cases} \tag{4.11}$$

$$\lambda^{k+1} = max\left(0, \lambda^{k+\frac{1}{2}}\right)$$

$$z_i^{k+\frac{1}{2}} = \begin{cases} \overline{u}_i^{k+1} + \frac{\phi_{\text{primal}}^{k+1}}{N_p}, & if\ \phi_{\text{primal}}^{k+1} \geq 0 \\ \overline{u}_i^{k+1} & \text{else} \end{cases} \tag{4.12}$$

$$z_i^{k+1} = max\left(0, \quad z_i^{k+\frac{1}{2}}\right)$$

$$\rho^{k+1} = \begin{cases} \rho^k \alpha_{\text{Incr}}, & if\ \phi_{\text{primal}}^{k+1} > \beta\phi_{\text{dual}}^{k+1} \\ \rho^k \alpha_{\text{Decr}}, & if\ \phi_{\text{primal}}^{k+1}\beta < \phi_{\text{dual}}^{k+1} \\ \rho^k & \text{else} \end{cases} \tag{4.13}$$

Table 4.2: Coordination parameters

PARAMETER	VALUE
Maximum iteration $[k_{max}]$	10
Initial dual variables $[\lambda^0]$	$100 * \aleph(0,1)$
Initial feasible global solutions $[z^0]$	Previous horizon allocations
Initial penalty $[\rho^0]$	1
Dual variable step-size decrement $[v]$	0.7
Primal-dual feasibility $[\beta]$	2
Penalty increment $[\alpha_{Incr}]$	1.1
Penalty decrement $[\alpha_{Decr}]$	0.9
Constraint violation tolerance $[eps]$	$1e-6$

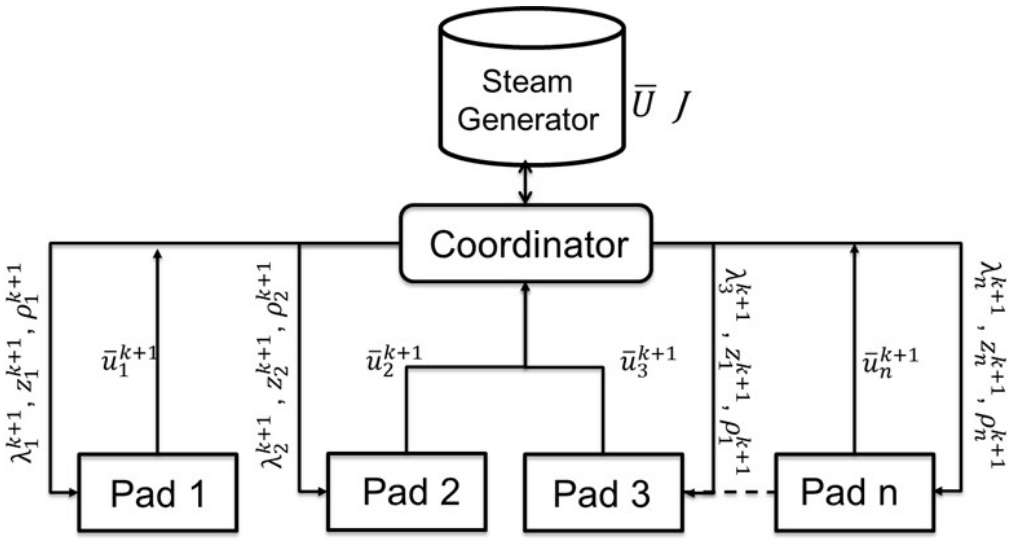

Figure 4.2: Communication scheme between the pads and the coordinator

Algorithm 1: Alternating Direction Method of Multipliers

Inputs: $k_{max}, eps, \alpha_{Decr}, \alpha_{Incr}, \beta, v, \lambda^0, z^0, \rho^0$.
Initialize: $k = 1$, *Convergence = False.*
while $\mathbf{k} \leq \mathbf{k_{max}} \wedge \neg$**Convergence** do

For each pad (**i**), do

$$\overline{\mathbf{u}}_{\mathbf{i,opt}} = \max_{\mathbf{u_i} \in \mathbf{U_i}} \mathbf{J_i}\left(\mathbf{u_i}\right) + \lambda^{\mathbf{k,T}}\left(\overline{\mathbf{u}}_{\mathbf{i}} - \mathbf{z}_{\mathbf{i}}^{\mathbf{k}}\right) + \frac{\rho^{\mathbf{k}}}{\mathbf{2}}\left\|\overline{\mathbf{u}}_{\mathbf{i}} - \mathbf{z}_{\mathbf{i}}^{\mathbf{k}}\right\|_{\mathbf{2}}^{\mathbf{2}}$$

end for

$\phi_{\text{primal}}^{\mathbf{k+1}} = \sum_{\mathbf{i=1}}^{\mathbf{N_P}} \overline{\mathbf{u}}_{\mathbf{i}}^{\mathbf{k+1}} - \overline{\mathbf{U}}\phi_{\text{dual}}^{\mathbf{k+1}} = \rho^{\mathbf{k}}\left|\overline{\mathbf{u}}^{\mathbf{k+1}} - \overline{\mathbf{u}}^{\mathbf{k}}\right|$
if $\phi_{\text{primal}}^{\mathbf{k+1}} <$ **eps** then
Convergence = True
else

$$\lambda^{\mathbf{k}+\frac{\mathbf{1}}{\mathbf{2}}} = \lambda^{\mathbf{k}} + \mathbf{v}\rho^{\mathbf{k}}\phi_{\text{primal}}^{\mathbf{k+1}}$$

$\lambda^{k+1} = max\left(0, \lambda^{k+\frac{1}{2}}\right)$

$$\mathbf{z}_{\mathbf{i}}^{\mathbf{k}+\frac{\mathbf{1}}{\mathbf{2}}} = \begin{cases} \overline{\mathbf{u}}_{\mathbf{i}}^{\mathbf{k+1}} + \frac{\phi_{\text{primal}}^{\mathbf{k+1}}}{\mathbf{N_P}}, & \textbf{if } \phi_{\text{primal}}^{\mathbf{k+1}} \geq \mathbf{0} \\ \overline{\mathbf{u}}_{\mathbf{i}}^{\mathbf{k+1}} & \text{else} \end{cases}$$

$$\mathbf{z}_{\mathbf{i}}^{\mathbf{k+1}} = \mathbf{max}\left(\mathbf{0},\ \mathbf{z}_{\mathbf{i}}^{\mathbf{k}+\frac{\mathbf{1}}{\mathbf{2}}}\right)$$

$$\rho^{\mathbf{k+1}} = \begin{cases} \rho^{\mathbf{k}}\alpha_{\text{Incr}}, & \textbf{if } \phi_{\text{primal}}^{\mathbf{k+1}} > \beta\phi_{\text{dual}}^{\mathbf{k+1}} \\ \rho^{\mathbf{k}}\alpha_{\text{Decr}}, & \textbf{if } \phi_{\text{primal}}^{\mathbf{k+1}}\beta < \phi_{\text{dual}}^{\mathbf{k+1}} \\ \rho^{\mathbf{k}} & \text{else} \end{cases}$$

end if

$$\mathbf{k} \leftarrow \mathbf{k} + \mathbf{1}$$

end while
Output: $\overline{\mathbf{u}}_{\text{opt}}$

4.3.3 RTO Implementation.

Algorithm 2 describes the steps involved in RTO; it uses real-time data from a heavy oil reservoir to develop a data analytic predictive model using a system identification approach. First, the digital heavy oil reservoir is represented using CMG-STARS (CMG, 2021). Next, a distributed optimization is performed for each pad. A constrained genetic algorithm (Blank and Deb, 2020) is used to optimize each pad. After a distributed nonlinear optimization using the prediction model, the optimally allocated steam is assigned to the heavy oil reservoir. Next, a data collecting system records the reservoir's reaction. Finally, the predictive model is updated using the freshly recorded reservoir response to improve forecast performance. The process exits the recursive cycle when it is no longer profitable to continue producing using SAGD or stopping time.

Two proposed RTO implementation is presented. First, with the alternating implementation, the objective of the horizon is alternated either based on time or pad average temperature. Then, in Algorithm 2, step 4 NPV or recovery for all pads is optimized for time-based alternation. For example, in this study, in the first three months, at step 4 of Algorithm 2, NPV is optimized by finding the minimum steam injection rates that recover most of the mobile bitumen saturation at an economical rate. The optimum injected steam at this stage slows the steam chamber temperature drop due to mobile bitumen depletion. Then, for the next six months, bitumen recovery is optimized. Recovering more of the bitumen initially in place means injecting steam at a higher rate for steam chamber growth to mobilize the immobile bitumen saturation. The steam chamber growth cycle stalling to drain mobile bitumen saturation and injecting at a high rate to expand the steam chamber is repeated until the end of optimization. The objective is to moderate steam chamber expansion and minimize heat losses to the surroundings while economically producing bitumen.

The second proposed implementation is based on the average pad temperature. Therefore, at the start of each horizon optimization (i.e., Algorithm

2, step 4), a check is done on the past three months of average pad temperature. If the average temperature in the pad stayed above $90 \circ C$ for the past three months, set the objective of optimization to NPV. Else, if the average temperature in the pad stayed below $80 \circ C$ for the past three months, set the objective of optimization to recovery to expand the steam chamber. The performance of the proposed implementation hinges on the data-driven model learning the physics of the SAGD process and optimization problem formulation. The model response will decrease steam chamber growth, steam injection, and liquid production rate over time during NPV optimization and vice versa during recovery optimization. For the first proposed case, all pads in the reservoir will either be optimizing NPV or recovery independent of steam chamber maturity. In the second proposed case, either all pads optimize NPV or recovery simultaneously, or some pads optimize NPV while the rest optimizes recovery. Equation 4.7 is a centralized optimization approach as used in software like CMG-CMOST. The second proposed case is possible for each pad with a different objective because the optimization problem has been decomposed (Equation 4.8). If a feasible solution is achieved, the second and third terms of Equation 4.8 will diminish. More importantly, in the ADMM iterative updating (Equation 4.9 - 4.13), the information required to coordinate is the optimum allocated steam or resource. Hence a different objective can be set for each pad, which makes this approach helpful when allocating steam in a multi-pad system pad with pads at different stages of steam chamber maturity.

Algorithm 2: Real-Time Multi-Pad Steam Allocation

For every time step **t = 7 days**.

1. Read the previous production and injection rates.
2. Normalize the previously recorded data based on each parameter's physical or operating constraint (range).
3. Identify the structure and parameters or update the parameters of the data-driven model
4. Perform distributed optimization using ADMM (Algorithm 1)
5. Apply optimal injection controls to the digital heavy oil reservoir
6. Record the response (production and injection rates) of the reservoir to the optimal control setpoints
7. $\mathbf{t = t + 1}$
8. Repeat steps $1 - 7$ until it is not profitable or the end of field life.

4.4 Reservoir Model

A synthetic 3D reservoir representative of the Western Canada oilfield for optimizing the multi-pad steam allocation consisting of four SAGD pads with 33 well-pairs is used. The reservoir has an average porosity of 0.31 and average horizontal and vertical permeabilities of 4372 mD and 3497 mD. Fig 4.3 displays the well-pad's permeability distribution, and Table 4.3 lists this study's reservoir properties.

During the pre-heating phase, each well-pair is heated for four months. The constraints for the injection wells were set at a maximum steam injection rate of 750 m^3/day (cold water equivalent, CWE) and a maximum injection pressure of 4000 kPa. The injection steam quality of 0.95 at a temperature of 250^oC. The production wells have a primary constraint of 2000 kPa bottom hole pressure and a secondary constraint of $1000m^3/day$ surface liquid rate. In addition, a maximum steam production rate of 10 m^3/day is set to mimic steam trap control. PAD-A consists of nine well-pairs, while PAD B to D consists of eight well pairs with all well-pairs with a length of 760 m to achieve an economical oil production rate (Jimenez, 2008). Normal SAGD operation is initiated after the circulation stage for two years, then RTO is initiated and lasts for three and half years. For the first two years, the steam injection is

designed to ensure that the average pad temperature is between 70^oC and 100^oC to ensure fluid mobility within each pad, like establishing inter-well fluid mobility and communication during the circulation phase (Shen, 2013). Pads A to D achieved average pad temperatures of 77^oC, 78^oC, 72^oC, and 90^oC, respectively.

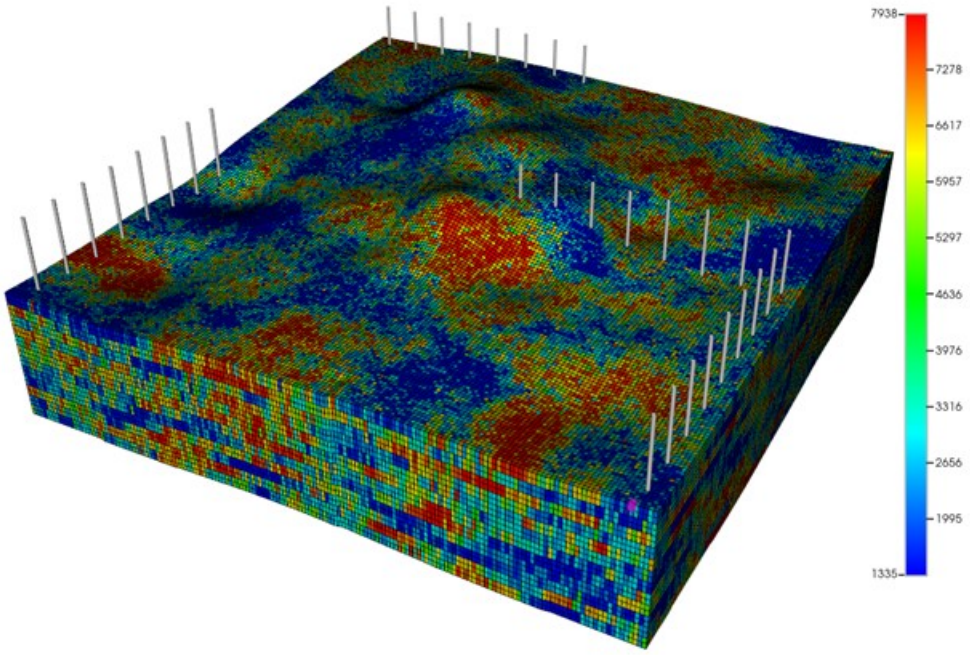

Figure 4.3: Permeability distribution

4.5 Results and Discussion

Multi-pad steam allocation optimization aims to enhance SAGD economics by lowering water and fuel consumption, which will reduce greenhouse gas emissions by reducing SOR. RTO treats each horizon optimization like a long-term optimization problem. The results for a multi-pad RTO that ensures long-term goals are met are presented. The first part of this section presents the validation of the data-driven model forecast performance to reservoir response. The second part presents the results of the different SAGD KPIs that guarantee that the RTO's long-term objectives are met. Six cases were created to evaluate the performance of optimization of short-term SAGD KPI that meets

Table 4.3: Reservoir model properties

PARAMETER	VALUE
Formation temperature [°C]	12
Initial reservoir pressure at $210m$ [Kpa]	1200
Average horizontal permeability [mD]	4372
Average vertical permeability [mD]	3497
Average porosity [fraction]	0.31
Average water saturation [fraction]	0.2
Steam injection pressure [kPa]	4000
Steam quality	0.95
Oil viscosity @ reservoir temperature [cP]	$1.42e6$
Rock heat capacity [J/m^3-C]	$2.3e6$
Thermal conductivity of Rock [J/m^3-day-C]	$2.7e5$
Thermal conductivity of Gas [J/m^3-day-C]	4000
Thermal conductivity of Oil [J/m^3-day-C]	$1.2e4$
Thermal conductivity of Water [J/m^3-day-C]	$5.4e4$

long-term goals. The first two cases (NPV and cSOR) are one of the main SAGD KPIs reported in the literature for long-term cost minimization optimization. RF and Temp are the other KPIs that indicate process efficiency. A particular KPI is optimized for each case in a single optimization study. Each case's performance relative to all four selected KPIs are compared at the RTO's end. The plots for this section are based on the response of the reservoir except when indicated

4.5.1 Data-Driven Reservoir Model Validation.

Two main models were used in this study. The first model is the pad's single input (steam rate) and single-output (average temperature). As shown in Fig 4.4, there is an excellent match between the data-driven model forecast and the response from the reservoir. The calibrated model used during optimization periods for forecasting the average temperature of the pad performance statistics is presented in Table 4.3. Column one, the correlation (r) indicative of the model timing errors, is one for all pads, which is the optimum expected. The bias (β) and variability ratios (γ) are the columns three and four, with both metrics at one optimum or close to one. KGE greater than 0.6 is considered to be a good model performance. Table 4.4, column five observed that

all pads recorded KGE' of approximately 0.97. The performance is consistent with the results in Fig 4.4. Column six, the skill score (ss) benchmarks the data-driven performance to a mean flow predictor with $KGE' \approx -0.4$. All data-driven model forecast in column six is greater than zero or close to one, indicating a nearly perfect forecast and better than the benchmark.

The second data-driven model is for each unique well-pair, single input (steam rate) and multi-output (Liquid rate, water-cut). Figs 4.5 and 4.6 show the evolution of the model forecasted performance and system response (numerical or digital reservoir) for Well_8 of the four pads. The plots show a close agreement between data-driven forecasted liquid rate and water cut correlates with the reservoir response. The calibrated data-driven model did not just pass the train-test threshold but also learned the SAGD process's physics. The curves of Figs 4.5 and 4.6 for all the pads show the model responding to steam rate perturbation during RTO. In Fig 4.5c, at approximately day 800, the data-driven model estimated liquid rate is zero because the model forecasted a wrong value at the time. The estimate is set to the physical or operational maximum or the minimum of that input or output. Tables 4.5 and 4.6 in the appendix show the statistical performance for the liquid rate and water cut forecast for wells within each pad. Similarly, to pad average temperature performance, the liquid rate and water cut forecast performance are in close agreement with the reservoir response except for the PAD_C Well_5 water cut forecast. The KGE and ss values for Well_5 are -1.337 and -0.6572, respectively, lower than the minimum threshold performance of greater than 0.6 and -0.4 for model acceptance. Even though the bias ratio is close to the optimum value of one, the KGE value is less than the minimum threshold because KGE cannot be more than the lowest value of its components (r, β,γ).

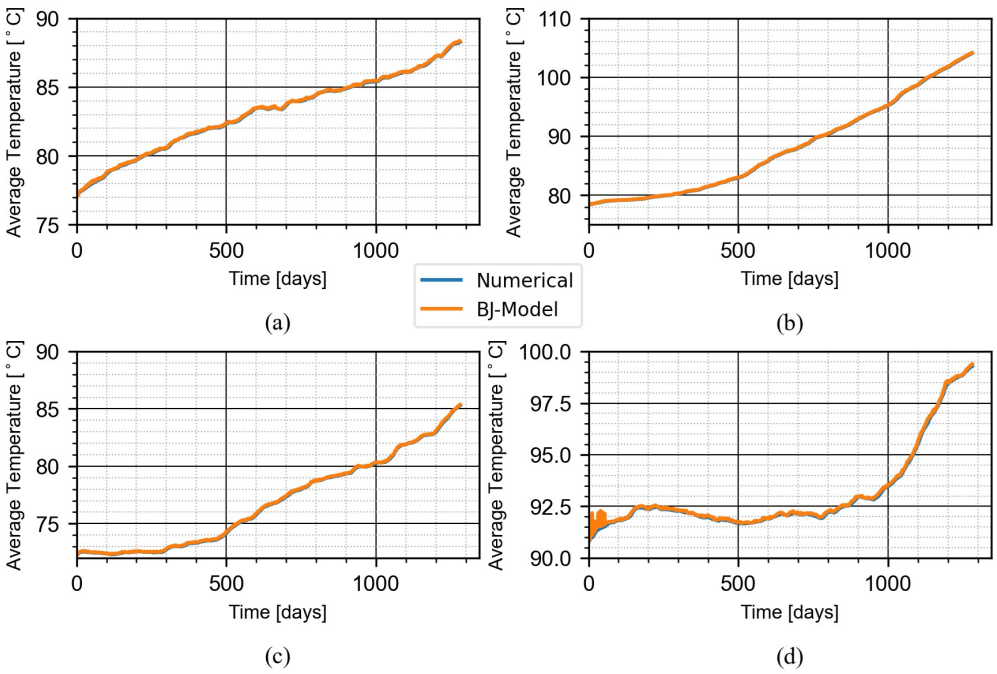

Figure 4.4: Forecasted (BJ-Model) and response (Numerical) average temperature during RTO for (a) PAD_A (b) PAD_B (c) PAD_C (d) PAD_D of bitumen recovery KPI.

Table 4.4: Average temperature model forecast dimensionless validation performance

	r	β	γ	KGE'	ss
PAD_A	1.000	0.999	0.98	0.977	0.9836
PAD_B	1.000	0.999	0.98	0.977	0.9833
PAD_C	1.000	1.000	0.975	0.975	0.9826
PAD_D	1.000	1.000	0.974	0.974	0.9816

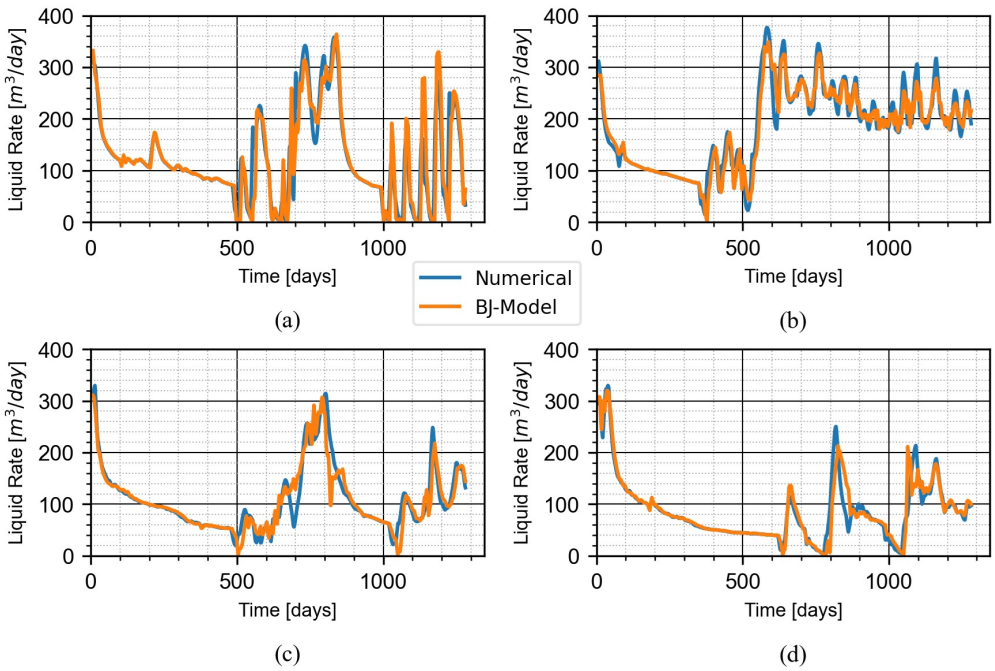

Figure 4.5: Forecasted (BJ-Model) and response (Numerical) liquid rate of well_8 during RTO for (a) PAD_A (b) PAD_B (c) PAD_C (d) PAD_D of bitumen recovery KPI.

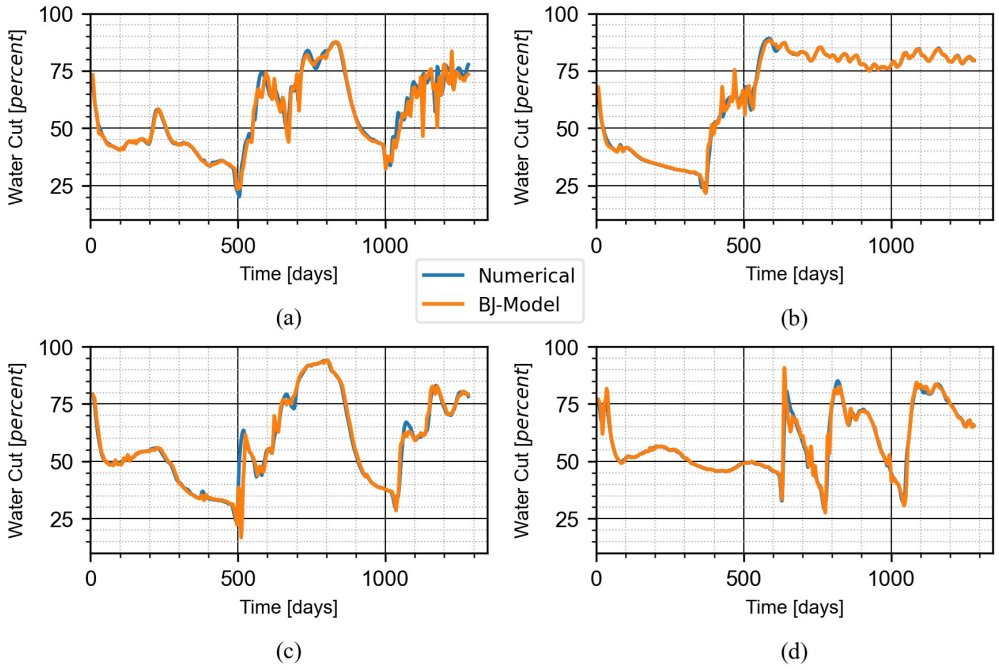

Figure 4.6: Forecasted (BJ-Model) and response (Numerical) water cut of well_8 during RTO for (a) PAD_A (b) PAD_B (c) PAD_C (d) PAD_D of bitumen recovery KPI.

Table 4.5: Liquid rate model forecast dimensionless validation performance

	r	β	γ	KGE'	ss	
PAD_A	**Well_1**	0.996	0.996	1.007	0.991	0.9935
	Well_2	0.999	1.000	0.998	0.998	0.9987
	Well_3	0.913	1.010	1.043	0.902	0.9306
	Well_4	0.949	1.000	0.976	0.943	0.9598
	Well_5	0.996	1.000	0.995	0.994	0.9955
	Well_6	0.995	1.000	0.989	0.988	0.9917
	Well_7	0.658	1.014	1.188	0.610	0.7234
	Well_8	0.864	1.000	1.047	0.856	0.8981
	Well_9	0.868	0.972	1.018	0.864	0.9034
PAD_B	**Well_1**	0.897	1.017	0.974	0.892	0.9236
	Well_2	0.912	1.023	0.982	0.907	0.9342
	Well_3	0.917	1.018	1.008	0.914	0.9392
	Well_4	0.996	0.999	1.007	0.992	0.994
	Well_5	0.995	1.000	0.993	0.991	0.9937
	Well_6	0.984	1.000	1.015	0.978	0.9844
	Well_7	0.945	1.003	0.994	0.945	0.9606
	Well_8	0.942	0.989	0.981	0.938	0.956
PAD_C	**Well_1**	0.985	1.001	0.981	0.976	0.9828
	Well_2	0.926	0.968	1.056	0.902	0.9306
	Well_3	0.975	0.994	0.990	0.972	0.9803
	Well_4	0.912	0.990	0.993	0.911	0.9372
	Well_5	0.981	1.050	1.009	0.946	0.9615
	Well_6	0.803	1.060	1.154	0.743	0.8174
	Well_7	0.991	1.004	0.997	0.990	0.9927
	Well_8	0.910	0.993	0.980	0.907	0.9343
PAD_D	**Well_1**	0.968	0.982	1.007	0.963	0.9736
	Well_2	0.896	1.047	1.025	0.883	0.9168
	Well_3	0.989	1.013	1.030	0.965	0.9752
	Well_4	0.979	1.017	0.984	0.968	0.9776
	Well_5	0.975	1.076	1.067	0.896	0.9261
	Well_6	0.777	0.993	1.079	0.764	0.8323
	Well_7	0.926	0.992	1.052	0.910	0.9359
	Well_8	0.919	1.014	1.008	0.918	0.9415

4.5.2 Key Performance Indicators.

Fig 4.7 shows the evolution of cumulative NPV at the end of the RTO for the individual pads. The optimization started two years after significant steam chamber development, and immobile bitumen in the pad was mobilized to be produced. When the optimization is initiated, the mobilized oil is produced, exposing the immobile bitumen in the pad to injected steam. For example, it can be observed in Fig 4.7a-c for pads A to C that NPV and cSOR cases cumulative NPV flattened by day 500 since the start of RTO. Steam supply is the main cost contributor to SAGD NPV estimation; since the NPV and cSOR KPI optimization finds the minimum steam that maximizes NPV, steam chamber growth is stalled. In long-term optimization, the optimizer finds steam allocation that ensures enough heat is injected to mobilize a significant amount of bitumen for the optimization period. In Fig 4.4d, the NPV flattened by day 700, and the discrepancy is due to the average pad temperature at the start of RTO. Pads A to D started with average pad temperatures of 77^oC, 78^oC, 72^oC, and 90^oC, respectively. It can be inferred that the higher the average pad temperature, the higher the amount of mobile oil saturation. Hence SAGD RTO with cost minimization goal, the mobilized oil is produced faster than injected steam to expand the steam chamber or mobilize the immobile bitumen.

On the other hand, the NPV for RF and Temp keeps increasing throughout the RTO because a significant amount of steam is injected to mobilize the immobile bitumen while depleting the mobilized one. The challenge with the RF and Temp cases is the high steam requirement to maximize the goals. This work introduces two additional case studies that alternate the NPV and RF optimization based on time and average pad temperature. From Fig 4.7, it can be observed that the two alternating cases resulted in similar NPV injecting a lower amount of steam for all pads. The drawback of NPV in selecting the optimum case is the lack of indicating which case requires a higher amount of steam to achieve the same NPV value. Hence an additional KPI can differentiate between the resource required and the environmental

Table 4.6: Water cut model forecast dimensionless validation performance

	r	β	γ	KGE'	ss	
PAD_A	**Well_1**	0.964	1.001	1.048	0.940	0.9575
	Well_2	0.854	1.001	1.029	0.851	0.8944
	Well_3	0.773	1.001	1.046	0.768	0.8356
	Well_4	0.922	1.001	1.027	0.917	0.9414
	Well_5	0.951	1.001	1.019	0.948	0.963
	Well_6	0.921	1.001	0.993	0.921	0.9438
	Well_7	0.887	1.003	1.005	0.886	0.9194
	Well_8	0.920	1.002	1.032	0.914	0.9389
	Well_9	0.806	1.010	1.269	0.668	0.7648
PAD_B	**Well_1**	0.932	1.003	1.020	0.929	0.9498
	Well_2	0.765	1.001	1.012	0.764	0.8327
	Well_3	0.848	1.001	1.069	0.833	0.8818
	Well_4	0.893	1.002	1.051	0.881	0.9157
	Well_5	0.957	1.001	1.020	0.953	0.9668
	Well_6	0.910	1.001	1.000	0.910	0.9362
	Well_7	0.958	1.001	1.019	0.954	0.9675
	Well_8	0.973	1.002	1.032	0.958	0.9703
PAD_C	**Well_1**	0.889	1.003	1.068	0.870	0.9076
	Well_2	0.817	1.002	1.059	0.808	0.8638
	Well_3	0.967	1.002	1.073	0.919	0.9429
	Well_4	0.565	0.986	1.482	0.351	0.5394
	Well_5	0.196	1.041	3.194	-1.337	-0.6572
	Well_6	0.862	1.014	1.016	0.861	0.9011
	Well_7	0.969	1.001	0.999	0.969	0.9781
	Well_8	0.878	1.006	1.048	0.869	0.9069
PAD_D	**Well_1**	0.996	1.005	1.013	0.986	0.9899
	Well_2	0.998	1.003	1.009	0.990	0.9932
	Well_3	0.972	0.999	0.977	0.964	0.9742
	Well_4	0.987	1.001	0.993	0.985	0.9896
	Well_5	0.991	1.001	1.022	0.976	0.9831
	Well_6	0.986	1.004	0.963	0.960	0.9717
	Well_7	0.986	1.003	1.037	0.960	0.9719
	Well_8	0.993	1.005	1.029	0.970	0.9787

impact.

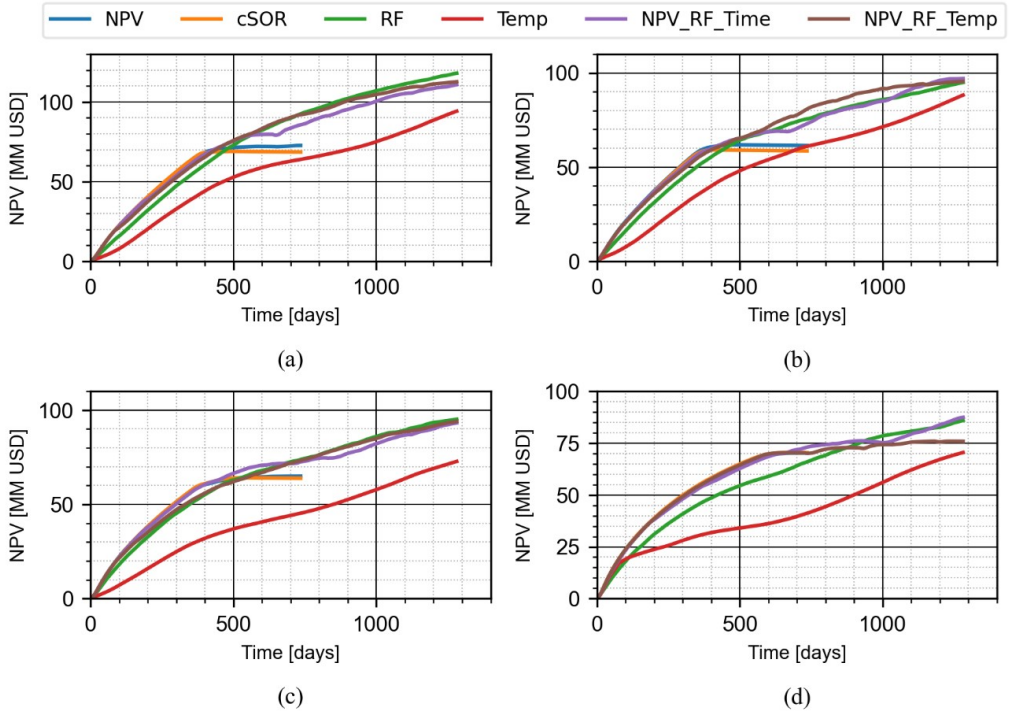

Figure 4.7: Cumulative NPV comparison for different KPIs (a) PAD_A (b) PAD_B (c) PAD_C (d) PAD_D

Fig 4.8 illustrates the evolution of cSOR for the four different pads. The cSOR decreased from the start of RTO for all cases except average pad temperature. cSOR performance stabilized below three for all cases except average pad temperature, indicative of a low carbon footprint, reduced resource requirements, and improved economic returns.

In contrast, the pad average temperature maximization leads to improved economic returns but a higher resource requirement and carbon footprint. Similar to NPV performance in Fig 4.7, in the NPV and cSOR cases, optimum cSOR performance was achieved before year two of RTO. The lowering of cSOR for Pads A-C (Fig 4.7a-c) after year one is due to the lowering steam requirement of bitumen production rates over time (i.e., flatlining of the curve). The RF cases for all pads recorded an elevated cSOR compared to NPV-RF alternation based on either time or temperature. The RF and Temp cases showed an elevated cSOR relative to cSOR and NPV cases because of the higher steam

allocation requirement to increase recovery or pad average temperature. RF case cSOR performance is significantly better than average pad temperature because it balances steam chamber growth and mobile oil depletion rate. The proposed scheme of alternating NPV and RF cases based on time and temperature showed a further improvement in cSOR compared to the RF case in all pads (Fig 4.8). Better cSOR performance should be commensurate with higher recovery for a SAGD recovery scheme to be recommended. Lower cSOR does not necessarily mean better performance. Reservoir heterogeneity can impede steam chamber growth leading to lower cSOR (Guo et al., 2018). Since the SAGD process goal is to recover proven oil while minimizing carbon footprint economically, a lower cSOR that achieves those goals is preferred.

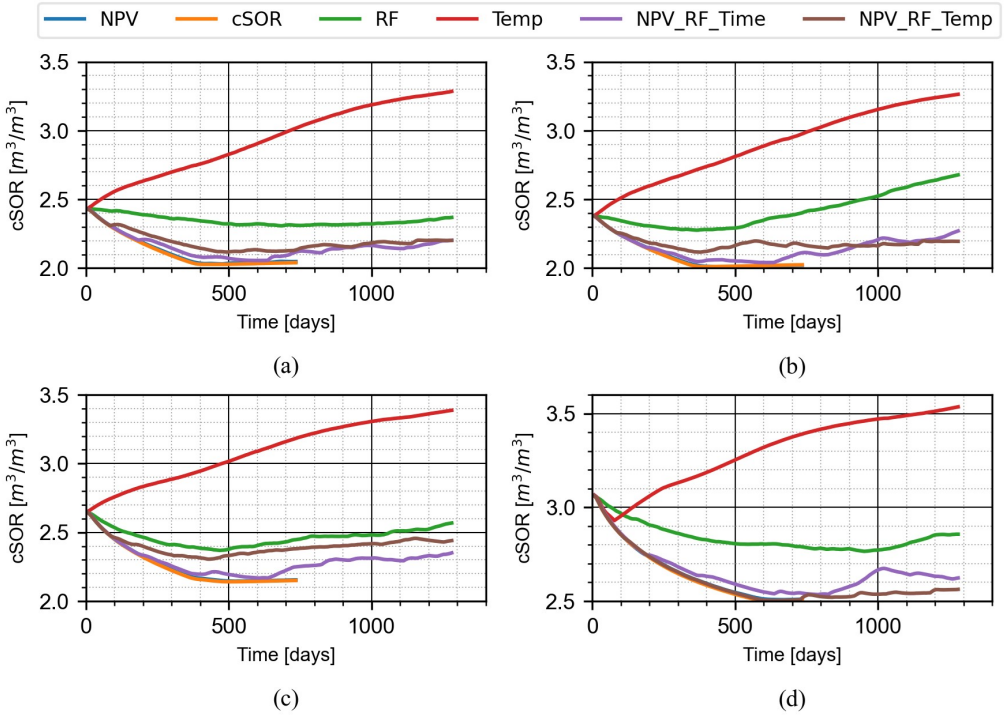

Figure 4.8: cSOR comparison for different KPIs (a) PAD_A (b) PAD_B (c) PAD_C (d) PAD_D

As shown in Fig 4.9, recovery performance for all pads follows economic performance as in Fig 4.7. The temperature values in Fig 4.7 are the recovery during the RTO period and not the cumulative from the start of SAGD recovery. For all pads, the order of performance can be ranked as Temp >

RF > NPV_RF_Time == NPV_RF_Temp > NPV == cSOR in terms of recovery. The recovery performance based on time supports the economic performance, as shown in Fig 4.4. When the recovery performance is compared with pore volume injected (PVI) of steam indicative of resource requirements, NPV_RF_Time == NPV_RF_Temp > RF > Temp. The recovery performance to PVI validates the cSOR performance, as shown in Fig 4.8. The NPV and cSOR recorded high recovery with the least amount of steam injected, as shown in Fig 4.8 for all pads. The trend validates the NPV performances as in Fig 4.7, which shows a steep increase in NPV and then flattened. As seen in Fig 4.9, the steam injection became too low to mobilize bitumen for recovery. For all the four pads, the Temp case recorded the highest recovery and amount of steam injected at the end of RTO. That translates to approximately two to three times and three to four times steam injected when the Temp case is compared to RF and proposed alternating cases. When the RF case is compared to proposed alternating cases, an additional recovery is achieved at the same PVI. For appreciable bitumen recovery, the average pad temperature must be significantly higher to mobilize the bitumen. Too high temperature leads to heat losses to the overburden and a high amount of steam produced, minimizing bitumen recovery efficiency.

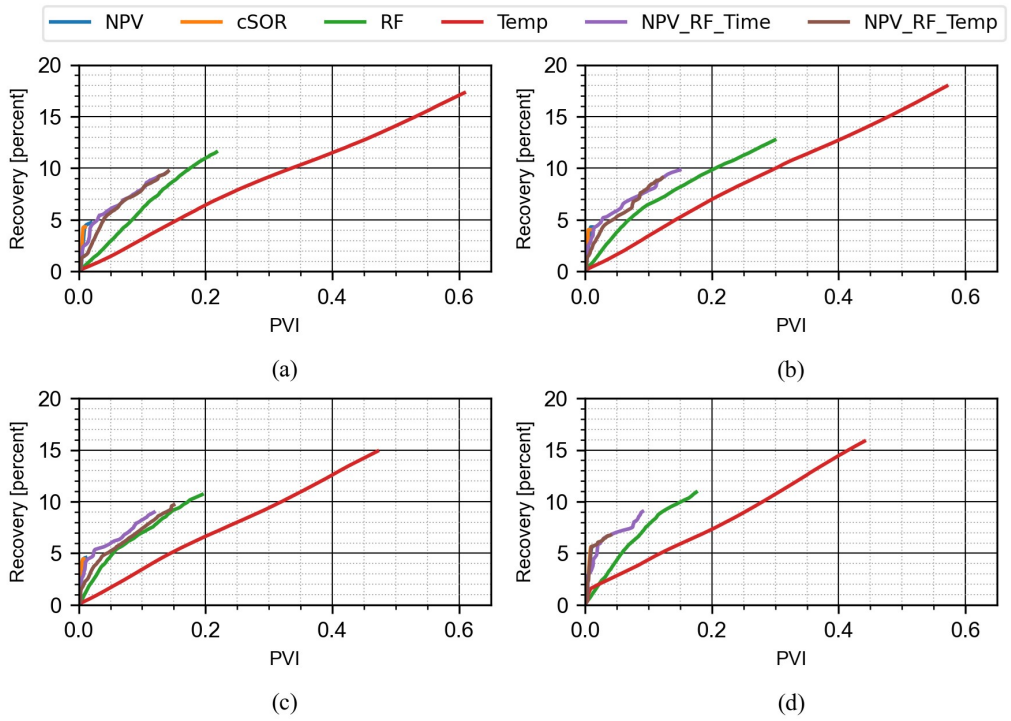

Figure 4.9: Recovery comparison for different KPIs (a) PAD_A (b) PAD_B (c) PAD_C (d) PAD_D

Fig 4.10 shows the pad average temperature indicator of steam chamber conformance. The reservoir model used in this study is heterogenous in permeability but does not have shale barriers that significantly impact steam chamber growth. The rate of temperature rise, as shown in Fig 4.10, will be subdued in a reservoir with shale barriers, but the trend will not be different. The decreasing temperature pad average temperature explains the early curtailment of NPV and cSOR cases. The lesson learned here is that, for cost minimization RTO, the average temperature in the reservoir or the steam chamber should reach maturity at the start-up phase if RTO is initiated at the normal phase. The cost minimization optimization will always be preferred at the blow-down phase, as shown in Fig 4.10. The decreasing temperature behavior is the goal of the blow-down phase, where steam is co-injected with non-condensable gas. The temperature performance further supports the use of the proposed alternating cases at the normal SAGD phase. For those cases, during the cost minimization or NPV RTO horizons, a decrease in average

pad temperature and an increase during recovery optimization horizons from the curves can be observed. In addition, the decrease and increase in temperature further validate the data-driven model that learned the SAGD process's physics. Suppose the model had fit the history without learning the physics of the SAGD process. In that case, the model will not always respond positively to an increase in temperature when optimizing recovery and average temperature or a decrease in temperature when minimizing cost, leading to lower steam injection. For the two proposed cases, the average temperature initially decreased before increasing for all pads since NPV was optimized for the alternating based on time in the first few months, followed by RF. Set optimizing NPV first three months, switch to RF optimization in the next six months, and repeat till the end of RTO. For the alternating based on temperature, there is a temperature rise in PAD A to C (Fig 4.7a-c), but the temperature dropped and stabilized at 80^oC. When the past six-month the average temperature is below 80^oC, switch to RF optimization and vice versa.

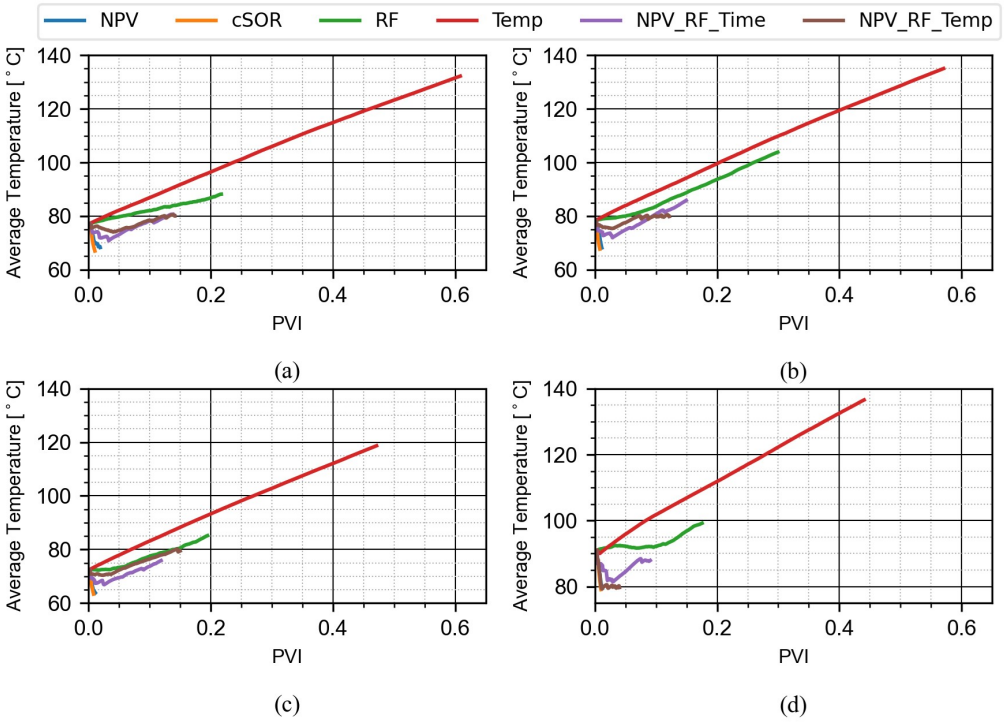

Figure 4.10: Recovery comparison for different KPIs (a) PAD_A (b) PAD_B (c) PAD_C (d) PAD_D

4.6 Conclusion

In this work, an ADMM-based scheme for multi-pad steam allocation optimization has been presented. The RTO workflow has effectively coordinated the steam allocation to independently operated well-pads. The workflow was implemented in this study to determine the impact of a short-term optimization problem formulation on the long-term performance of SAGD. The following conclusions were drawn based on the results of the study.

1. Cost minimization-based RTO is ineffective in meeting long-term normal phase SAGD operations performance goals.

2. Short-term optimization of recovery and steam chamber growth RTO can attain long-term SAGD performance goals at a higher resource requirement than cost minimization.

3. RTO with a short-term recovery goal requires less than two to three times more steam than steam chamber growth optimization.

4. The proposed alternating cost minimization and recovery optimization outperform individual cost and recovery optimization for the normal SAGD operations phase by less than three to four times the steam requirement.

The proposed workflow has a significant potential for multi-pad real-time steam allocation decisions in bitumen recovery.

Chapter 5

Multi-Criteria Real-Time Optimization of Multi-Pad Steam Allocation[1]

5.1 Introduction

The production of bitumen in situ accounts for a considerable percentage of Alberta's main energy output. Therefore, efficient SAGD operations must adopt decisions, recovery procedures, and technical inputs that reduce operating costs and greenhouse gas (GHG) emissions-related environmental consequences. Over the years, the expansion of oil sand operations has increased total emissions but drop in GHG emissions per barrel (Millington, 2020). Canadian Energy Research Institute (CERI) scenario-based analysis on energy requirements and GHG emission outlook for 2015 to 2050 showed the application of technology to increase energy efficiency and process improvements of decreasing reservoir quality could decrease energy requirements by 31.1% and GHG emission by 47.6% of SAGD operations without decreasing production (Murillo, 2015). Based on these CERI reports, this work presents technology such as RTO as a short-term SAGD process optimization tool to improve ultimate recovery and decrease energy requirement GHG emissions in the long term.

The joint goal of maximizing production and decreasing energy requirement requires a multi-objective formulation of the optimization problem. One

[1]A version has been submitted to Journal of Petroleum Science and Engineering 2022

approach to multi-objective optimization is aggregating the objectives into a single weighted objective (Al-Gosayir et al., 2012; Awotunde and Sibaweihi, 2012). However, the main drawback of the weighted aggregation is the selection of the appropriate weights to balance the objectives. A way to mitigate the above drawback is to run multiple realizations of the weight distribution and use a criterion such as the Sharpe ratio (Capolei et al., 2015) or Modigliani's risk-adjusted measure (Sibaweihi and Trivedi, 2022) to select the optimum control strategy. However, the above approach becomes computationally expensive with increasing design variables. In this work, a multi-objective optimization approach will be adopted due to recent advances in algorithm efficiency. Several applications of multi-objective optimization for bitumen recovery process optimization have been reported. For example, Coimbra et al. (2019) generated non-dominated solutions for steam alternating solvent process with a joint objective of maximizing oil recovery and minimizing solvent usage. Similarly, Ma and Leung (2020) investigated the impact of reservoir heterogeneity and solution gas in maximizing oil recovery and minimizing solvent usage in optimizing the warm solvent injection recovery process. Mayo-Molina and Leung (2021) optimized bitumen recovery and cumulative steam-oil-ratio (cSOR) of steam alternating solvent process reservoir with varying shale barrier size, location, and proportion. Hunyinbo et al. (2021) presented three objectives of oil recovery, solvent loss, and injected fluid enthalpy of multi-objective optimization of a warm vaporized solvent injection process with phase behavior constraints. In this work, a comparison of combinations of joint objectives ranging from two to four is studied.

Several SAGD RTO studies have been presented over the years. RTO computation requirements are reduced by using a data-driven model. Therefore, the critical design questions for the RTO workflow must be addressed: the type of data-driven model, design variables, and objective. Vembadi et al. (2018) used model predictive control (MPC) to maximize the joint objectives of steam chamber growth and SAGD process net present value (NPV) by using optimal rates and subcool temperature as decision variables. The multi-input multi-output MPC control structure outperformed the multi-input

single-output control structure for predicting the steam trap of the SAGD process with liquid production and steam injection rates as manipulated variables (Purkayastha et al., 2018). Our most recent research shows that when compared to the first-principle model's out-of-train-test response, the multi-input multi-output Box-Jenkins control structure data-driven model RTO achieves excellent results Sibaweihi and Trivedi (2022). Sibaweihi et al. (2021) presented the SAGD RTO process with a single input (steam rate), single output (oil rate), and output-error control structure data-driven model to optimize an NPV of well-pad of varying reservoir quality and variable steam availability. Patel and Trivedi (2020) presented an RTO process that controls steam chamber conformity by optimizing subcool setpoints using linear and nonlinear MPC. The data-driven proxy model used in the preceding study accelerates the simulation of the SAGD process. Guevara et al. (2021) developed a reinforcement learning strategy for long-term production optimization of the SAGD process. RTO has a decision-making time horizon ranging from a few days to a few weeks (Foss et al., 2009). In this study, the Box-Jenkins data-driven model will be used to make short-term decisions to meet long-term goals.

Long-term operational decisions are broken down using the RTO approach to meet long-term targets. Meanwhile, the RTO method lessens the need for computational resources during optimization through temporal decomposition and data-driven proxy models. As the SAGD process develops, additional wells pads come online, reducing available steam. With an increase in the number of wells (an optimization variable), the optimization problem becomes more complex, necessitating more computational time. Studies aiming to optimize SAGD are typically conducted on a single pad (Guo et al., 2018; Sibaweihi and Trivedi, 2022). Very few researchers have tried to find the optimal number of pads for SAGD. With the method described by Card et al. (2014), the computational time for a multi-pad, multi-million grid cell SAGD model can be reduced from nearly a month to just seven days. For a ten-year simulation, Kumar et al. (2020) presented a workflow for a multi-pad reservoir model of a SAGD steam allocation that uses 15 pads and runs in less than twenty-four hours without sacrificing accuracy. The authors em-

ployed AI and machine learning algorithms to fine-tune the model's numerical parameters and gridding it dynamically. Multi-pad SAGD operations with constrained steam availability of interconnected well-pads benefit greatly from decomposition-based optimization methods. For example, the Dantzig-Wolfe decomposition approach (Gunnerud et al., 2009) and Lagrangian decomposition (Foss et al., 2009; Krishnamoorthy et al., 2018,?) are effective in RTO because they break the original optimization problem into smaller problems. We will employ Maxeiner and Engell (2017) inequality-constrained ADMM (Boyd et al., 2010) version in this study. Our study extends the inequality-constrained ADMM for multi-criteria optimization, and to the best of our knowledge, this study is the first application for SAGD RTO.

Optimizing the SAGD process helps determine the operating strategies to manage SAGD reservoirs. The performance of the management is assessed based on economic, environmental, and engineering efficiencies. The economic performance is assessed based on NPV and cumulative steam oil ratio (cSOR). The cSOR also doubles as the environmental performance measure, with lower values representing reduced GHG emissions due to lower water and fuel requirements. Finally, steam conformance or temperature distribution is indicative of engineering performance. In addition, ultimate bitumen recovery is influenced by steam chamber expansion, conductive heating, and infill wells (Strobl et al., 2016) is also an engineering performance indicator. So, it is essential to define the RTO problem in a way that considers the three efficiency measures so that SAGD's long-term performance is not affected.

In the past, there have been studies on different approaches to optimize short- and long-term optimization. van Essen et al. (2011) investigated bi-objective hierarchical short- and long-term performance optimization as secondary and primary objectives, respectively, while constraining short-term performance to optimal long-term performance. Long-term and short-term NPV were improved by using uncertainty in the reservoir description, as demonstrated by Chen et al. (2012). To achieve this, they focused on maximizing NPV performance over the next year or two while maintaining a good NPV throughout the project's lifetime. Hasan et al. (2013) provided a strategy

that optimizes long and short-term goals using a multi-objective approach and places upper and lower constraints on the objectives based on previous rankings of the preference of long and short-term goal performances. A bi-objective long- and short-term NPV optimization alternative based on hierarchical joint optimization of long-term NPV performance and time-varying well control was put forth by Shirangi et al. (2017). The outer loop keeps cash flows from falling below the amount of capital invested over time while optimizing NPV within the bounds of the modified internal rate of return. The inner loop optimizes the well controls. The long-short optimization problem does not apply to the RTO workflow in the studies mentioned above because decisions are made based on the anticipated short-term response. The formulation's hierarchical structure also raises the cost of computation. Finally, Al-Aghbari et al. (2022) investigated various multi-objective function combinations to optimize waterflood management's short- and long-term performance. This study suggests that a multi-pad SAGD RTO workflow uses a multi-objective approach to meet short-term and long-term performance goals. Previous studies used long-term optimization workflows to meet short- and long-term performance goals.

The previously reported works have focused on different objective combinations. This work contribution presents a study of different multi-objective combinations with a recommendation for which combinations are optimal in RTO in the short-long-term. A compromised programming approach is used to select the optimal control strategy at each control horizon. A combination of four different SAGD KPIs will be implemented. The KPIs implemented are NPV, cSOR, recovery factor (RF), and average pad temperature. Five unique cases of a combination of two KPIs and three cases of three or four unique combinations will be optimized in a multi-criteria optimization framework. The remainder of the article is structured as follows: (1) Data-driven model construction, (2) multi-criteria distributed real-time steam allocation, (3) reservoir model, (4) findings and discussion, and (5) conclusion.

5.2 Data-Driven Model Development

Collecting data from the SAGD reservoir is the first step in using a reservoir simulator. Next, a zero mean noise is applied to the recorded data and normalized between 0 and 100. This transformation is governed by the feature's minimum and maximum engineering, environmental, and device constraints. Finally, after the data have been cleaned and prepared, the Box-Jenkins approach is applied to train the data-driven model by minimizing the prediction error with MATLAB System Identification Toolbox (MATLAB, 2021).

Two data-driven models will be employed in this work. First, at the well to forecast the production parameters (i.e., liquid rate, water-cut) and at the pad, to forecast the average pad temperature. The Box-Jenkins polynomial structure (Equationuation 5.1) is used to model SAGD process dynamics. The inputs ($u(t)$) for both models at any time (t) is the steam injection rate and the output ($\widehat{y}(t)$) liquid rate or average pad temperature for the well or pad. The first term of the right-hand side of Equation 5.1 is the process, and the disturbance transfer functions model is the second term. The backward shift operator (z^{-1}) of the two terms relates the past inputs to the current output. The steps followed in training and validating both models have been outlined in Sibaweihi and Trivedi (2022).

Box-Jenkins Model (BJ)

$$\hat{y}(t) = \frac{B(z^{-1})}{F(z^{-1})}u(t) + \frac{C(z^{-1})}{D(z^{-1})}e(t) \tag{5.1}$$

$$B(z^{-1}) = b_1 z^{-1} + \cdots + b_{nb} z^{-nb}$$
$$C(z^{-1}) = 1 + c_1 z^{-1} + \cdots + c_{nc} z^{-nc}$$
$$D(z^{-1}) = 1 + d z^{-1} + \cdots + d_{nd} z^{-nd}$$
$$F(z^{-1}) = 1 + f_1 z^{-1} + \cdots + f_{nf} z^{-nf}$$

5.2.1 Data-Driven Model Forecast Validation.

Three performance metrics will be utilized: Pearson correlation (r) defined in Equation 5.2, modified Kling-Gupta efficiency (KGE$'$) which is Equation 5.3, and the skill score (ss) as in Equation 5.4. The KGE$'$ mitigates r to outliers

(Legates & McCabe, 1999). The performance metric KGE$'$ is decomposed into r, bias (β), and variability (γ) ratios. The first term r correlates with measured (m) outputs (y) and the mean of measured outputs ($\overline{y}$) to the data-driven model's forecast (f) outputs ($\widehat{y}_i$) and the mean of the outputs $\left(\overline{\widehat{y}}\right)$. The second term β is the ratio of the mean (μ) of the forecasted and measured outputs. The γ term relates to the standard deviations (σ) ratios of the model outputs to measured outputs.

Pearson Correlation

$$r = \frac{\sum_{t=1}^{N_p} \left(y_t - \overline{y}\right)\left(\widehat{y}_t - \overline{\widehat{y}}\right)}{\sqrt{\sum_{t=1}^{N_p} \left(y_i - \overline{y}\right)^2}\sqrt{\sum_{t=1}^{N_p} \left(\widehat{y}_t - \overline{\widehat{y}}\right)^2}}, \qquad -1 \leq r \leq 1 \tag{5.2}$$

Modified Kling-Gupta Efficiency (Kling et al., 2012)

$$KGE\prime = 1 - \sqrt{\left(r-1\right)^2 + \left(\beta - 1\right)^2 + \left(\gamma - 1\right)^2}, \tag{5.3}$$

$$-0.41 < KGE\prime \leq 1$$

$$\beta = \frac{\mu_f}{\mu_m}$$

$$\gamma = \frac{\sigma_f/\mu_f}{\sigma_m/\mu_m}$$

Skill score (Knoben et al., 2019)

$$ss = \frac{\text{KGE}'_{\text{model}} - \text{KGE}'_{\text{benchmark}}}{1 - \text{KGE}'_{\text{benchmark}}} \tag{5.4}$$

5.3 Multi-criteria Distributed Real-time Steam Allocation

5.3.1 Optimization Problem.

As established in the introduction, RTO decisions are based on the short-term response from the reservoir. Hence, balancing steam chamber growth, maximizing ultimate recovery, and positive economic returns can be challenging to manage with a single objective if no significant steam chamber is established prior to RTO implementation. Four different SAGD KPIs are jointly implemented in this work. The first KPI is the NPV (Equation 5.5), a metric for economic returns. Where the steam injection rate (u) represents the cash outflows or cost, the decision variable of optimization. For each well (j) at the time (t), the revenue is estimated from the oil production rate $[\widehat{y}_{o,j}(t)]$. The other cost terms are produced water $[\widehat{y}_{w,j}(t)]$, transportation and blending of oil, royalty rate at each prediction horizon (P) for all wells (N_w). The allocation of steam to each well-pair is constrained subject to ($s.t.$) minimum ($u_j^{\min}$), and maximum ($u_j^{\max}$) steam injection rate. Instabilities in the SAGD steam allocation changes (Δu_j) are constrained between the next prediction horizons to a minimum ($\Delta u_j^{\min}$) and maximum ($\Delta u_j^{\max}$) steam injection rate for each well-pair in the pad. The steam available $u_j^{\max}$ is limited, which is denoted by $\overline{u}$. Table 5.1 shows the input of the NPV parameters used in the optimization. They are based on major SAGD project operating costs in Canada (Alexey, 2018). The second KPI is the cSOR (Equation 5.6), an economic and environmental metric. cSOR is not an alternative to NPV, estimated in this work as the ratio of cumulative steam injected to oil produced from the start to the time optimization conducted (T) during the SAGD process. RF (Equation 5.7) is the ratio of cumulative oil produced to oil initially in place (OOIP). The last KPI is the average pad temperature indicative of the steam chamber conformance. In field applications, this can be estimated from thermocouple readings.

$$J(\mathbf{u}) = \sum_{j=1}^{N_w} \sum_{t=1}^{P} \frac{(p_o \widehat{y}_{o,j}(t) - p_w \widehat{y}_{w,j}(t) - p_r p_o \widehat{y}_{o,j}(t) - p_s u_{s,j}(t) - p_{\text{otbc}} \widehat{y}_{o,j}(t))}{(1+D)^{\Delta t}} \tag{5.5}$$

$$\begin{gathered} \text{s.t.} \;\; u_j^{\min} \leq u_j \leq u_j^{\max} \\ \Delta u_j^{\min} \leq \Delta u_j \leq \Delta u_j^{\max} \\ \textstyle\sum_{j=1}^{N_w} \mathbf{u}_j \leq \overline{u} \end{gathered}$$

$$\text{cSOR}(\mathbf{u}) = \frac{\sum_{t=1}^{T} \sum_{j=1}^{N_w} u_{s,j}(t)}{\sum_{t=1}^{T} \sum_{j=1}^{N_w} \widehat{y}_{o,j}(t)} \tag{5.6}$$

$$\text{RF}(\mathbf{u}) = \frac{\sum_{t=1}^{T} \sum_{j=1}^{N_w} \widehat{y}_{o,j}(t)}{\text{OOIP}} \tag{5.7}$$

Table 5.1: Economic input parameters

Description	Value
Price of oil [p_o]	60 USD/bbl.
Steam processing cost [p_s]	6 USD/bbl.
Produced water processing cost [p_w]	1.96 USD/bbl.
the transportation and blending cost of oil [p_{otbc}]	4.95 USD/bbl.
Royalty rate [p_r]	2%
Discount factor (D)	10%

Equation 5.8 is the single objective function for a multi-pad optimization of the SAGD process. Where (J) is the optimized KPI for each pad (i). The pads share the same steam supply and hence the sum of all steam allocations to each pad ($\overline{\mathbf{u}}_i$) should be equal to or less than the maximum available steam ($\overline{U}$). A centralized optimization structure has been the focus of earlier works with multi-pad optimization (Card et al., 2014; Kumar et al., 2020). The multi-criteria optimization in this study reformulates Equation 5.8 as expressed in Equation 5.9 and optimized to determined a non-dominated solutions set (Pareto-optimal set). Different combinations of selected KPIs (m) ranging from two to four will be implemented in this study. An additional constraint with a slack variable (z_i) is added to 5.9 to decompose it to individual pad scale problems.

$$\max_{u_i \in U_i \forall_i} \sum_{i=1}^{N_p} J_i\left(\mathbf{u}_i\right) \tag{5.8}$$

$$\text{s.t.} \qquad \textstyle\sum_{i=1}^{N_p} \overline{\mathbf{u}}_i \leq \overline{U}$$

$$J_m\left(\mathbf{u}\right) = \left\{ \sum_{i=1}^{N_p} \mathrm{NPV}\left(\mathbf{u}\right),\ \sum_{i=1}^{N_p} \frac{1}{\mathrm{cSOR}\left(\mathbf{u}\right)}, \sum_{i=1}^{N_p} \mathrm{RF}\left(\mathbf{u}\right), \sum_{i=1}^{N_p} \mathrm{Temp}\left(\mathbf{u}\right) \right\}, \tag{5.9}$$

$$m = 1, 2, \ldots, M$$
$$\text{s.t.} \textstyle\sum_{i=1}^{N_p} \overline{\mathbf{u}}_i \leq \overline{U}$$
$$\textstyle\sum_{i=1}^{N_p} z_i = \overline{U}$$

5.3.2 Multi-criteria Distributed Optimization.

The maximum steam availability constraint in Equation 5.9 is relaxed by dual decomposition (second term) and a quadratic penalty term as in Equation 5.10. The average allocated steam at each iteration (k) is multiplied by the dual variable ($\lambda^{k,T}$), the marginal cost to relax the constraint (the first penalty term or the second term of Equation 5.10). The third term or second penalty term (ρ^k) guarantee that each pad utilizes its allocated resource and guides the solution towards global feasibility. Equation 5.7 is parallelized by the coordinator sending a vector of globally feasible solutions ($\mathbf{z}_i^k$) and dual vector ($\lambda^{k,T}$) to each KPI (m) and pad (i) as defined by Equation 5.11. In the classic ADMM for a single objective optimization, the two penalty terms become negligible when global feasibility is attained. By this motivation, in a multi-criteria optimization, the two penalty terms must be added to at least one of the KPIs being jointly optimized. This study applies the penalty term to all KPIs optimized for each pad.

$$\max_{u_i \in U_i \forall_i} \sum_{i=1}^{N_p} J_i\left(\overline{\mathbf{u}}_i\right) + \lambda^{k,T} \sum_{i=1}^{N_p} \left(\overline{\mathbf{u}}_i - \mathbf{z}_i^k\right) + \frac{\rho^k}{2} \sum_{i=1}^{N_p} \left\|\overline{\mathbf{u}}_i - \mathbf{z}_i^k\right\|_2^2 \tag{5.10}$$

$$J_{m,i}\left(\mathbf{u}\right) + \lambda^{k,T}\left(\overline{\mathbf{u}}_{m,i} - \mathbf{z}_{m,i}^k\right) + \frac{\rho^k}{2}\left\|\overline{\mathbf{u}}_{m,i} - \mathbf{z}_{m,i}^k\right\|_2^2 \ \forall_{m,i} \tag{5.11}$$

ADMM iteratively solves the constrained multi-criteria optimization problem (Equation 5.9) by a series of unconstrained problems with a penalty (Equation 5.11). At each iteration, the coordinator communicates the dual variables ($\lambda^{k,T}$), penalty (ρ^k) and feasible global solutions ($\mathbf{z}_i^k$) to each pad to perform unconstrained optimization and return the optimum steam allocation to the pad (Fig 5.1). The optimum is selected from a set of non-dominated solution using a compromise programming approach. If the sum of the returned optimum steam allocation to each pad ($\overline{\mathbf{u}}_i$) is greater than the available steam ($\overline{U}$) update ($\lambda^{k,T}$, ρ^k, $\mathbf{z}_i^k$) using Equation 5.14 - 5.16, else convergence has been achieved. Table 5.2 shows the ADMM coordination parameters in this study. The step-by-step procedure for multi-pad multi-criteria RTO workflow is described in Algorithm 1.

$$\phi_{\text{primal}}^{k+1} = \sum_{i=1}^{N_p} \overline{\mathbf{u}}_i{}^{k+1} - \overline{U} \tag{5.12}$$

$$\phi_{\text{dual}}^{k+1} = \rho^k \left|\overline{u}^{k+1} - \overline{u}^k\right| \tag{5.13}$$

$$\lambda^{k+\frac{1}{2}} = \begin{cases} \lambda^k + \nu\rho^k\phi_{primal}^{k+1} & if \phi_{primal}^{k+1} \geq 0 \\ \lambda^k + \rho^k\phi_{primal}^{k+1} & if \phi_{primal}^{k+1} < 0 \end{cases} \tag{5.14}$$

$$\lambda^{k+1} = max\left(0, \lambda^{k+\frac{1}{2}}\right)$$

$$z_i^{k+\frac{1}{2}} = \begin{cases} \overline{u}_i^{k+1} + \frac{\phi_{\text{primal}}^{k+1}}{N_p}, & if\ \phi_{\text{primal}}^{k+1} \geq 0 \\ \overline{u}_i^{k+1} & \text{else} \end{cases} \tag{5.15}$$

$$z_i^{k+1} = max\left(0, \quad z_i^{k+\frac{1}{2}}\right)$$

Table 5.2: Coordination parameters

PARAMETER	VALUE
Maximum iteration $[k_{max}]$	10
Initial dual variables $[\lambda^0]$	$100 * \aleph(0,1)$
Initial feasible global solutions $[z^0]$	Previous horizon allocations
Initial penalty $[\rho^0]$	1
Dual variable step-size decrement $[v]$	0.7
Primal-dual feasibility $[\beta]$	2
Penalty increment $[\alpha_{Incr}]$	1.1
Penalty decrement $[\alpha_{Decr}]$	0.9
Constraint violation tolerance $[eps]$	$1e-6$

$$\rho^{k+1} = \begin{cases} \rho^k \alpha_{\text{Incr}}, & if\ \phi^{k+1}_{\text{primal}} > \beta \phi^{k+1}_{\text{dual}} \\ \rho^k \alpha_{\text{Decr}}, & if\ \phi^{k+1}_{\text{primal}} \beta < \phi^{k+1}_{\text{dual}} \\ \rho^k & \text{else} \end{cases} \tag{5.16}$$

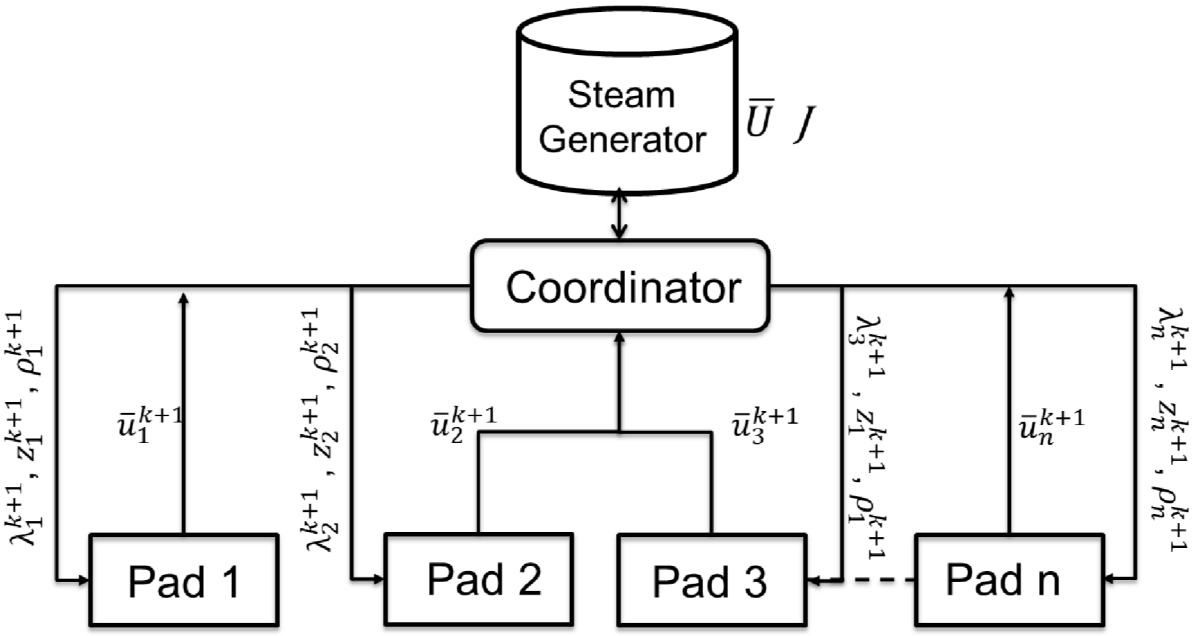

Figure 5.1: Communication scheme between the pads and the coordinator

Algorithm 1: Alternating Direction Method of Multipliers

Inputs: $k_{max}, eps, \alpha_{Decr}, \alpha_{Incr}, \beta, v, \lambda^0, z^0, \rho^0$.
Initialize: $k = 1$, *Convergence = False*.
while $\mathbf{k} \leq \mathbf{k}_{\max} \wedge \neg$**Convergence** do

For each pad (**i**), do

$$\overline{\mathbf{u}}_{\mathbf{i,opt}} = \mathbf{J}_{\mathbf{m,i}}(\mathbf{u}) + \lambda^{\mathbf{k,T}}\left(\overline{\mathbf{u}}_{\mathbf{m,i}} - \mathbf{z}^k_{m,i}\right) + \frac{\rho^{\mathbf{k}}}{\mathbf{2}}\left\|\overline{\mathbf{u}}_{\mathbf{m,i}} - \mathbf{z}^{\mathbf{k}}_{\mathbf{m,i}}\right\|^{\mathbf{2}}_{\mathbf{2}}$$

end for

$\phi^{\mathbf{k+1}}_{\text{primal}} = \sum_{\mathbf{i=1}}^{\mathbf{N_P}} \overline{\mathbf{u}}_{\mathbf{i}}{}^{\mathbf{k+1}} - \overline{\mathbf{U}}\phi^{\mathbf{k+1}}_{\text{dual}} = \rho^{\mathbf{k}}\left|\overline{\mathbf{u}}^{\mathbf{k+1}} - \overline{\mathbf{u}}^{\mathbf{k}}\right|$
if $\phi^{\mathbf{k+1}}_{\text{primal}} <$ **eps** then
Convergence = True
else

$$\lambda^{\mathbf{k}+\frac{\mathbf{1}}{\mathbf{2}}} = \lambda^{\mathbf{k}} + \mathbf{v}\rho^{\mathbf{k}}\phi^{\mathbf{k+1}}_{\text{primal}}$$

$$\lambda^{\mathbf{k+1}} = \mathbf{max}\left(\mathbf{0},\, \lambda^{\mathbf{k}+\frac{\mathbf{1}}{\mathbf{2}}}\right)$$

$$\mathbf{z}_{\mathbf{i}}^{\mathbf{k}+\frac{\mathbf{1}}{\mathbf{2}}} = \begin{cases} \overline{\mathbf{u}}_{\mathbf{i}}^{\mathbf{k+1}} + \frac{\phi^{\mathbf{k+1}}_{\text{primal}}}{\mathbf{N_P}}, & \mathbf{if}\ \phi^{\mathbf{k+1}}_{\text{primal}} \geq \mathbf{0} \\ \overline{\mathbf{u}}_{\mathbf{i}}^{\mathbf{k+1}} & \text{else} \end{cases}$$

$$\mathbf{z}_{\mathbf{i}}^{\mathbf{k+1}} = \mathbf{max}\left(\mathbf{0},\, \mathbf{z}_{\mathbf{i}}^{\mathbf{k}+\frac{\mathbf{1}}{\mathbf{2}}}\right)$$

$$\rho^{\mathbf{k+1}} = \begin{cases} \rho^{\mathbf{k}}\alpha_{\text{Incr}}, & \mathbf{if}\ \phi^{\mathbf{k+1}}_{\text{primal}} > \beta\phi^{\mathbf{k+1}}_{\text{dual}} \\ \rho^{\mathbf{k}}\alpha_{\text{Decr}}, & \mathbf{if}\ \phi^{\mathbf{k+1}}_{\text{primal}}\beta < \phi^{\mathbf{k+1}}_{\text{dual}} \\ \rho^{\mathbf{k}} & \text{else} \end{cases}$$

end if

$$\mathbf{k} \leftarrow \mathbf{k} + \mathbf{1}$$

end while
Output: $\overline{\mathbf{u}}_{\text{opt}}$

5.3.3 RTO Implementation.

The RTO workflow extracts and transforms the reservoir's last three months' historical data for data-driven model training and testing at each control horizon. This study represents the heavy oil reservoir using CMG-STARS (CMG, 2021). After the data-driven model passes testing, a multi-criterion distributed optimization using a non-dominated sorting genetic algorithm (Blank and Deb, 2020) is performed. At the end of the optimization, a series of non-dominating solutions are returned. Finally, the compromise programming method (Blank and Deb, 2020) measures the deviation of each KPI from its ideal value. The non-dominated with the minimum deviation is set as the optimum control setpoints. Algorithm 2 describes the steps involved in the multi-criteria RTO.

Algorithm 2: Real-Time Multi-Pad Steam Allocation

For every time step $\mathbf{t} = \mathbf{7\ days}$.

1. Read the previous production and injection rates.
2. Normalize the previously recorded data based on each parameter's physical or operating constraint (range).
3. Identify the structure and parameters or update the parameters of the data-driven model
4. Perform distributed optimization using ADMM (Algorithm 1)
5. Use compromise programming method to perform multi-criteria decision making
6. Apply optimal injection controls from compromise programming to the digital heavy oil reservoir
7. Record the response (production and injection rates) of the reservoir to the optimal control setpoints
8. $\mathbf{t} = \mathbf{t} + \mathbf{1}$
9. Repeat steps $1 - 7$ until it is not profitable or the end of field life.

5.4 Reservoir Model

Fig 5.2 is a fictitious reservoir based on Western Canadian oilfields. The reservoir model comprises 33 well-pairs 760 m long that are heated for four months during the pre-heating phase. The vertical distance between well-pairs averaged $5m$, while the aerial distance averaged 80 m. Each production well had a minimum bottom hole pressure of 2000 kPa and a maximum steam production of 10 $m3/day$. The injection wells are set to operate at 0.95 steam quality and a maximum temperature of 250^oC. The ideal temperature for fluid mobility and well-pair communication is between 70 and 100^oC. (Shen, 2013). After two years of normal SAGD before starting RTO, the average temperatures of the well-pads ranged from 72 to 90^oC, indicating significant steam chamber growth. The reservoir properties used in this study are summarized in Table 5.3.

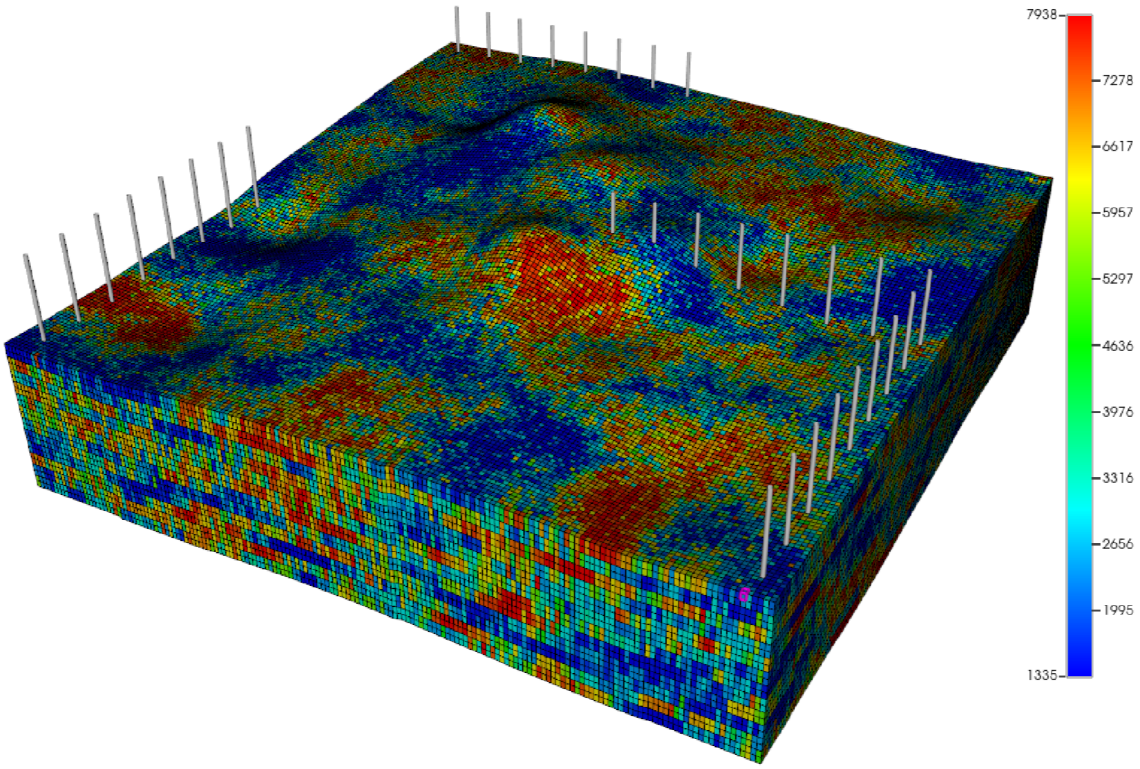

Figure 5.2: Permeability distribution

Table 5.3: Reservoir model properties

PARAMETER	VALUE
Formation temperature [°C]	12
Initial reservoir pressure at $210m$ [Kpa]	1200
Average horizontal permeability [mD]	4372
Average vertical permeability [mD]	3497
Average porosity [fraction]	0.31
Average water saturation [fraction]	0.2
Steam injection pressure [kPa]	4000
Steam quality	0.95
Oil viscosity @ reservoir temperature [cP]	$1.42e6$
Rock heat capacity [J/m^3-C]	$2.3e6$
Thermal conductivity of Rock [J/m^3-day-C]	$2.7e5$
Thermal conductivity of Gas [J/m^3-day-C]	4000
Thermal conductivity of Oil [J/m^3-day-C]	$1.2e4$
Thermal conductivity of Water [J/m^3-day-C]	$5.4e4$

5.5 Results and Discussion

The results of a multi-criteria multi-pad steam allocation proposed approach performance are presented for different combinations of the SAGD process KPI. The performance of each KPI combination is assessed on a multi-pad synthetic western Canadian reservoir. The first part of this section presents the validation of the data-driven model forecast performance to reservoir response. The second part presents the results of the different SAGD KPIs combinations. The first five cases are combinations of two different KPIs, the other three have two different combinations of three, and the last is the combination of all four. The KPIs are classified in this work as weak and strong cost minimizer and steam chamber growth. The NPV is weak (i.e., the same NPV can be due to high or low steam injection), while cSOR is strong (i.e., low is because of low steam injection and high is because of high steam injection) cost minimizer. RF is a weak steam chamber growth KPI because the KPI balances between high steam injection to mobilize bitumen and the production of mobile bitumen. At the same time, Average Temperature (aveTemp) only focuses on steam chamber growth. The plots for this section are based on the response of the reservoir during the RTO period.

5.5.1 Data-Driven Reservoir Model Validation.

The forecasted performance of the data-driven model and the reservoir response are compared Figs 5.3-5.5. The figures show that the evolution between data-driven forecasted water cut, liquid, and oil rates correlates with the reservoir response. The calibrated data-driven model forecasted out of sample train-test data performance compared to the response model showed it learned the physics of the SAGD process. Figs 5.3 to 5.5 for all the pads show the Well 5 performance of NPV-aveTemp joint KPI RTO. The liquid rate (Fig 5.3) forecast to the r, *KGE'*, and *ss* metrics show the model performance close to the target value of one for each metric. However, for the water cut (Fig 5.4), from day 1200, the data-driven model estimated water cut for Well 5 (Fig. 5.4b) is wrong, which is reflected in the performance of all three metrics. Before day 1200, the water cut performance for all metrics is excellent. Similarly, in Fig 5.4d, the model overpredicted between days 900 and 1000 compared to the reservoir performance. The below-par performance of the model in Figs. 5.4b and 5.4d reflected in the oil rate (Fig 5.5) performance of Well 5 of PAD_B (Fig. 5.5b) and PAD_D (Fig 5.5d).

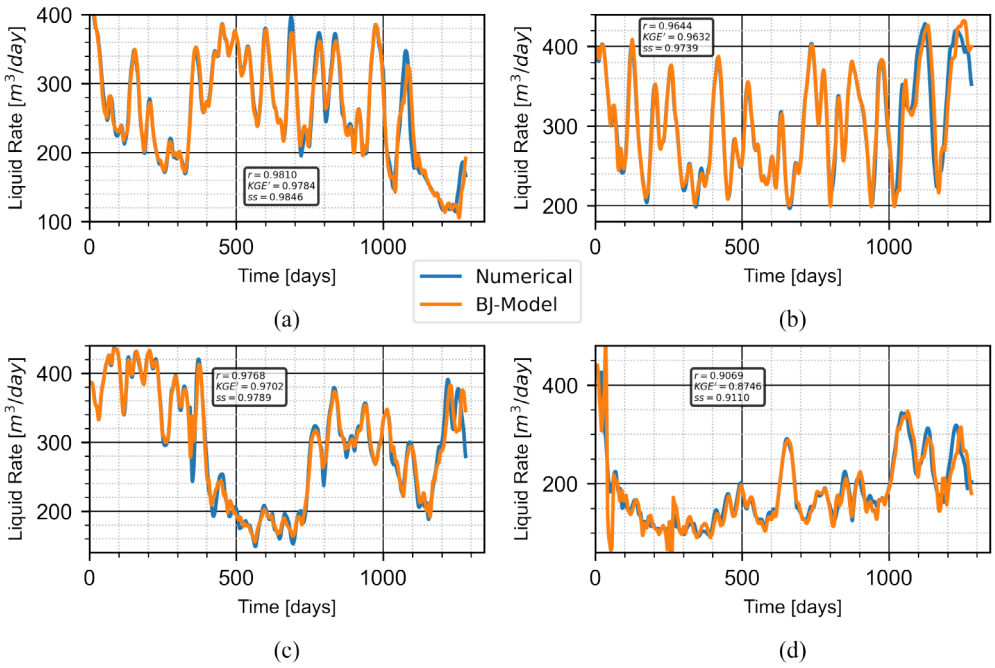

Figure 5.3: Forecasted (BJ-Model) and response (Numerical) liquid rate of well_5 during RTO for (a) PAD_A (b) PAD_B (c) PAD_C (d) PAD_D of bitumen recovery KPI.

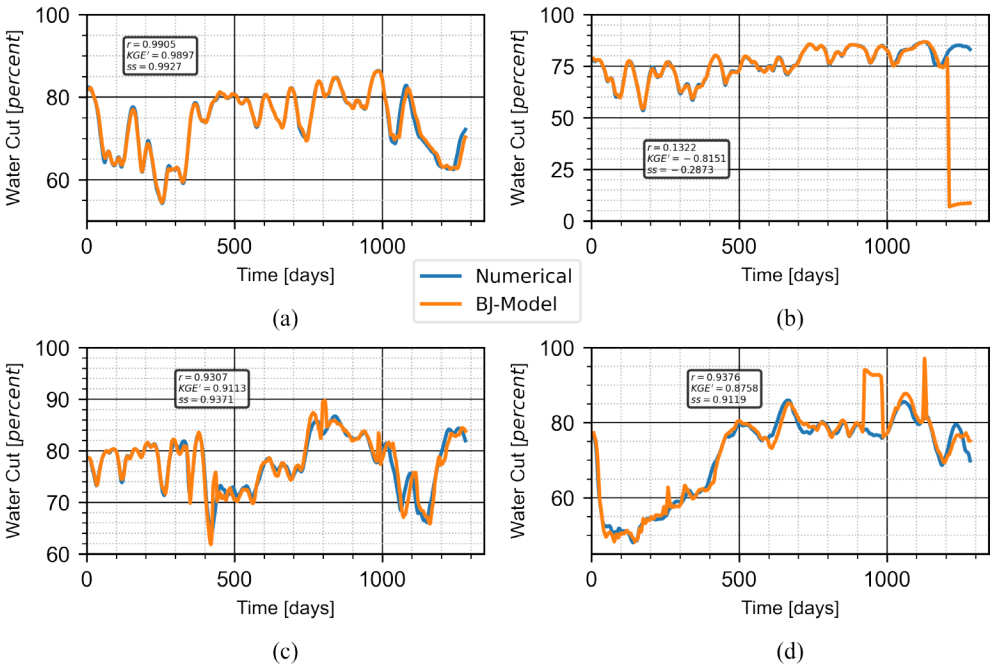

Figure 5.4: Forecasted (BJ-Model) and response (Numerical) water cut of well_5 during RTO for (a) PAD_A (b) PAD_B (c) PAD_C (d) PAD_D of bitumen recovery KPI.

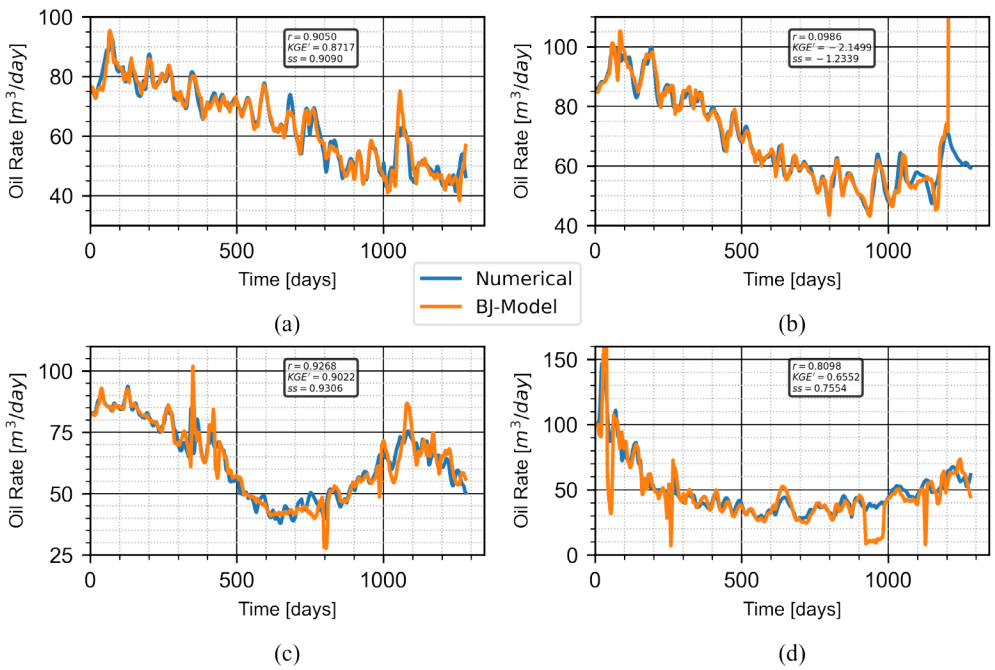

Figure 5.5: Estimated (BJ-Model) and response (Numerical) oil rate of well_5 during RTO for (a) PAD_A (b) PAD_B (c) PAD_C (d) PAD_D of bitumen recovery KPI.

5.5.2 Key Performance Indicators.

Fig 5.6 shows the evolution of cumulative NPV at the end of the RTO for all combinations of KPIs that must include NPV for the individual pads. What Fig 5.6 shows for Figs 5.6a, 5.6b, and 5.6c, the gradient of the cumulative NPV rise slowed by day 500 for the NPV_RF case but slowed by day 800 for PAD_D (Fig 5.6d). The delay in Fig 5.6d is because the average pad temperature was higher at the start of RTO in PAD_D than in PAD A-C. Also, the cumulative NPV slows because NPV KPI minimizes the amount of steam allocation over time. The KPI combinations with at least NPV_aveTemp show a consistent steep rise in the gradient of the cumulative NPV for all pads throughout the RTO. The steep rise of cumulative NPV is due to the higher steam chamber growth of at least NPV_aveTemp compared to NPV_RF combinations. The NPV_aveTemp showed the best performance in all four PADS at the end of RTO. Based on the gradient of the cumulative NPV rise in all four PADs, it can be inferred that NPV_aveTemp KPI combination with or without cSOR

and RF shows better performance in long-term SAGD process NPV KPI optimization. The NPV performance of the combinations for all pads is ranked as NPV_aveTemp > NPV_cSOR_RF_aveTemp > NPV_RF_aveTemp > NPV_RF.

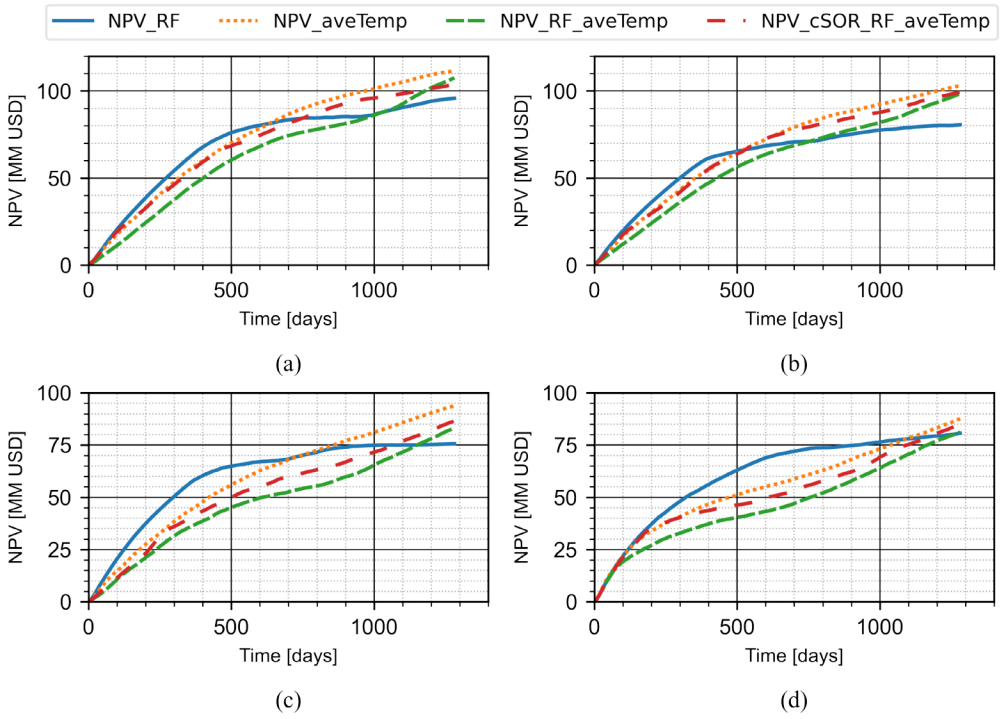

Figure 5.6: Cumulative NPV comparison for different joint NPV and other KPIs (a) PAD_A (b) PAD_B (c) PAD_C (d) PAD_D

The trend in the evolution of cumulative NPV (Fig 5.7) for KPI combinations with at least cSOR follows that of NPV as expected. However, the lower performance of the cumulative NPV with cSOR_RF is significantly lower than when the combinations have aveTemp KPI. The above statement is further confirmed, as shown in Fig 5.8. The performance in Figs 5.6-5.8 confirms the statement of the problem to optimize NPV that there should be a balance between the economic and steam chamber growth KPIs. Additionally, what Figs 5.6-5.8 show that though RF KPI leads to an increase in the steam chamber, its combination with economic KPIs depends on the average temperature at the start of RTO. The temperature at the start of RTO also affected the difference in performance between NPV_RF and cSOR_RF cases. Increasing average temperature minimizes the difference between the two cases, as shown

in Fig 5.8. In Fig. 5.8a, the difference looks higher because PAD_A has nine wells while the rest of the PADs have eight wells. The performance of cumulative NPV with at least aveTemp KPI, as in Fig 5.9 shows RTO of NPV KPI performance, is relatively the same for all joint KPI optimization with aveTemp.

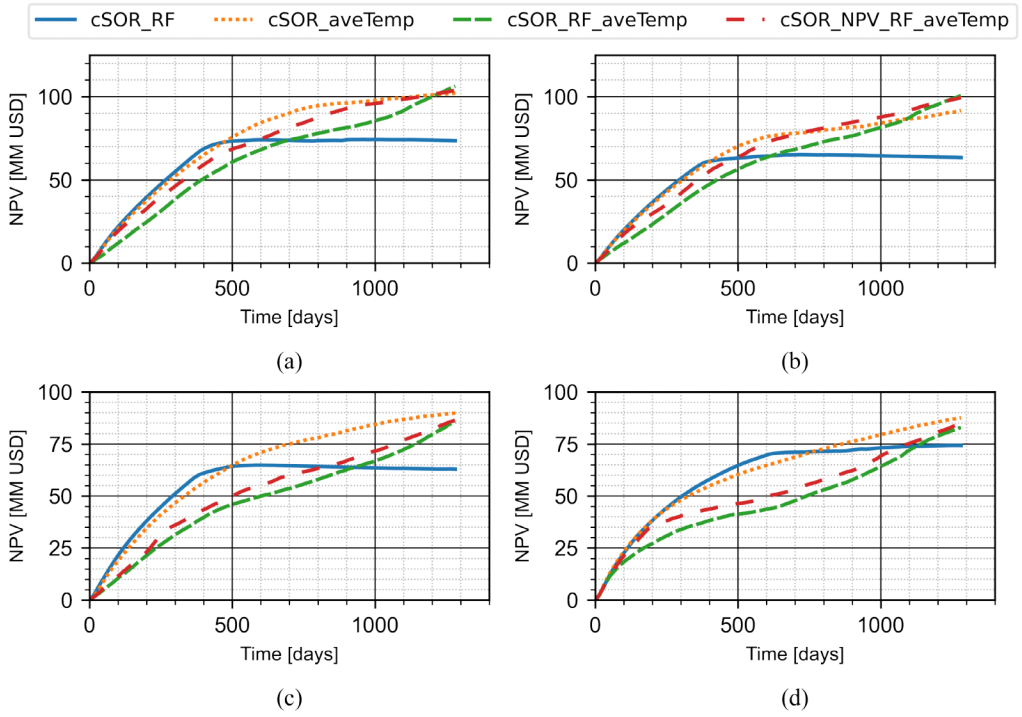

Figure 5.7: Cumulative NPV comparison for different joint cSOR and other KPIs (a) PAD_A (b) PAD_B (c) PAD_C (d) PAD_D

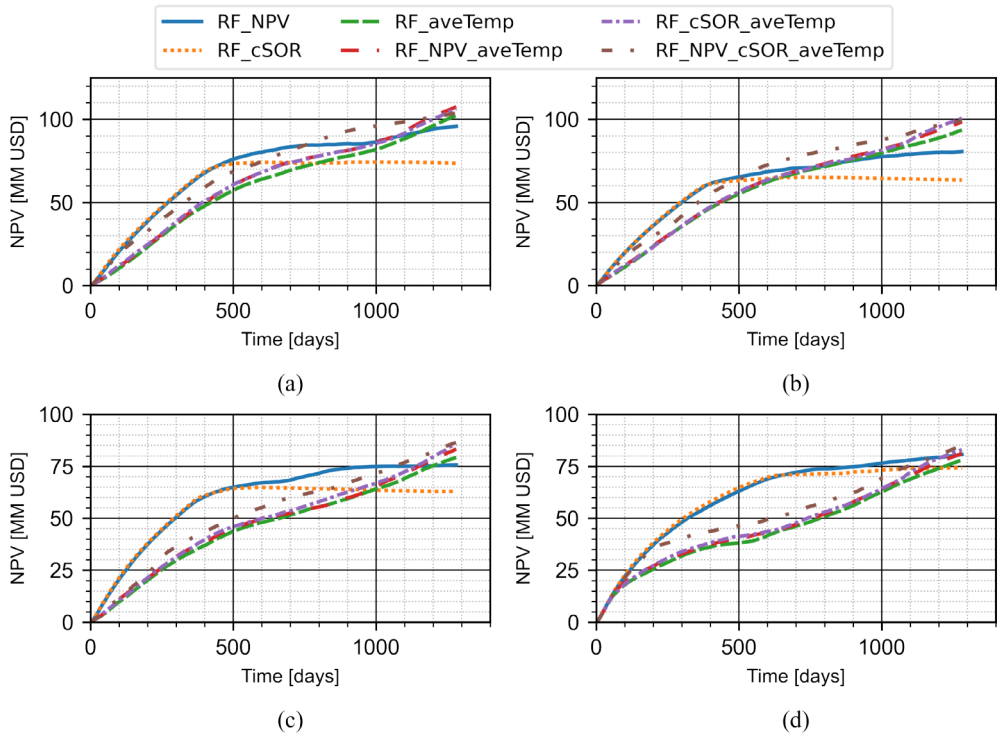

Figure 5.8: Cumulative NPV comparison for different joint RF and other KPIs (a) PAD_A (b) PAD_B (c) PAD_C (d) PAD_D

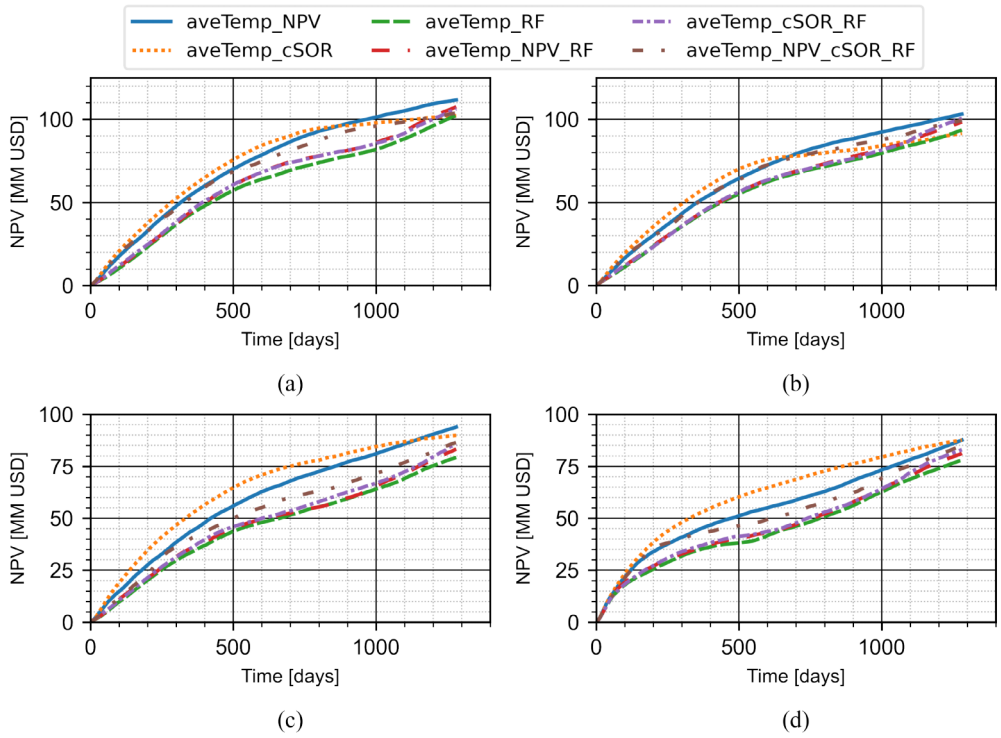

Figure 5.9: Cumulative NPV comparison for different joint average temperature and other KPIs (a) PAD_A (b) PAD_B (c) PAD_C (d) PAD_D

Fig 5.10 shows the evolution of cumulative NPV at the end of the RTO for all the joint KPI combinations. It can be inferred from Fig 5.10 that in all the pads, the economic-aveTemp joint KPI outperforms all KPI combinations. Hence, a combination of either cSOR-aveTemp or NPV-aveTemp KPIs is preferred over three or four KPI combinations if the objective is solely NPV optimization. The three or four joint objectives' performance is lower than the economic-aveTemp joint KPI because RF and aveTemp increase steam allocation, which is the main cost contributor to lowering cumulative NPV. The NPV performance of the combinations for all pads is ranked as NPV_aveTemp > cSOR_aveTemp > NPV_cSOR_RF_aveTemp > NPV_RF_aveTemp > RF_aveTemp > RF_aveTemp > NPV_RF > cSOR_RF. The NPV KPI does not show the resource required to achieve the forecast and the impact of the SAGD process on the environment. Hence, the joint NPV-cSOR performance of each case helps determine the optimal KPI combinations.

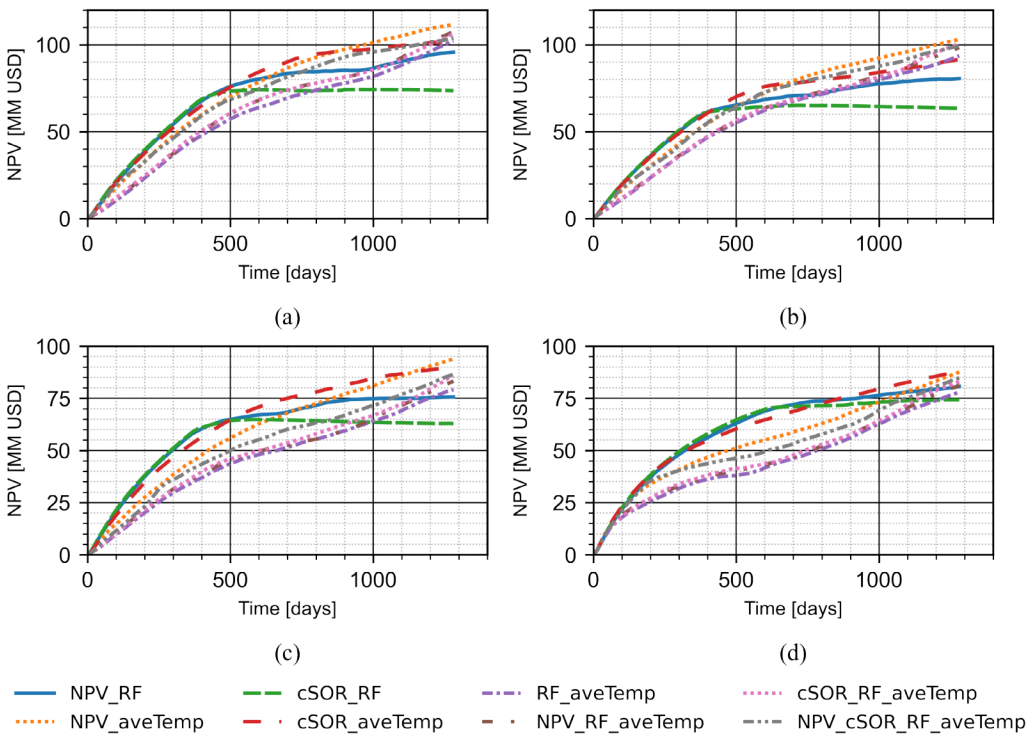

Figure 5.10: Cumulative NPV comparison for different KPIs (a) PAD_A (b) PAD_B (c) PAD_C (d) PAD_D

Fig 5.11 illustrates the evolution of cSOR for joint KPI optimizations of NPV and other KPI combinations of the four different pads. Lower cSOR performance indicates a low carbon footprint, reduced resource requirements, and improved economic returns. The performance at the end of RTO cSOR for all the cases fell between the typical SAGD process range of two to five. All cases with aveTemp in Fig 5.11 have an elevated cSOR relative to NPV_RF. The elevated cSOR results from the higher steam injection, leading to increased mobile bitumen saturation. NPV_RF case for PADs A - C (Fig. 5.11a, 5.11b, and 5.11c) saw a decrease in cSOR until about day 500 when it flattened before an increase and flattened. The behavior is consistent with cumulative NPV (Fig. 5.6a, 5.6b, and 5.6c), which saw a similar trend. Whenever the cSOR drops, the joint objective is influenced significantly by the NPV, leading to mobilized oil production. The rise of cSOR means RF or aveTemp is the main influencing KPI of the joint objective. The cSOR performance of the combinations for all pads is ranked as NPV_aveTemp > NPV_cSOR_RF_aveTemp

> NPV_RF_aveTemp > NPV_RF. Though lower cSOR is preferred, the low cSOR of NPV RF is due to decreasing bitumen production by the end of the RTO.

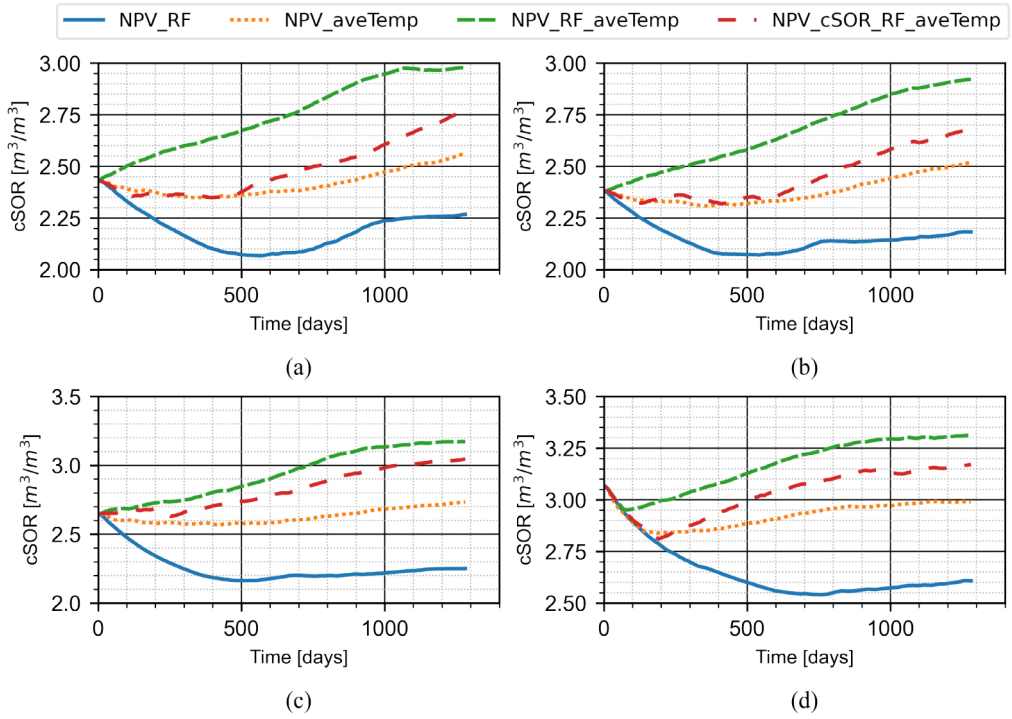

Figure 5.11: cSOR comparison for different joint NPV and other KPIs (a) PAD_A (b) PAD_B (c) PAD_C (d) PAD_D

The trend in the evolution of cumulative cSOR (Fig 5.12) for KPI combinations with at least cSOR shows that for two joint KPIs, cSOR dominates, while for three or four, RF_aveTemp dominates. However, cSOR_RF combinations had similar cSOR performance as cSOR_aveTemp that did not translate into optimum cumulative NPV (Fig 5.7). It can be inferred that, for a combination of economic and recovery KPIs, the economic KPI dominates, as further confirmed in Figs 5.13-5.14. In Fig 5.9, the cumulative NPV performance for all combinations with aveTemp is relatively the same for all cases, but there is a clear separation with cSOR performance (Fig 5.14). Based on the cSOR performance in Fig 5.14, the performance ranking in Fig 5.7 can be rearranged as cSOR_aveTemp > NPV_aveTemp > aveTemp_NPV_cSOR_RF > aveTemp_cSOR_RF ≈ aveTemp_NPV_RF > aveTemp_RF. The rankings above

are based on the required resource and environmental impact. Though both cSOR and NPV are expected to minimize the required resource for allocation, what Fig 5.14 shows is that cSOR is a strong KPI for reducing steam allocation relative to NPV KPI. The combined effect of NPV_cSOR can be observed with the aveTemp_NPV_cSOR_RF case for all pads (Fig 5.14), significantly lowering the required steam allocation.

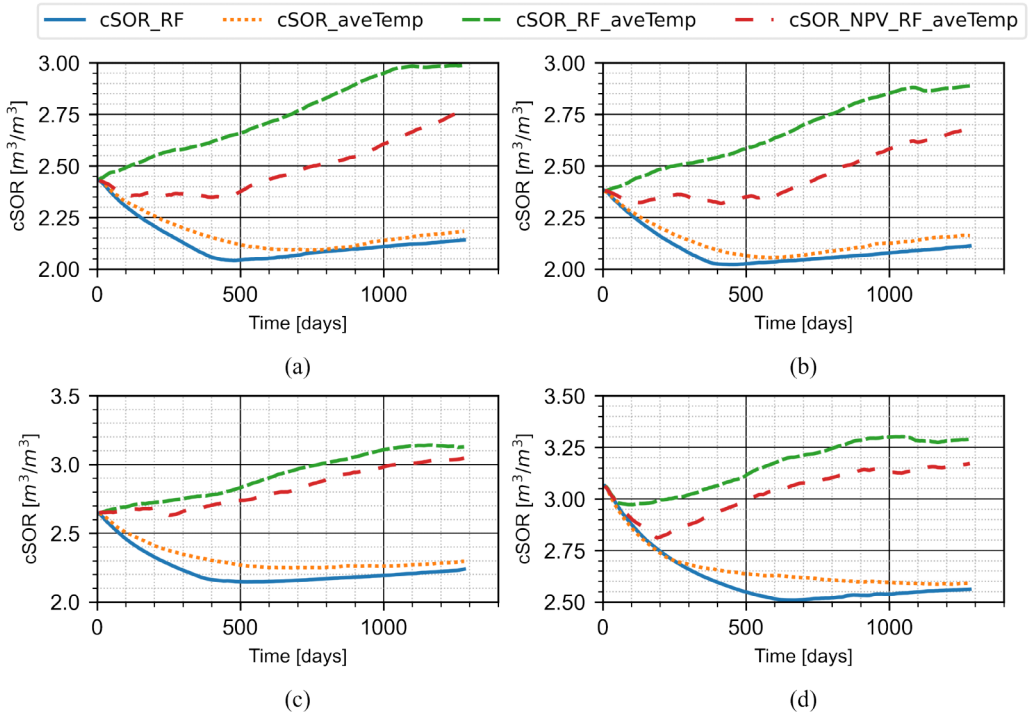

Figure 5.12: cSOR comparison for different joint cSOR and other KPIs (a) PAD_A (b) PAD_B (c) PAD_C (d) PAD_D

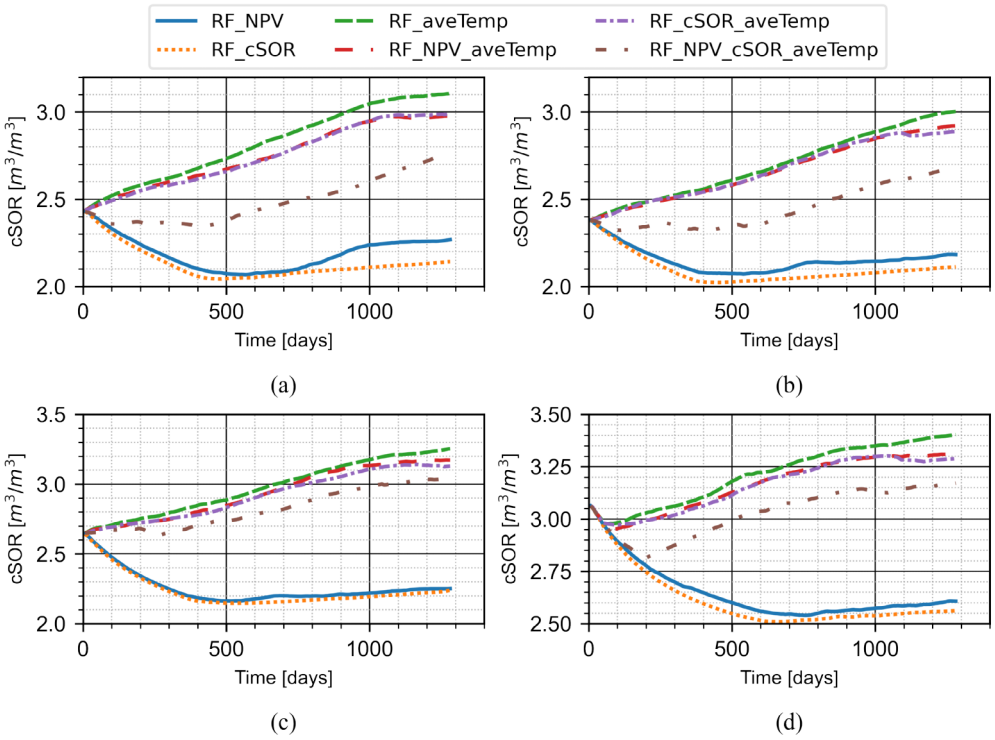

Figure 5.13: cSOR comparison for different joint RF and other KPIs (a) PAD_A (b) PAD_B (c) PAD_C (d) PAD_D

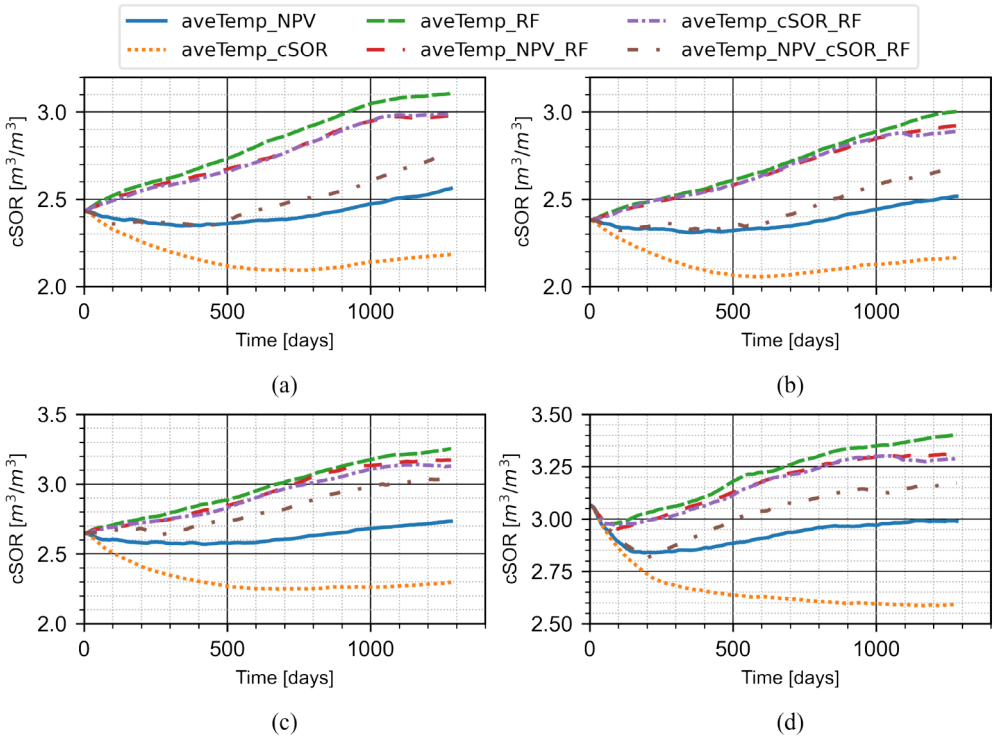

Figure 5.14: cSOR comparison for different joint average temperature and other KPIs (a) PAD_A (b) PAD_B (c) PAD_C (d) PAD_D

Fig 5.15 illustrates the evolution of cSOR for the four different pads. Except for cSOR_aveTemp, all cases with aveTemp showed an increasing cSOR over time. NPV_aveTemp case showed a median cSOR performance relative to all cases. Based on the performance in Fig 5.15 the performance ranking for all cases can be rearranged as cSOR_aveTemp > NPV_aveTemp > aveTemp_NPV_cSOR_RF > aveTemp_cSOR_RF ≈ aveTemp_NPV_RF > aveTemp_RF > NPV_RF > cSOR_RF . NPV_RF case combines weak resource minimizer (NPV) and weak steam chamber growth KPIs, leading to better performance than strong resource minimizer (cSOR) with weak steam chamber growth KPIs. What can be concluded is from Figs 5.10 and 5.15 strong resource minimizer and steam chamber growth KPIs are required to achieve an optimal balance between maximizing economic returns and minimizing the required resource.

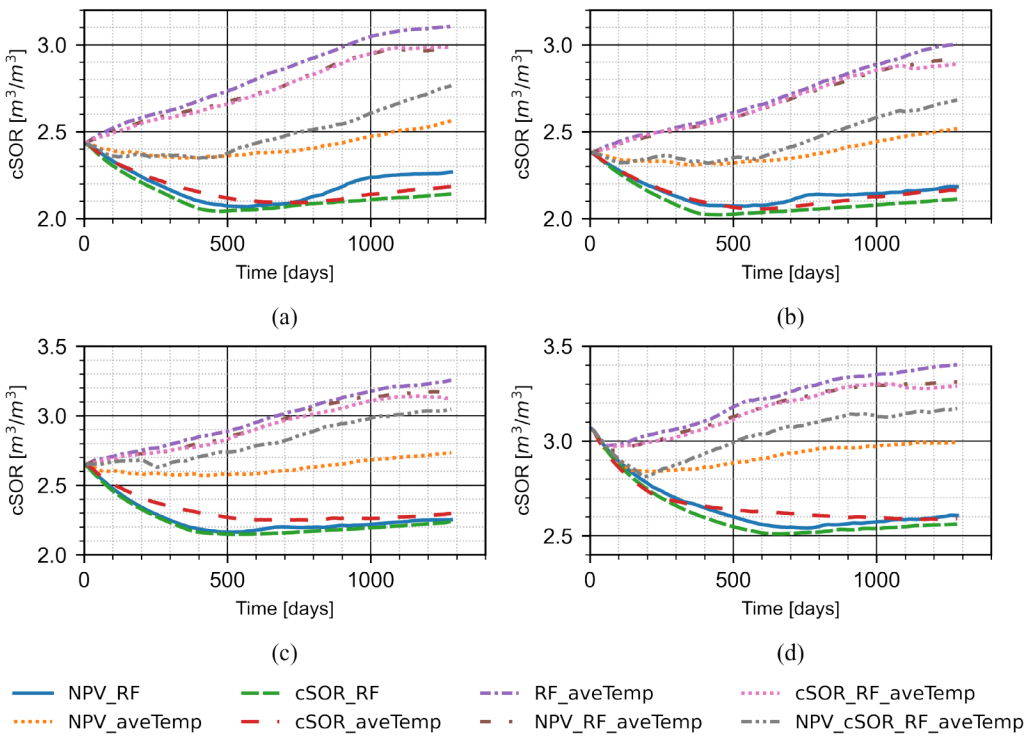

Figure 5.15: cSOR comparison for different KPIs (a) PAD_A (b) PAD_B (c) PAD_C (d) PAD_D

As shown in Fig 5.16, recovery performance for all pads shows NPV_RF recovers more bitumen per pore volume of steam injected. On a per pore volume injected basis, two joint KPI optimization recovers more bitumen than three or four joint KPI. At 0.2 PVI, NPV_cSOR_RF_aveTemp case recovers between $0.5 to 1.5\%$ more bitumen recovery for all pads. The additional recovery can be attributed to the addition of the cSOR KPI, which leads to the increased production of mobilized bitumen. Also, lower cSOR (Fig 5.11) was achieved, which means a lower steam requirement and emission. The NPV (Fig 5.6) and cSOR (Fig 5.11) performance at the end of RTO is approximately the same for all cases. Hence the performance in terms of recovery per pore volume injected (PVI) shows NPV_aveTemp is the best combination. NPV_RF shows better performance for all pads but is not recommended if, at the start of RTO average pad temperature is 90^oC and below.

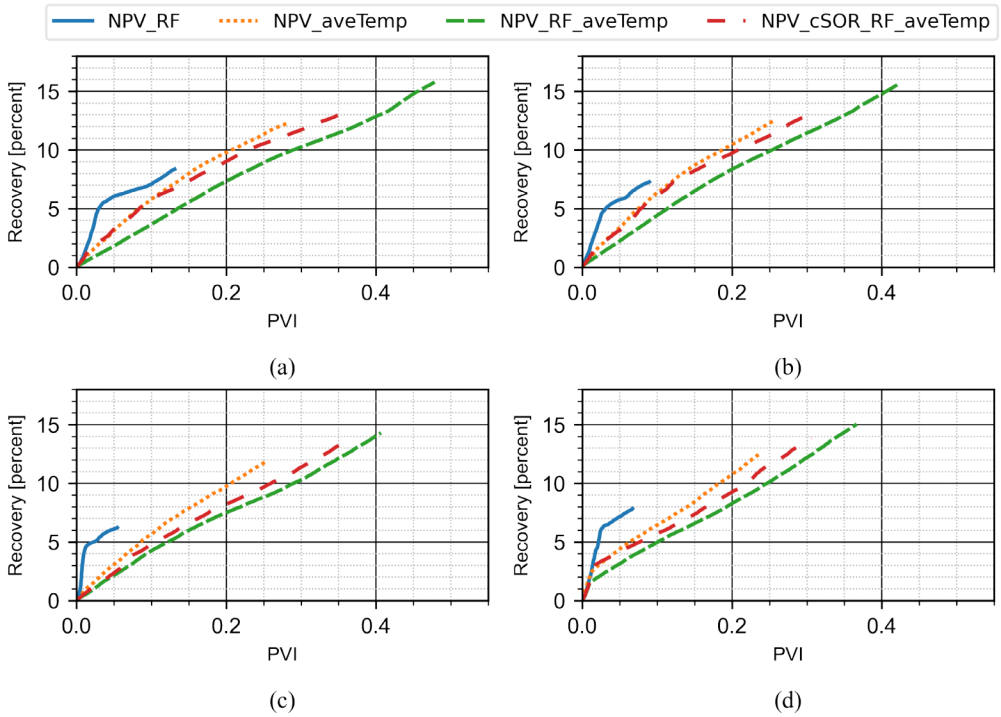

Figure 5.16: Recovery comparison for different joint NPV and other KPIs (a) PAD_A (b) PAD_B (c) PAD_C (d) PAD_D

Fig 5.17 trend for recovery performance of KPI combinations of cSOR with other SAGD KPI is consistent with NPV with other SAGD KPI (Fig 5.16). cSOR KPI combined with other KPIs of SAGD achieves the same performance at a lower PVI than NPV combinations, as in Fig 5.16. In Fig 5.18, it can be seen that RF_cSOR recovery performance terminates early because less steam is injected. The NPV (Fig 5.8) performance evolution of all KPI combinations with RF_aveTemp without cSOR was relatively the same at the end of RTO following the recovery performance in Fig 5.18. Addition of cSOR KPI to the combination lowered the steam injected between 0.07 to 0.23 pore volume and hence cSOR performance in Fig 5.13.

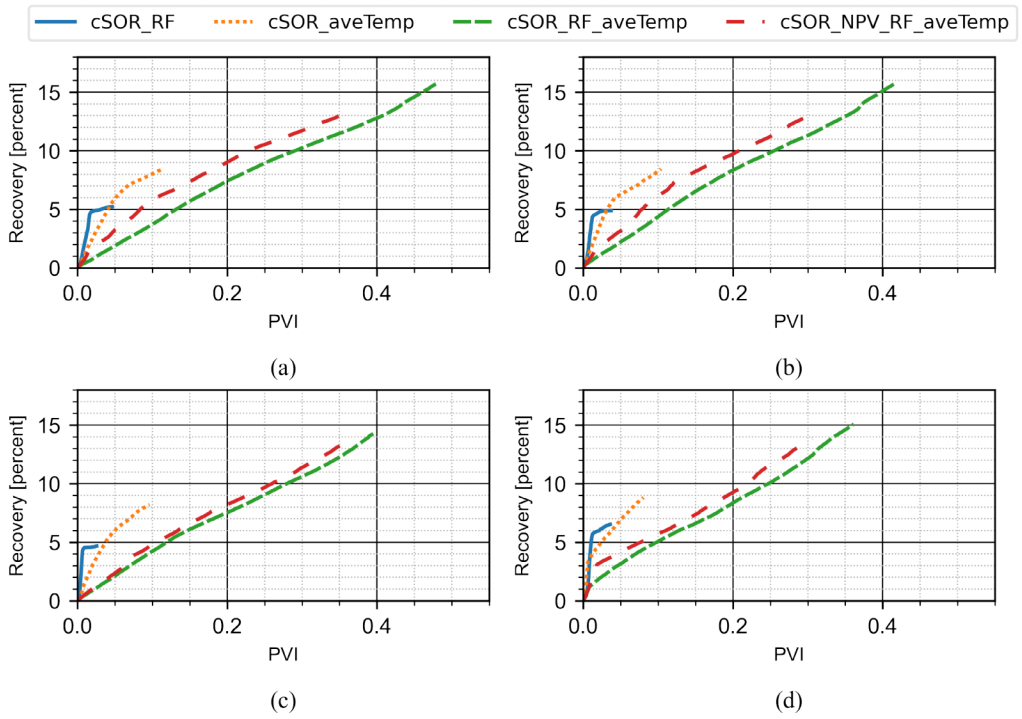

Figure 5.17: Recovery comparison for different joint cSOR and other KPIs (a) PAD_A (b) PAD_B (c) PAD_C (d) PAD_D

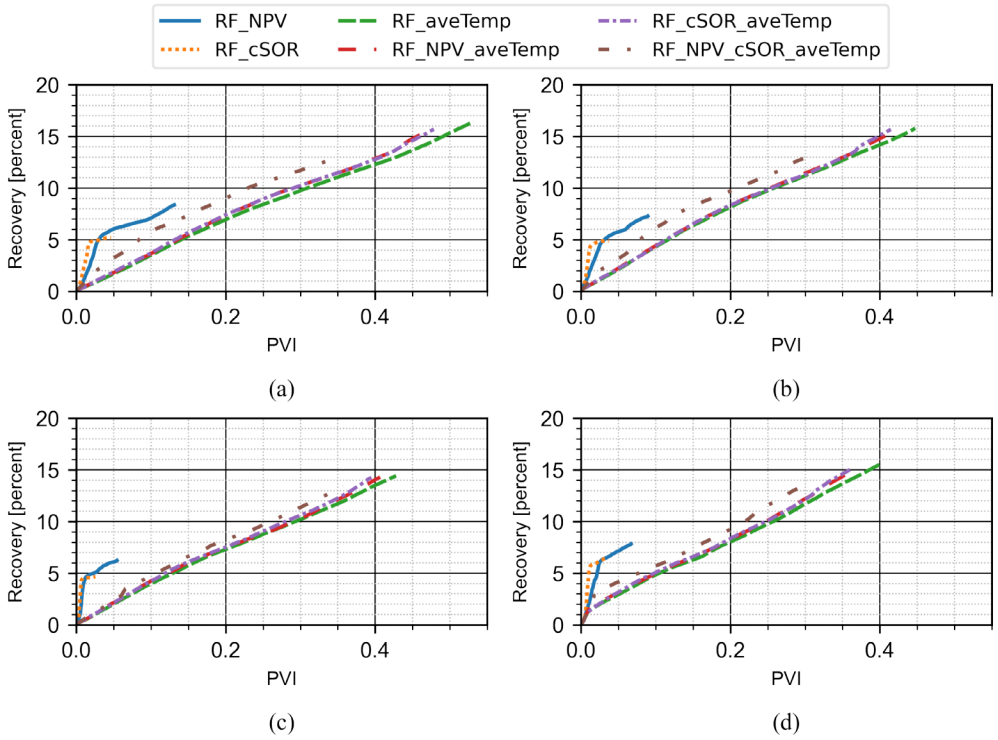

Figure 5.18: Recovery comparison for different joint RF and other KPIs (a) PAD_A (b) PAD_B (c) PAD_C (d) PAD_D

The recovery performance for all combinations with aveTemp shows that aveTemp_cSOR and aveTemp_RF had the minimum and the maximum, respectively, at the end of RTO (Fig 5.19). Ranking by the PVI bases, aveTemp_cSOR $>$ aveTemp_NPV $\approx$ aveTemp_NPV_cSOR_RF $>$ aveTemp_cSOR_RF $\approx$ aveTemp_NPV_RF $\approx$ aveTemp_RF. What can be deduced from the rankings is that a strong cost minimizer can balance the effect of strong steam chamber growth KPI. Hence at the same PVI combination of cSOR or NPV with aveTemp and RF recovery is between 1 to 4% higher.

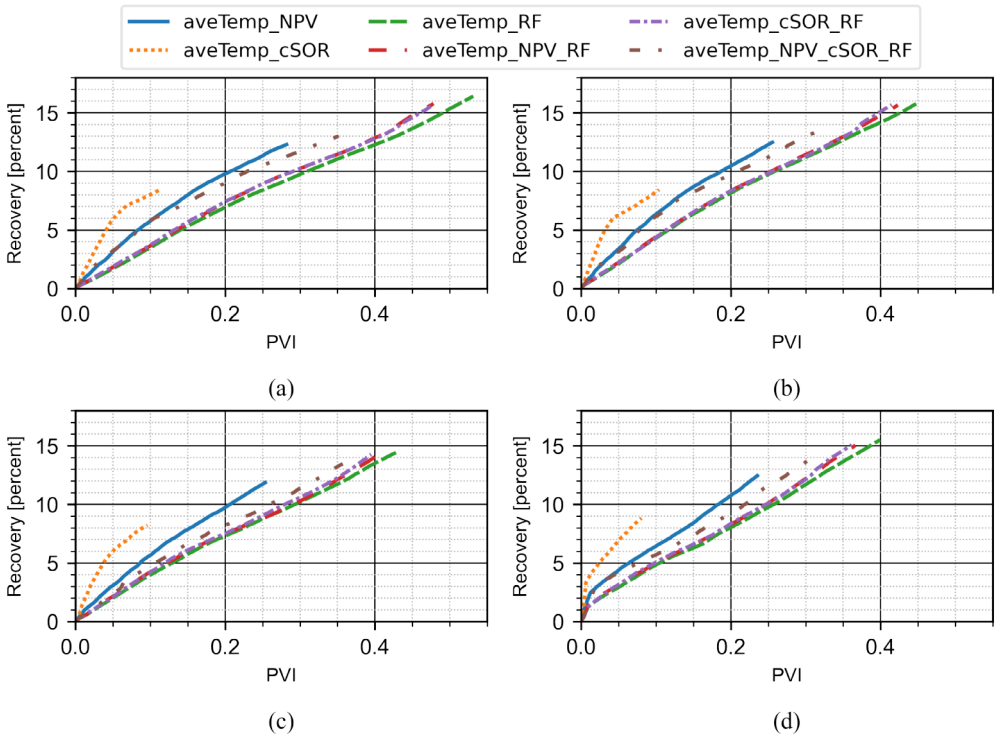

Figure 5.19: Recovery comparison for different joint average temperature and other KPIs (a) PAD_A (b) PAD_B (c) PAD_C (d) PAD_D

Fig 5.20 shows the recovery performance for all pads at the end of RTO. The recovery values in Fig 5.20 are the recovery due to the RTO. The order of performance rankings for all cases RF_aveTemp > cSOR_RF_aveTemp ≈ NPV_RF_aveTemp > NPV_cSOR_RF_aveTemp > NPV_aveTemp > cSOR_aveTemp > NPV_RF > cSOR_RF. The goal of RTO is to minimize the amount of steam injected while maximizing recovery and economic returns. Based on PVI, the recovery performance is re-ordered as cSOR_aveTemp > NPV_aveTemp > NPV_cSOR_RF_aveTemp > cSOR_RF_aveTemp ≈ NPV_RF_aveTemp > RF_aveTemp > NPV_RF ≈ cSOR_RF . From Fig 5.20, NPV_RF and cSOR_RF recorded high recovery with PVI for all pads. However, both cases are ranked lower because of the NPV performance (Fig 5.10).

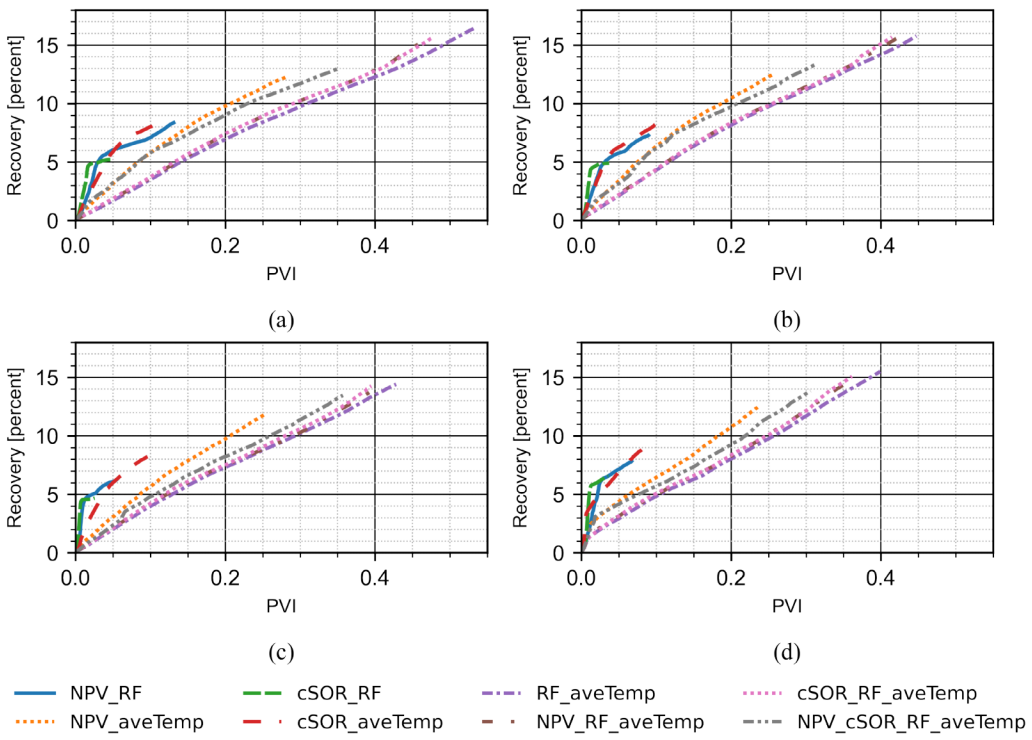

Figure 5.20: Recovery comparison for different KPIs (a) PAD_A (b) PAD_B (c) PAD_C (d) PAD_D

The fluid balance is one of the operational decisions that causes SAGD to perform below expectation (Yeung, 2019). The cases studied showed the impact of optimally balancing the injected steam influence on the economic, thermal efficiency, and environmental impact of the SAGD process. A study by Edmunds and Chhina (2001) found that the economics of SAGD projects is more affected by the steam oil ratio than the production rate, consistent with the results presented in this study. The best combination of cSOR_aveTemp had the optimal economic (Fig 5.10), thermal efficiency, and low greenhouse gas emission (Fig 5.15) had lower recovery indicative of a low production rate at the end of RTO. The use of steam oil ratio alone as an objective can lead to poor performance in heterogeneous reservoirs (Guo et al., 2018), and hence as shown in this work, a joint goal with steam chamber conformance. The decreasing temperature in Fig 5.21 pad average temperature explains the poor performance of the NPV_RF and cSOR_RF cases due to an imbalance in production favor, causing a temperature drop. The recovery performance (Fig

5.20) of the NPV_RF and cSOR_RF cases showed improving performance on PVI and similar behavior with economic (Fig 5.10) and thermal efficiency (Fig 5.15) performance initially but poor performance after two years of RTO. The behavior of NPV_RF and cSOR_RF cases shows that the combinations are not recommended for the normal phase of SAGD operations. Hence, the lesson learned here is that the average temperature in the reservoir or the steam chamber should reach maturity at the start-up phase if RTO will always be preferred at the blow-down phase. The decreasing temperature behavior is the goal of the blow-down phase, where steam is co-injected with non-condensable gas. Another observation from Fig 5.21 is that NPV_aveTemp is excellent in expanding the steam chamber (i.e., higher temperature indicative of higher steam chamber volume) compared to cSOR_aveTemp.

Nevertheless, on average, cSOR_aveTemp recovers two percent more oil on PVI. Additionally, a combination of three or four KPIs performance is lower than a combination of two SAGD operations RTO considering the aggregated performance of all KPIs as shown in this study. Therefore, the conclusions on the rankings in this study will not hold at the blow-down phase. In addition, starting RTO at a much higher temperature, cSOR_RF and NPV_RF combinations will be preferred based on lower resource requirements. Finally, the study used a heterogenous reservoir with no shale barriers, which impedes steam chamber growth. However, the authors contend there will be no change in the order of performance rankings even though there will be a reduction in each KPI metric.

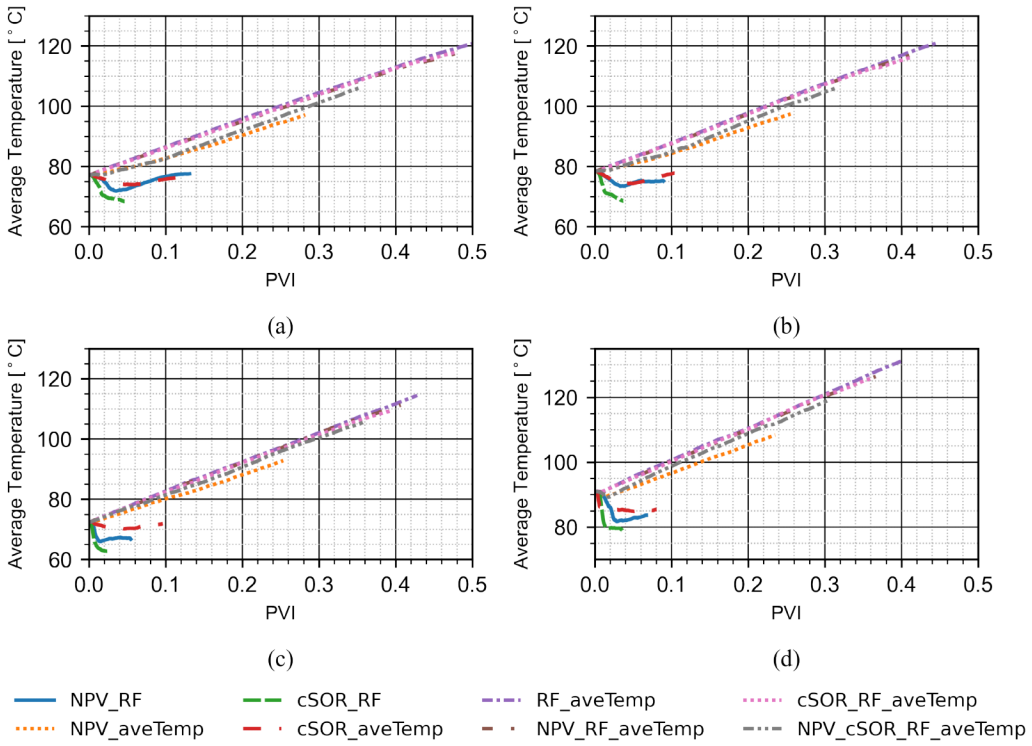

Figure 5.21: Temperature comparison for different KPIs (a) PAD_A (b) PAD_B (c) PAD_C (d) PAD_D

5.6 Conclusion

An ADMM-based strategy for optimizing the allocation of steam across multiple criteria and pads has been presented in this work. Furthermore, the workflow was set up so that the optimal KPI combination can be identified for a short-term optimization problem formulation that has the potential to accomplish long-term performance goals for SAGD KPIs. Based on the research findings, the following are the conclusions.

1. cSOR_aveTemp combination is the most effective in meeting long-term normal phase SAGD operations performance goals.

2. KPI combination of three or four RTO can attain long-term SAGD recovery and economic performance goals at a higher resource requirement.

3. cSOR_aveTemp KPI combination requires approximately less than three to five times steam than cSOR_RF_aveTemp, NPV_RF_aveTemp, and

NPV_cSOR_RF_aveTemp to generate the approximately same amount of economic returns optimization.

4. cSOR_aveTemp KPI combination requires less than two to three times more steam than NPV_aveTemp to generate the approximately same amount of economic returns optimization.

The proposed workflow has a significant potential for multi-criteria multi-pad real-time steam allocation decisions in bitumen recovery.

Chapter 6

Concluding Remarks and Recommendations

6.1 Concluding Remarks

RTO workflow has the ability to improve on reservoir management operations decisions short and long-term goals. Application of RTO to prioritize steam allocation, robust economic uncertainty management, and multi-pad challenges have been addressed in this study. Each approach used in addressing the challenges listed are verified using a field-scale model and the outcome of the proposed improvements to RTO workflow are presented.

A proactive steam prioritization allocation workflow that can determine the effect of steam injection pattern on heavy oil recovery by using system identification to a changing steam availability. The strength of the proposed method is observable from the results as NPV is increased between 25% to 50% compared to the base case with a constant steam injection pattern in all cases examined. Due to the efficient use of available steam, the steam-to-oil ratio was decreased between 5% to 15%. Steam prioritization outperforms no steam prioritization scenario with an additional NPV increase between 14.7% to 25% when compared individually to the base case.

The study proposes data-driven input-output normalization to incorporate operating constraints based on their physical range. The workflow includes model training-updating based on the concept of forgetting factor to adapt the data-driven model to the current state of the reservoir. A robust opti-

mization problem scheme in which economic risk is mitigated by formulating the objective as a tradeoff of expected returns and risk is managed in real-time. A modified Modigliani's risk-adjusted performance has been implemented to minimize the possibility of selecting the wrong optimal risk-return tradeoff of non-symmetric return realizations in this work. Application of the proposed workflow on a synthetic reservoir with steam NCG co-injection showed the data-driven calibrated model forecast performance shows a reasonable agreement with the synthetic reservoir throughout the optimization period. In addition, the optimization study with the proposed workflow also showed a NPV increase of approximately 25%–77% and a decrease in the cumulative cSOR from 4.5 to 6.7% compared to continuous steam injection base case. The reduction in cSOR indicates a lower steam requirement. An increase in methane sequestered demonstrates workflow ability to reduce greenhouse gas emissions while improving SAGD NCG co-injection KPIs.

In this contribution, ADMM and a dynamic data-driven model to reduce the computational cost of RTO. ADMM coordinates in real-time field-wide use of shared steam generation which grows the steam chamber without negatively affecting the long-term economic performance. A SAGD field with four pads with 33 well-pairs shows that for all four pads, an economic-based KPI limits the achievement of long-term goals because it cannot account for the future state beyond the horizon under consideration due to hindered steam chamber growth. For the steam chamber expansion and bitumen recovery KPI, high recovery and economic performance are achieved, but with a high resource requirement, leading to a high carbon footprint. On the other hand, an alternating economic and bitumen recovery KPI achieves high economic performance while minimizing resource requirements that decrease carbon footprint.

This work presents a study of multiple combinations of SAGD KPIs for a multi-pad real-time steam allocation. The KPI combinations used in this study are NPV, cSOR, RF, and aveTemp. A dynamic data-driven model based on the Box-Jenkins model structure is used to model the SAGD recovery process and a first principle simulator as a proxy for an actual reservoir. A multi- and many-objective optimization of real-time multi-pad steam allocation using

the ADMM is proposed. A compromise programming approach guides the decision-maker choice of the optimum control setpoints of the nondominated solutions at each horizon. At the end of three and half years of RTO, the optimal KPI combination is ranked based on the aggregated performance of NPV, cSOR, and RF of SAGD multi-pad steam allocation. A representative western Canadian reservoir model with four pads and 33 well pairs is used for this study. The aggregated performance of this study's results showed that joint optimization of an economic and a steam chamber growth KPIs of two is better than a combination of three or four. The choice of the joint economic and steam chamber growth KPIs depends on the average pad temperature at the start of RTO to achieve optimal fluid balance in the long term. cSOR or NPV with RF joint KPI performs optimally at average pad temperatures above 90^oC while cSOR or NPV with aveTemp below 90^oC at the start of RTO to achieve injected and produced fluid balance. Optimum economic return, recovery, and greenhouse gas emission of the SAGD process are achieved with cSOR KPI as the primary economic objective.

The contributions towards improving real-time SAGD operations optimizations in this research is summarized as follows:

1. A steam prioritization approach for real-time SAGD operations optimization that leads to improvement in NPV while reducing cSOR with varying steam availability at each control horizon.

2. A forgetting factor approach to adapt a data-driven model with input-output normalized to incorporate operating constraints based on their physical range.

3. A modified Modigliani's risk-adjusted performance for selecting the optimal risk-return tradeoff of non-symmetric return realizations in real-time economic robust optimization.

4. A control framework for multi-pad single and multi-criteria real-time optimization that leads optimize short-term objectives while achieving

long-term goals by balancing the steam chamber growth with increasing bitumen recovery, lowering cSOR, and maximizing economic returns.

5. An alternating single objective real-time optimization based on time and temperature which leads to balancing the steam chamber growth with increasing bitumen recovery, lowering cSOR, and maximizing economic returns as an alternative to multi-criteria real-time optimization.

6.2 Recommendations

Although in this research, attempts were made to improve on the applicability of RTO workflow on a reservoir management there still remain additional work to be done. The following recommendations suggested below can improve on the efficiency of RTO workflow.

- The proposed steam allocation prioritization is based on the individual well KPI being optimized performance. Application of the well-pair productivity and injectivity indices can further be explored.

- The data-driven model performance when close to lower limits of the outputs degrades significantly. Training of the data-driven with a multi-objective KGE objective which learns the correlation, bias and the variance of the past data can be an alternative to improve forecasting performance.

- Due to computational resource limitations the validation test for were tested for normal and wind-down phases separately. Additionally, the proposed improvements to RTO workflow were tested separately. With more computational resource, the improvements can be integrated and tested from the build-up through normal and to wind-down phase.

- In this research it was assumed all well-pairs and well-pads start producing at the same time. An improvement of the workflow that accounts different well-pairs and well-pads with different maturity or years of operation competing for a limited resource can be explored.

- Robust optimization with additional candidate uncertain variables instead of only the oil price as tested in this work can be investigated.

Bibliography

Aackermann, P. E. (2015). Stochastic optimization and risk management in the production optimization of oil reservoirs. Master's thesis, Technical University of Denmark, Department of Applied Mathematics and Computer Science, Richard Petersens Plads, Building 324, DK-2800 Kgs. Lyngby, Denmark, compute@compute.dtu.dk. DTU supervisor: John Bagterp Jørgensen, jbjo@dtu.dk, DTU Compute.

Aboorvanathan, R., A. Hossini, C. Dong, V. Dehdari, and J. Feeney (2019, 9). Sagd production optimization through preferential steam allocation. In *SPE Annual Technical Conference and Exhibition*, Calgary, Alberta, Canada. Society of Petroleum Engineers. https://doi.org/10.2118/195984-MS.

Al-Aghbari, M., M. Al-Wadhahi, and A. M. Gujarathi (2022). Multi-objective optimization of brugge field for short-term and long-term waterflood management. *Arabian Journal for Science and Engineering 47*(9), 11069–11087. https://doi.org/10.1007/s13369-021-05614-7.

Al-Gosayir, M., J. Leung, and T. Babadagli (2012, 11). Design of solvent-assisted sagd processes in heterogeneous reservoirs using hybrid optimization techniques. *Journal of Canadian Petroleum Technology 51*, 437–448. https://doi.org/10.2118/149010-PA.

Alexey (2018, 8). Major sagd projects in canada. http://sellsidehandbook.com/2018/08/04/major-oil-sands-projects-in-canada/. Accessed: 2022-11-13.

Anderson, T. W. and D. A. Darling (1952). Asymptotic Theory of Certain

"Goodness of Fit" Criteria Based on Stochastic Processes. *The Annals of Mathematical Statistics 23*(2), 193–212.

Austin-Adigio, M. and I. Gates (2019). Non-condensable gas Co-Injection with steam for oil sands recovery. *Energy 179*, 736–746.

Awotunde, A. A. and N. Sibaweihi (2012, 12). Consideration of voidage replacement ratio in well placement optimization. In *SPE Kuwait International Petroleum Conference and Exhibition 2012*, Volume 2, Kuwait City, Kuwait, pp. 763–775. Society of Petroleum Engineers. https://doi.org/10.2118/163354-MS.

Awotunde, A. A. and N. Sibaweihi (2014). Consideration of voidage-replacement ratio in well-placement optimization. *SPE Economics & Management 6*, 40–54. https://doi.org/10.2118/163354-PA.

Benders, J. F. (1962, 12). Partitioning procedures for solving mixed-variables programming problems. *Numer. Math. 4*, 238–252. https://doi.org/10.1007/BF01386316.

Blank, J. and K. Deb (2020). Pymoo: Multi-objective optimization in python. *IEEE Access 8*, 89497–89509. https://doi.org/10.1109/ACCESS.2020.2990567.

Boyd, S., N. Parikh, E. Chu, B. Peleato, and J. Eckstein (2010). Distributed optimization and statistical learning via the alternating direction method of multipliers. *Foundations and Trends in Machine Learning 3*, 1–122. https://doi.org/10.1561/2200000016.

Boyd, S., L. Xiao, A. Mutapcic, and J. Mattingley (2008). Notes on decomposition methods: Notes for ee364b. Stanford University. https://see.stanford.edu/materials/lsocoee364b/08-decomposition_notes.pdf.

Butler, R. (1999). The Steam And Gas Push (SAGP). *Journal of Canadian Petroleum Technology 38*(03). https://doi.org/10.2118/99-03-05.

Butler, R., Q. Jiang, and C. Yee (2000, 08). Steam and Gas Push (SAGP)-3;Recent Theoretical Developments and Laboratory Results. *Journal of Canadian Petroleum Technology 39*(08). https://doi.org/10.2118/00-08-04.

Butler, R. M. (1991). *Thermal recovery of oil and bitumen*. Englewood Cliffs, N.J., USA: Prentice Hall.

Capolei, A., E. Suwartadi, B. Foss, and J. B. Jørgensen (2015, 1). A mean–variance objective for robust production optimization in uncertain geological scenarios. *Journal of Petroleum Science and Engineering 125*, 23–37. https://doi.org/10.1016/J.PETROL.2014.11.015.

Card, C. C., A. Kumar, J. C. Close, A. Kjosavik, H. Agustsson, and M. M. Picone (2014, 2). A new and practical workflow for large multipad sagd simulation—an oil-sands case study. *Journal of Canadian Petroleum Technology 53*, 14–31. https://doi.org/10.2118/165511-PA.

Chen, B., R.-M. Fonseca, O. Leeuwenburgh, and A. C. Reynolds (2017). Minimizing the risk in the robust life-cycle production optimization using stochastic simplex approximate gradient. *Journal of Petroleum Science and Engineering 153*, 331 – 344. https://doi.org/10.1016/j.petrol.2017.04.001.

Chen, C., G. Li, and A. C. Reynolds (2012). Robust Constrained Optimization of Short- and Long-Term Net Present Value for Closed-Loop Reservoir Management. *SPE Journal 17*(03), 849–864. https://doi.org/10.2118/141314-PA.

Cheng, R., J. F. Forbes, and W. S. Yip (2007, 6). Price-driven coordination method for solving plant-wide mpc problems. *Journal of Process Control 17*, 429–438. https://doi.org/10.1016/j.jprocont.2006.04.003.

CMG (2018). *STARS Thermal & Advanced Processes Simulator*. Calgary, Alberta, Canada: Computer Modelling Group.

CMG (2020). *STARS Thermal & Advanced Processes Simulator*. Calgary, Alberta, Canada: Computer Modelling Group.

CMG (2021). *STARS Thermal & Advanced Processes Simulator*. Calgary, Alberta, Canada: Computer Modelling Group.

Coimbra, L., Z. Ma, and J. Y. Leung (2019, 4). Practical application of pareto-based multi-objective optimization and proxy modeling for steam alternating solvent process design. In *SPE Western Regional Meeting Proceedings*, San Jose, California, USA. Society of Petroleum Engineers. https://doi.org/10.2118/195247-MS.

Conte, C., T. Summers, M. N. Zeilinger, M. Morari, and C. N. Jones (2012, 12). Computational aspects of distributed optimization in model predictive control. In *2012 IEEE 51st IEEE Conference on Decision and Control (CDC)*, pp. 6819–6824. https://doi.org/10.1109/CDC.2012.6426138.

Dantzig, G. B. and P. Wolfe (1960, 2). Decomposition principle for linear programs. *Operations Research 8*, 101–111. https://doi.org/10.1287/opre.8.1.101.

Dehdari, V., C. Dong, and E. Marron (2017, 02). Calibrating a semi-analytic sagd forecasting model to 3d heterogeneous reservoir simulations. In *SPE Canada Heavy Oil Technical Conference 2017*, Calgary, Alberta, Canada. Society of Petroleum Engineers. https://doi.org/10.2118/184980-ms.

Delamaide, E. (2018, 03). Senlac, the Forgotten SAGD Project. *SPE Reservoir Evaluation & Engineering 21*(03), 789–805. https://doi.org/10.2118/183721-PA.

Detpunyawat, P. (2017). Sagd in reservoirs with top and bottom water zones. Master's thesis, University of Calgary, Calgary, Alberta, Canada. https://prism.ucalgary.ca/handle/11023/4139.

Devon, C. (2017, 12). 2017 performance presentation devon canada corporation jackfish sagd project. https://static.

aer.ca/prd/documents/oilsands/insitu-presentations/2017AthabascaDevonJackfishSAGD10097.pdf. Accessed: 2022-11-13.

Doan, G. T., B. Harschnitz, N. Shiga, E. Pennacchioli, and B. Park (2014, 6). Ncg co-injection at hangingstone demonstration project – case study and analysis. In *SPE Heavy Oil Conference Canada 2014*, Calgary, Alberta, Canada. Society of Petroleum Engineers. https://doi.org/10.2118/170068-MS.

Edmunds, N. and H. Chhina (2001). Economic optimum operating pressure for sagd projects in alberta. *Journal of Canadian Petroleum Technology 40*, 13–17. https://doi.org/10.2118/01-12-DAS.

Elgsaeter, S. M., O. Slupphaug, and T. A. Johansen (2008, 02). Production optimization: System identification and uncertainty estimation. In *SPE Intelligent Energy Conference and Exhibition*, Amsterdam, Netherlands. Society of Petroleum Engineers. https://doi.org/10.2118/112186-ms.

Escobar, E., P. Valko, W. J. Lee, and M. G. Rodriguez (2000, 1). Optimization methodology for cyclic steam injection with horizontal wells. In *SPE/CIM International Conference on Horizontal Well Technology*, Calgary, Alberta, Canada. Society of Petroleum Engineers. https://doi.org/10.2118/65525-MS.

Farahi, M. M. M., M. Ahmadi, and B. Dabir (2021). Model-based waterflooding optimization using multi-objective approach for efficient reservoir management. *Journal of Petroleum Science and Engineering 196*, 107988. https://doi.org/10.1016/j.petrol.2020.107988.

Fedutenko, E., C. Yang, C. Card, and L. X. Nghiem (2014). Time-dependent neural network based proxy modeling of sagd process. In *SPE Heavy Oil Conference Canada 2014*, Calgary, Alberta, Canada. https://doi.org/10.2118/170085-MS.

Foss, B., V. Gunnerud, and M. D. Diez (2009, 12). Lagrangian decomposi-

tion of oil-production optimization applied to the troll west oil rim. *SPE Journal 14*, 646–652. https://doi.org/10.2118/118299-PA.

Frenette, C. T., M. Saeedi, and J. L. Henke (2016, 1). Integrated economic model for evaluation and optimization of cyclic-steam-stimulation projects. *SPE Economics & Management 8*, 11–22. https://doi.org/10.2118/169859-PA.

Gonzalez, L. E., P. Ficocelli, and T. Bostick (2012). Real time optimization of sagd wells. In *SPE Heavy Oil Conference*. Society of Petroleum Engineers. https://doi.org/10.2118/157923-ms.

Guevara, J. L., R. Patel, and J. Trivedi (2021, 11). Optimization of steam injection in sagd using reinforcement learning. *Journal of Petroleum Science and Engineering 206*, 108735. https://doi.org/10.1016/j.petrol.2021.108735.

Guevara, J. L., R. G. Patel, and J. J. Trivedi (2018, 12). Optimization of steam injection for heavy oil reservoirs using reinforcement learning. In *SPE International Heavy Oil Conference and Exhibition*, Kuwait City, Kuwait. Society of Petroleum Engineers. https://doi.org/10.2118/193769-MS.

Gunnerud, V., B. Foss, B. Nygreen, R. Vestbø, and N. C. Walberg (2009, 1). Dantzig-wolfe decomposition for real-time optimization - applied to the troll west oil rim. *IFAC Proceedings Volumes 42*, 69–75. https://doi.org/10.3182/20090712-4-TR-2008.00012.

Guo, T., J. Wang, and I. D. Gates (2018, 9). Pad-scale control improves sagd performance. *Petroleum 4*, 318–328. https://doi.org/10.1016/j.petlm.2018.06.001.

Hanssen, G., B. Foss, and A. Teixeira (2015). Production optimization under uncertainty with constraint handling kristian. *IFAC-PapersOnLine 48*, 62 – 67. https://doi.org/10.1016/j.ifacol.2015.08.011.

Hao, M. and A. Popa (2015, 3). Steam generators optimization using a modified quantum-behaved particle swarm optimization (qpso) algorithm. In *SPE Digital Energy Conference and Exhibition*, Woodlands, Texas, USA. Society of Petroleum Engineers. https://doi.org/SPE-173391-MS.

Hasan, A., B. Foss, S. Krogstad, V. Gunnerud, and A. Teixeira (2013). Decision Analysis for Long-term and Short-term Production Optimization Applied to the Voador. In *SPE Reservoir Characterisation and Simulation Conference and Exhibition*, Abu Dhabi, UAE. https://doi.org/10.2118/166027-MS.

Holanda, R. W., E. Gildin, and J. L. Jensen (2015). Improved Waterflood Analysis Using the Capacitance-Resistance Model Within a Control Systems Framework. In *SPE Latin America and Caribbean Petroleum Engineering Conference*, Quito, Ecuador. https://doi.org/10.2118/177106-MS.

HomChaudhuri, B. (2013, 06). *Price-Based Distributed Optimization in Large-Scale Networked Systems*. Ph. D. thesis, University of Cincinnati, Cincinnati, Ohio, USA.

Hourfar, F., B. Moshiri, K. Salahshoor, M. Zaare-Mehrjerdi, and P. Pourafshary (2016, 10). Adaptive modeling of waterflooding process in oil reservoirs. *Journal of Petroleum Science and Engineering 146*, 702–713. https://doi.org/10.1016/j.petrol.2016.06.038.

Huang, B. and R. Kadali (2008). *Dynamic modeling, predictive control and performance monitoring. A data-driven subspace approach*, Volume 374 of *Lect. Notes Control Inf. Sci.* London: Springer.

Huang, Z. and Z. Chen (2021). Comparison of different machine learning algorithms for predicting the sagd production performance. *Journal of Petroleum Science and Engineering 202*, 108559. https://doi.org/10.1016/j.petrol.2021.108559.

Huang, Z., R. Li, and Z. Chen (2023). Integration of data-driven models

for dynamic prediction of the sagd production performance with field data. *Fuel 332*, 126171. https://doi.org/10.1016/j.fuel.2022.126171.

Hunyinbo, S., P. Azom, A. Ben-Zvi, and J. Y. Leung (2022). A Machine Learning Approach to Real-Time Uncertainty Assessment of SAGD Forecasts. *SPE Journal*, 1–13. https://doi.org/10.2118/208962-PA.

Hunyinbo, S., Z. Ma, and J. Y. Leung (2021, 10). Incorporating phase behavior constraints in the multi-objective optimization of a warm vaporized solvent injection process. *Journal of Petroleum Science and Engineering 205*, 108949. https://doi.org/10.1016/J.PETROL.2021.108949.

Jansen, J.-D., D. R. Brouwer, G. Naevdal, and C. P. J. W. van Kruijsdijk (2005). Closed-loop reservoir management. *First Break 23*. https://doi.org/10.3997/1365-2397.2005002.

Jimenez, J. (2008, 12). The field performance of sagd projects in canada. In *International Petroleum Technology Conference*, Kuala Lumpur, Malaysia. Society of Petroleum Engineers. https://doi.org/10.2523/IPTC-12860-MS.

Johansson, B., P. Soldati, and M. Johansson (2006, 8). Mathematical decomposition techniques for distributed cross-layer optimization of data networks. *IEEE Journal on Selected Areas in Communications 24*, 1535–1547. https://doi.org/10.1109/JSAC.2006.879364.

Jones, J. A. and P. Dwivedi (2018, 4). An integrated workflow approach to manage steamflood operations. In *SPE Western Regional Meeting*, Garden Grove, California, USA. Society of Petroleum Engineers. https://doi.org/10.2118/190064-MS.

Kim, M. and H. Shin (2017). Development and field application of proxy models for predicting the shale barrier size using sagd production data. In *SPE/IATMI Asia Pacific Oil & Gas Conference and Exhibition*, Jakarta, Indonesia. Society of Petroleum Engineers. https://doi.org/10.2118/186925-MS.

Kling, H., M. Fuchs, and M. Paulin (2012). Runoff conditions in the upper Danube basin under an ensemble of climate change scenarios. *Journal of Hydrology 424-425*, 264–277. https://doi.org/10.1016/j.jhydrol.2012.01.011.

Knoben, W. J., J. E. Freer, and R. A. Woods (2019, 10). Technical note: Inherent benchmark or not? comparing nash-sutcliffe and kling-gupta efficiency scores. *Hydrology and Earth System Sciences 23*, 4323–4331. https://doi.org/10.5194/HESS-23-4323-2019.

Knudsen, B. R., I. E. Grossmann, B. Foss, and A. R. Conn (2014, 4). Lagrangian relaxation based decomposition for well scheduling in shale-gas systems. *Computers & Chemical Engineering 63*, 234–249. https://doi.org/10.1016/J.COMPCHEMENG.2014.02.005.

Krishnamoorthy, D., M. A. Aguiar, B. Foss, and S. Skogestad (2018, 10). A distributed optimization strategy for large scale oil and gas production systems. *2018 IEEE Conference on Control Technology and Applications, CCTA 2018*, 521–526. https://doi.org/10.1109/CCTA.2018.8511385.

Krishnamoorthy, D., B. Foss, and S. Skogestad (2018, 1). A distributed algorithm for scenario-based model predictive control using primal decomposition. *IFAC-PapersOnLine 51*, 351–356. https://doi.org/10.1016/J.IFACOL.2018.09.325.

Kumar, A. and H. Hassanzadeh (2021). A qualitative study of the impact of random shale barriers on sagd performance using data analytics and machine learning. *Journal of Petroleum Science and Engineering 205*, 108950. https://doi.org/10.1016/j.petrol.2021.108950.

Kumar, A., A. Novlesky, E. Bityutsky, P. Koci, and J. Wightman (2018, 12). Field surveillance and ai based steam allocation optimization workflow for mature brownfield steam floods. In *SPE International Heavy Oil Conference and Exhibition*, Kuwait City, Kuwait. Society of Petroleum Engineers. https://doi.org/10.2118/193700-MS.

Kumar, A., G. Warren, K. Joslin, A. Abraham, and J. Close (2020, 9). Steam allocation optimization in full field multi-pad sagd reservoir. In *SPE Canada Heavy Oil Conference*, Calgary, Alberta, Canada. Society of Petroleum Engineers. https://doi.org/10.2118/199907-MS.

Legates, D. R. and G. J. McCabe (1999, 1). Evaluating the use of "goodness-of-fit" measures in hydrologic and hydroclimatic model validation. *Water Resources Research 35*, 233–241. https://doi.org/10.1029/1998WR900018.

Ljung, L. (1999). *System identification: theory for the user*. Upper Saddle River, NJ: Prentice Hall PTR.

Ma, Z. and J. Y. Leung (2019). Integration of deep learning and data analytics for sagd temperature and production analysis. In *SPE Reservoir Simulation Conference*, Galveston, Texas, USA. Society of Petroleum Engineers. https://doi.org/10.2118/193829-MS.

Ma, Z. and J. Y. Leung (2020, 8). Design of warm solvent injection processes for heterogeneous heavy oil reservoirs: A hybrid workflow of multi-objective optimization and proxy models. *Journal of Petroleum Science and Engineering 191*, 107186. https://doi.org/10.1016/J.PETROL.2020.107186.

Ma, Z., J. Y. Leung, S. Zanon, and P. Dzurman (2015, 11). Practical implementation of knowledge-based approaches for steam-assisted gravity drainage production analysis. *Expert Systems with Applications 42*, 7326–7343. https://doi.org/10.1016/j.eswa.2015.05.047.

Manchuk, J. G. and C. V. Deutsch (2013, 5). Optimization of drainage-area configurations to maximize recovery from sagd operations. *Journal of Canadian Petroleum Technology 52*, 233–242. https://doi.org/10.2118/165573-PA.

Maremi, A., E. Ben-Awuah, and Y. Pourrahimian (2020). An automated production targeting goal programming framework for oil sands mine planning considering organic rich solids. *Mining Technology*, 1–15.

Markowitz, H. M. (1952). Portfolio selection. *Journal of Finance 7*, 77–91.

MATLAB (2018). System identification toolbox.

MATLAB (2021). System identification toolbox.

Maxeiner, L. S. and S. Engell (2017, 7). Hierarchical mpc of batch reactors with shared resources. *IFAC-PapersOnLine 50*, 12041–12046. https://doi.org/10.1016/J.IFACOL.2017.08.2103.

Mayo-Molina, I. and J. Y. Leung (2021). Design of optimal operational parameters for steam-alternating-solvent processes in heterogeneous reservoirs - a multi-objective optimization approach. In *Society of Petroleum Engineers - SPE Europec featured at 82nd EAGE Conference and Exhibition, EURO 2021*, Volume 2. Society of Petroleum Engineers. https://doi.org/10.2118/205120-MS.

MEG, E. (2017). Christina lake regional project: 2016/2017 performance presentation. in situ performance presentations. https://static.aer.ca/prd/documents/oilsands/insitu-presentations/2017MEGChristinaLakeSAGD10773.pdf. Accessed: 2022-11-13.

Mendoza, A. M. and A. Kantzas (2020, 9). Simulation of non-condensable gases co-injection in steam assisted gravity drainage: State of the art and important mechanisms. In *SPE Canada Heavy Oil Conference*, Calgary, Alberta, Canada. Society of Petroleum Engineers. https://doi.org/10.2118/199930-MS.

Millington, D. (2019). Canadian oil sands supply costs and development projects (2019-2039). Technical report, Canadian Energy Research Institute. https://doi.org/https://ceri.ca/studies/canadian-oil-sands-supply-costs-and-development-projects-2019-2039, Accessed: 2022-11-13.

Millington, D. (2020). Canadian oil sands production and emissions outlook (2020-2039). Technical report, Canadian Energy Research Institute,

Calgary, AB. https://doi.org/https://ceri.ca/assets/files/Study%20191%20Full%20Report.pdf, Accessed: 2022-11-13.

Modigliani, F. and M. Leah (1997). Risk-adjusted performance. *Journal of portfolio management 23*, 45.

Mohajer, M. M., C. E. P. Damas, A. J. B. Silva, and A. Al-Kinani (2010, 1). An integrated framework for sagd real-time optimization. In *SPE Intelligent Energy Conference and Exhibition*, Utrecht, Netherlands. Society of Petroleum Engineers. https://doi.org/10.2118/128426-MS.

Mohankumar, Y., Z. Li, and B. Huang (2020, 5). Integrated well pad development scheduling with steam injection control in steam-assisted gravity drainage. *Journal of Process Control 89*, 45–57. https://doi.org/10.1016/J.JPROCONT.2020.03.008.

Murillo, C. A. (2015, 8). Oil sands industry energy requirements and greenhouse gas (ghg) emissions outlook (2015-2050). Technical report, Canadian Energy Research Institute, Calgary, Alberta, Canada. https://doi.org/https://ceri.ca/assets/files/Study_151_Full_Report.pdf, Accessed: 2022-11-13.

Nourozieh, H., E. Ranjbar, A. Kumar, and C. C. Card (2017). Impact, mitigation and optimization strategies when low oil prices alter long term sagd project implementation. In *SPE Canada Heavy Oil Technical Conference*, Calgary, Alberta, Canada. Society of Petroleum Engineers. https://doi.org/10.2118/185007-MS.

NRCAN, N. R. (2016). what-are-oil-sands. Natural Resources Canada. https://doi.org/https://www.nrcan.gc.ca/our-natural-resources/energy-sources-distribution/fossil-fuels/crude-oil/what-are-oil-sands/18089, Accessed: 2022-11-11.

Ockree, M., K. G. Brown, J. Frantz, M. Deasy, and R. John (2018, 10). Integrating big data analytics into development planning optimiza-

tion. In *SPE/AAPG Eastern Regional Meeting*, Pittsburgh, Pennslyvania, USA. Society of Petroleum Engineers. https://doi.org/10.2118/191796-18ERM-MS.

Patel, A. N., D. Davis, C. F. Guthrie, D. Tuk, T. T. Nguyen, and J. Williams (2005, 1). Optimizing cyclic steam oil production with genetic algorithms. In *SPE Western Regional Meeting*, Irvine, California, USA. Society of Petroleum Engineers. https://doi.org/10.2118/93906-MS.

Patel, K., E. M. Aske, and M. Fredriksen (2014, 5). Use of model-predictive control for automating sagd well-pair operations: A simulation study. *SPE Production & Operations 29*, 105–113. https://doi.org/10.2118/165535-pa.

Patel, R. G., V. Prasad, and J. J. Trivedi (2018). Real-Time Production Optimization of Steam-Assisted-Gravity-Drainage Reservoirs Using Adaptive and Gain-Scheduled Model-Predictive Control: An Application to a Field Model. *SPE Production & Operations 34*(01), 72–89. https://doi.org/10.2118/185688-PA.

Patel, R. G., V. Prasad, and J. J. Trivedi (2019, 2). Real-time production optimization of steam-assisted-gravity-drainage reservoirs using adaptive and gain-scheduled model-predictive control: An application to a field model. *SPE Production & Operations 34*(01), 72–89. https://doi.org/10.2118/185688-pa.

Patel, R. G. and J. J. Trivedi (2017). Sagd real-time production optimization using adaptive and gain-scheduled model-predictive-control: A field case study. In *SPE Western Regional Meeting Proceedings*, Bakersfield, California, USA. https://doi.org/10.2118/185688-ms.

Patel, R. G. and J. J. Trivedi (2020, 8). Nonlinear model predictive control of steam-assisted-gravity-drainage well operations for real-time production optimization. *SPE Production & Operations 35*, 564–578. https://doi.org/10.2118/201212-PA.

Pezier, J. and A. White (2006). The Relative Merits of Investable Hedge Fund Indices and of Funds of Hedge Funds in Optimal Passive Portfolios. Technical Report icma-dp2006-10, Henley Business School, University of Reading. https://econpapers.repec.org/paper/rdgicmadp/icma-dp2006-10.htm.

Popa, A. S., E. Grijalva, S. Cassidy, J. Medel, and A. Cover (2015, 9). Intelligent use of big data for heavy oil reservoir management. In *SPE Annual Technical Conference and Exhibition*, Houston, Texas, USA. Society of Petroleum Engineers. https://doi.org/10.2118/174912-MS.

Prakash, J., N. Sibaweihi, R. G. Patel, and J. J. Trivedi (2020, 09). Data-Driven Steam Optimization for SAGD. In *SPE Canada Heavy Oil Conference*, Virtual. https://doi.org/10.2118/199908-MS.

Purkayastha, S. N., I. D. Gates, and M. Trifkovic (2015, 1). Model-predictive-control (mpc) of steam trap subcool in steam-assisted gravity drainage (sagd). *IFAC-PapersOnLine 48*, 539–544. https://doi.org/10.1016/j.ifacol.2015.09.023.

Purkayastha, S. N., I. D. Gates, and M. Trifkovic (2018, 8). Real-time multivariable model predictive control for steam-assisted gravity drainage. *AIChE Journal 64*, 3034–3041. https://doi.org/10.1002/AIC.16098.

Renard, G., D. Dembele, J. Lessi, and J. L. Mari (1998). System identification approach applied to watercut analysis in waterflooded layered reservoirs. In *SPE Symposium on Improved Oil Recovery*. https://doi.org/10.2523/39606-ms.

Robinson, B., J. Kenny, I. L. Hernandez-Hdez, J. A. Bernal, and R. Chelak (2005, 1). Geostatistical modeling integral to effective design and evaluation of sagd processes of an athabasca oilsands reservoir, a case study. In *SPE International Thermal Operations and Heavy Oil Symposium*, Calgary, Alberta, Canada. Society of Petroleum Engineers. https://doi.org/10.2118/97743-MS.

Rockafellar, R. T. and S. Uryasev (2002). Conditional value-at-risk for general loss distributions. *Journal of banking & finance 26*, 1443–1471.

Salehinia, S., Y. Salehinia, F. Alimadadi, and S. H. Sadati (2016, 11). Forecasting density, oil formation volume factor and bubble point pressure of crude oil systems based on nonlinear system identification approach. *Journal of Petroleum Science and Engineering 147*, 47–55. https://doi.org/10.1016/j.petrol.2016.05.008.

Santos, S. M. G., A. T. F. S. Gaspar, and D. J. Schiozer (2017). Risk management in petroleum development projects: Technical and economic indicators to define a robust production strategy. *Journal of Petroleum Science and Engineering 151*, 116 – 127. https://doi.org/10.1016/j.petrol.2017.01.035.

Saputelli, L., M. Nikolaou, and M. J. Economides (2006, 3). Real-time reservoir management: A multiscale adaptive optimization and control approach. *Comput Geosci 10*, 61–96. https://doi.org/10.1007/s10596-005-9011-5.

Shahandeh, H., S. Rahim, and Z. Li (2016). Strategic optimization of the oil sands development with sagd: Drainage area arrangement and development planning. *Journal of Petroleum Science and Engineering 137*. https://doi.org/10.1016/j.petrol.2015.11.023.

Shen, C. (2013, 1). Sagd for heavy oil recovery. *Enhanced Oil Recovery Field Case Studies*, 413–445. https://doi.org/10.1016/B978-0-12-386545-8.00017-8.

Shirangi, M. G., O. Volkov, and L. J. Durlofsky (2017). Joint Optimization of Economic Project Life and Well Controls. In *SPE Reservoir Simulation Conference*, Montgomery, Texas, USA. https://doi.org/10.2118/182642-MS.

Sibaweihi, N., R. G. Patel, J. L. Guevara, I. D. Gates, and J. J. Trivedi (2019, 4). Real-time steam allocation workflow using machine learning for digital

heavy oil reservoirs. In *SPE Western Regional Meeting Proceedings*, San Jose, California, USA. Society of Petroleum Engineers. https://doi.org/10.2118/195312-MS.

Sibaweihi, N., R. G. Patel, J. L. Guevara, I. D. Gates, and J. J. Trivedi (2021). Real-time steam allocation workflow using machine learning for digital heavy oil reservoirs. *Journal of Petroleum Science and Engineering 199*, 108168. https://doi.org/10.1016/j.petrol.2020.108168.

Sibaweihi, N. and J. Trivedi (2022, 4). Risk management and optimization in real-time noncondensable gas co-injection under economic uncertainty. *SPE Reservoir Evaluation & Engineering*, 1–21. https://doi.org/10.2118/209591-PA.

Siraj, M. (2017, May). *Reducing the effect of uncertainty in robust optimization for oil recovery*. Ph. D. thesis, Technische Universiteit Eindhoven. Proefschrift.

Siraj, M. M., P. M. J. den Hof, and J. D. Jansen (2015, 12). Risk management in oil reservoir water-flooding under economic uncertainty. *2015 54th IEEE Conference on Decision and Control (CDC)*, 7542–7547. https://doi.org/10.1109/CDC.2015.7403410.

Siraj, M. M., P. M. J. V. den Hof, and J. D. Jansen (2017, 7). An adaptive robust optimization scheme for water-flooding optimization in oil reservoirs using residual analysis. *IFAC-PapersOnLine 50*, 11275–11280. https://doi.org/10.1016/j.ifacol.2017.08.1632.

Strobl, R., D. Gray, C. Flowers, Y. Wang, and A. Boustani (2016, 3). Steam assisted gravity drainage – new perspectives on recovery mechanisms and production. In *Geoconvention*, Calgary, Alberta, Canada. https://geoconvention.com/wp-content/uploads/abstracts/2016/050_GC2016_Steam_Assisted_Gravity_Drainage_New_Perspectives.pdf.

Sun, Q. and T. Ertekin (2015). The development of artificial-neural-network-based universal proxies to study steam assisted gravity drainage (sagd) and

cyclic steam stimulation (css) processes. In *SPE Western Regional Meeting*, Garden Grove, California, USA. Society of Petroleum Engineers. https://doi.org/10.2118/174074-MS.

van Essen, G. M., P. M. Van den Hof, and J. D. Jansen (2011). Hierarchical Long-Term and Short-Term Production Optimization. *SPE Journal 16*(01), 191–199. https://doi.org/10.2118/124332-PA.

Vanegas, J. W. P., C. V. Deutsch, and L. B. Cunha (2008). Uncertainty assessment of sagd performance using a proxy model based on butler's theory. In *SPE Annual Technical Conference and Exhibition*, Denver, Colorado, USA. Society of Petroleum Engineers. https://doi.org/10.2118/115662-MS.

Vembadi, S. S., R. G. Patel, J. J. Trivedi, and V. Prasad (2018, 6). Real-time feedback control of sagd wells using model predictive control to optimize steam chamber development under uncertainty. *The Canadian Journal of Chemical Engineering 96*, 1290–1305.

Vittoratos, E., G. R. Scott, and C. I. Beattie (1990, 2). Cold lake cyclic steam stimulation: A multiwell process. *SPE Reservoir Engineering 5*, 19–24. https://doi.org/10.2118/17422-PA.

Wang, C., G. Li, and A. C. Reynolds (2009). Production optimization in closed-loop reservoir management. *SPE Journal 14*, 506–523. https://doi.org/10.2118/109805-PA.

Yang, C., C. Card, and L. Nghiem (2009). Economic optimization and uncertainty assessment of commercial sagd operations. *Journal of Canadian Petroleum Technology 48*, 8.

Yang, C., C. Card, L. X. Nghiem, and E. Fedutenko (2011). Robust optimization of sagd operations under geological uncertainties. In *SPE Reservoir Simulation Symposium*, Woodlands, Texas, USA. Society of Petroleum Engineers. https://doi.org/10.2118/141676-MS.

Yao, S., J. J. Trivedi, and V. Prasad (2015, 8). Proxy modeling of the production profiles of sagd reservoirs based on system identification. *Ind. Eng. Chem. Res. 54*, 8356–8367. https://doi.org/10.1021/ie502258z.

Yee, C. and A. Stroich (2004). Flue Gas Injection Into a Mature SAGD Steam Chamber at the Dover Project (Formerly UTF). *Journal of Canadian Petroleum Technology 43*(01). https://doi.org/10.2118/04-01-06.

Yeung, K. C. (2019, 7). Why some sagd projects perform below expectations. *Canadian Heavy Oil Association*. https://choa.ab.ca/why-some-sagd-projects-perform-below-expectations/.

Yu, Y., S. Liu, Y. Liu, Y. Bao, L. Zhang, and Y. Dong (2021). Data-driven proxy model for forecasting of cumulative oil production during the steam-assisted gravity drainage process. *ACS Omega 6*(17), 11497–11509. https://doi.org/10.1021/acsomega.1c00617.

Zheng, J., J. Y. Leung, R. P. Sawatzky, and J. M. Alvarez (2016, 6). A proxy model for predicting sagd production from reservoirs containing shale barriers. In *SPE Canada Heavy Oil Technical Conference*, Calgary, Alberta, Canada. Society of Petroleum Engineers. https://doi.org/10.2118/180715-MS.